

Fig 4. Surface morphologies of PbS produced using 600 W microwave power for 15 min. (a-f) are AC, AT, CA, NA, NC and NT, respectively.

Different product morphologies were influenced by lead and sulfur sources which have different structure formulas. Nucleation and growth of the particles can play roles in the morphology. The crystal growth of some preferred structures or planes relates to the surface energy of the planes in the specified condition. It is described as the shape selective surface absorption process [13]. The amount of starting agents in the solution also has the influence on different orientation of the particles which reflects nucleation and growth of the crystals. The particle orientations were increased with the increasing in the amount of starting agents [14]. Phase with the lowest free energy is thermodynamically stable, and has more chance to exist in the process [15]. This reflects the product morphologies. Apart from the above, crystal growth is influenced by the solubility of the precursors in the particular solvent and synthesized temperature which reflects the morphologies [13]. Microwave powers and irradiation times also have the influence on the product shape, size and crystallinity.

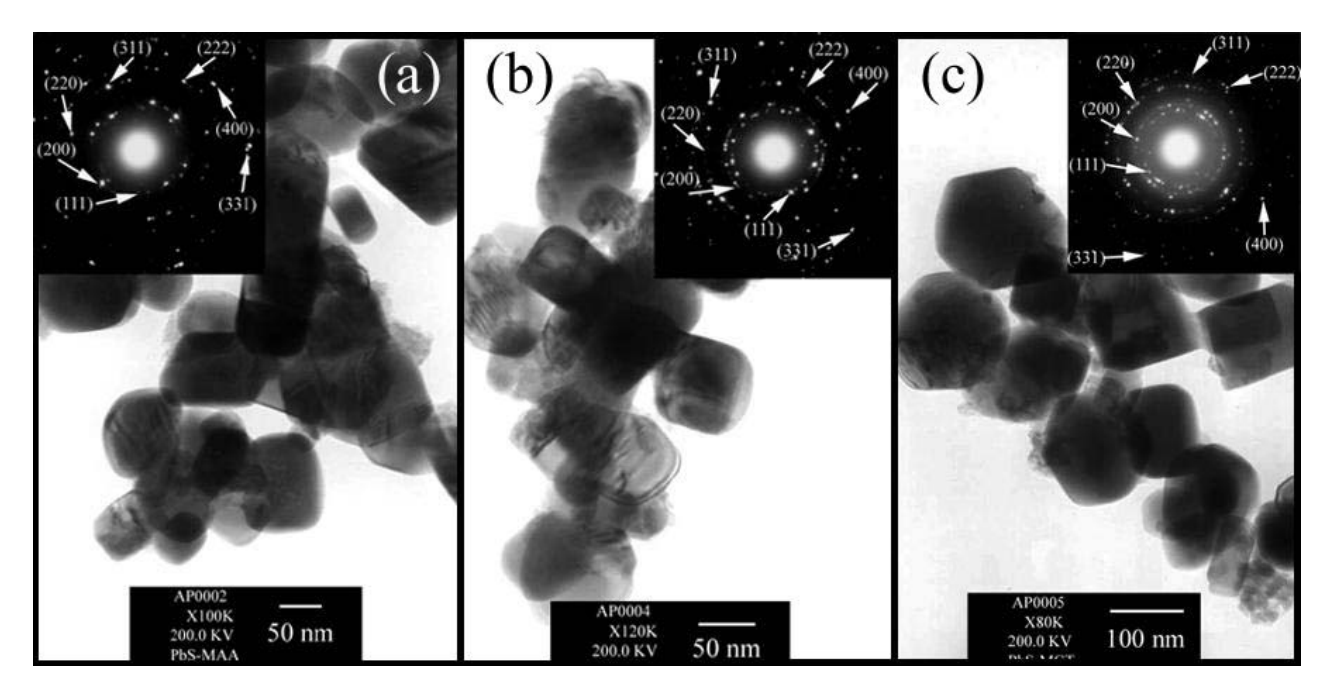


Fig 5. TEM images and SAED patterns of PbS produced using 600 W microwave power for 15 min. (a-c) are AA, CC and CT, respectively.

Their SAED patterns (Fig 5) compose of a number of bright spots arranging into concentric rings. They show the character of crystalline products. Electron beam diffracts from the crystallographic planes of the unit cells composing the products. The interpreted patterns [16,17] correspond to (111), (200), (220), (311), (222), (400) and (331). Comparing the diffraction planes to those of the JCPDS software [11], they were specified as cubic PbS.

The AT and NC products were also analyzed using TEM. Their morphologies (Figs 6a and 6d) are in accord with those of the SEM images (Figs 4b and 4e). SAED patterns (Figs 6b and 6e) appear as symmetric and systematic array of bright spots showing that a number of atoms are arranged in their crystal lattices. The patterns were interpreted [18], and specified as cubic PbS crystal [11]. Calculated electron beams [18] are in the [310] and [001] directions for AT and NC products, respectively. They are the directions that electron beams were sent to the crystal facets. Diffraction patterns for AT and NC with [310] and [001] zone axes were simulated (Figs 6c and 6f), respectively [19]. The simulated spots with the specified crystallographic planes are in systematic and symmetric arrays. Comparing the interpreted and simulated patterns, they are in good accord. The a\*, b\* and c\* lattice vectors for both patterns are in the [100], [010] and [001] directions, respectively. For

one crystal structure, the corresponding lattice vectors are the same although their zone axes are different. Additional concentric rings were also detected for the AT product (Fig 6b). They were caused by the C grid.

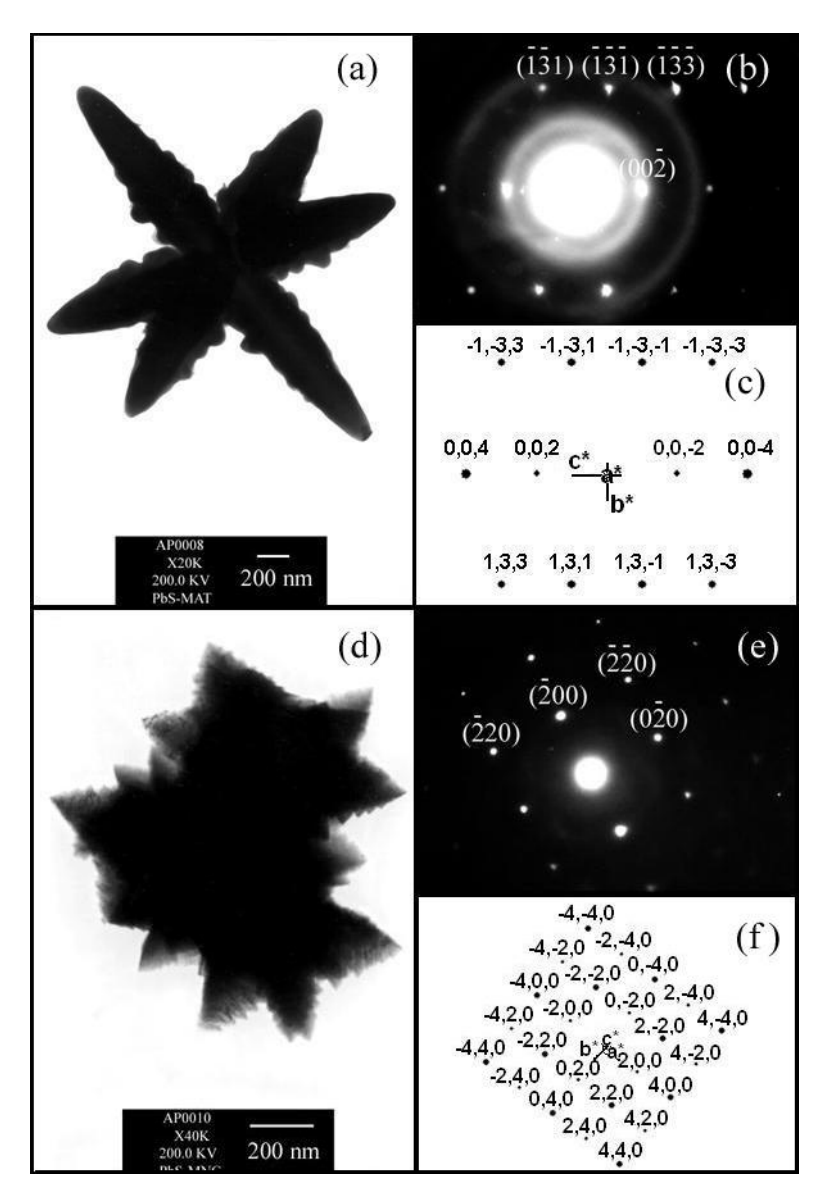


Fig 6. TEM images, and SAED and simulated patterns of PbS produced using 600 W microwave power for 15 min. (a-c) and (d-f) are for AT and NC, respectively.

A definite existence of the products was analyzed using a Raman spectrometer. Test specimens are non-destructive and are able to re-used for other purposes. Generally, Raman shifts correspond to the longitudinal optical (LO) mode in crystalline semiconductors. Transverse optical (TO) and surface phonon (SP) modes are not detectable due to symmetry restrictions and low intensities, respectively [20]. The detection of SP mode is possible in the nanostructured materials of which the

surface to volume ratio is large. This shows that surface roughness and crystallite size can play the role in the Raman spectra [20]. For the present research, the spectra (Fig 7) contain prominent bands at the same wavenumbers although the products have different morphologies (synthesized using different lead and sulfur sources). They imply that the vibrations are independent of the morphologies. The frequencies are influenced by some parameters, such as the atomic masses of Pb and S, and vibration constant of bonding between Pb and S atoms arranged in the lattice. Among the different spectra, their peaks are at 138, 273 and 439 cm<sup>-1</sup>. The peak below 150 cm<sup>-1</sup> is tentatively attributable to the so-called plasma line of the excitation laser [21,22]. The 273 cm<sup>-1</sup> peak corresponds to two-phonon process [21]. The peak at 439 cm<sup>-1</sup> is allowed in the rock-salt structure [23]. It was specified as the first overtone mode [22], which involves two phonons with equal but opposite k [23]. The fundamental LO of the rock-salt structure at approximately 219.5 cm<sup>-1</sup> was unable to detect due to the rising in intensity of baseline (disorder in PbS lattice) at low wavenumbers. Baseline intensity covered the fundamental LO mode, which was forbidden [22,23].

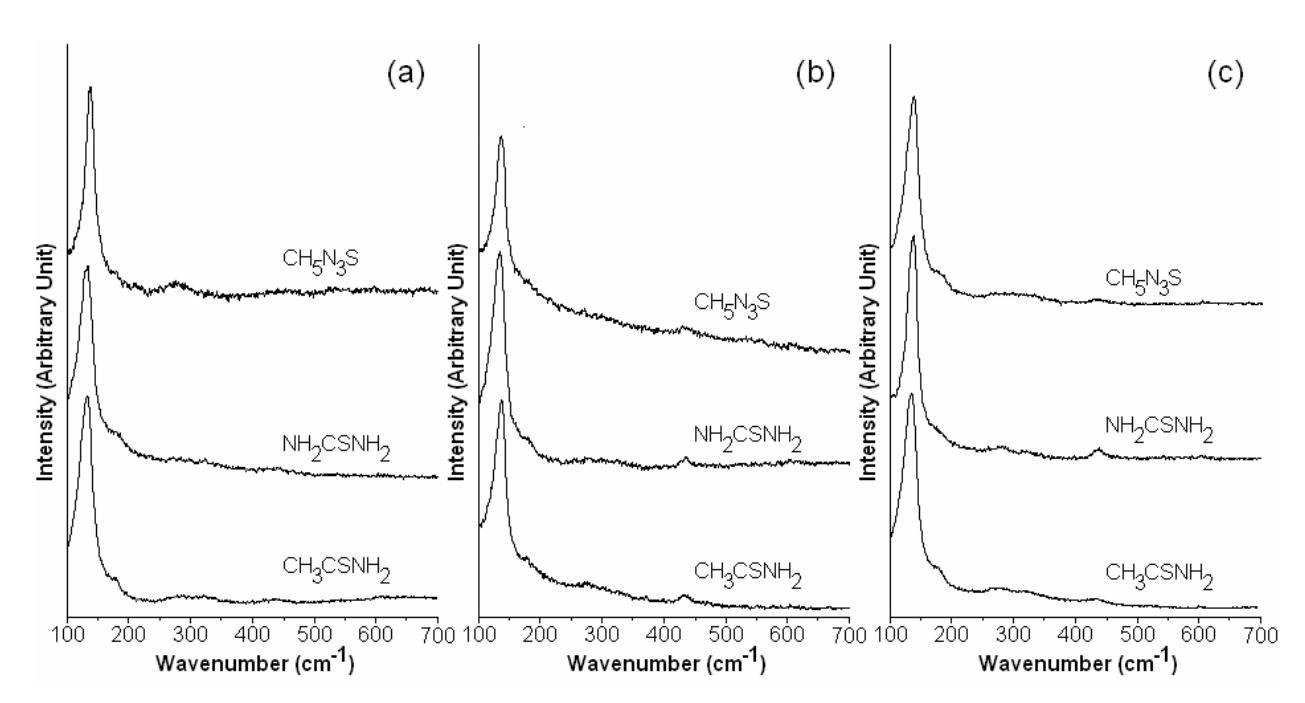


Fig 7. Raman spectra of PbS produced from (a-c) Pb(CH<sub>3</sub>COO)<sub>2</sub>.H<sub>2</sub>O, PbCl<sub>2</sub>.2.5H<sub>2</sub>O and Pb(NO<sub>3</sub>)<sub>2</sub> and different sulfur sources, using 600 W microwave power for 15 min, respectively.

#### **Conclusions**

Different shapes and sizes of PbS crystals were successfully produced from different lead and sulfur sources in propylene glycol using the cyclic microwave radiation at different powers and prolonged times. XRD, SAED and Raman analyses revealed the presence of PbS phase with the first overtone mode at 439 cm<sup>-1</sup>. The crystalline degree was increased with the increasing in the microwave powers and prolonged times. The nano-sized particles, hexapods, cubes, ferns and magic squares were characterized using SEM and TEM. They were influenced by the microwave powers, prolonged times and starting agents.

#### References

- [1] S. Wang, A. Pan, H. Yin, Y. He, Y. Lei, Z. Xu, B. Zou, Mater. Lett. 60 (2006) 1242.
- [2] L. Xu, W. Zhang, Y. Ding, W. Yu, J. Xing, F. Li, Y. Qian, J. Cryst. Growth 273 (2004) 213.
- [3] L. Dong, Y. Chu, Y. Liu, M. Li, F. Yang, L. Li, J. Coll. Interf. Sci. 301 (2006) 503.
- [4] G. Zhou, M. Lü, Z. Xiu, S. Wang, H. Zhang, Y. Zhou, S. Wang, J. Phys. Chem. B 110 (2006) 6543.
- [5] P. Zhao, G. Chen, Y. Hu, X. He, K. Wu, Y. Cheng, K. Huang, J. Cryst. Growth 303 (2007) 632.
- [6] S.F. Wang, F. Gu, M.K. Lü, Langmuir 22 (2006) 398.
- [7] Y.J. Yang, Coll. Surf. A 276 (2006) 192.
- [8] S.F. Wang, F. Gu, M.K. Lü, D.Z. Wang, Z.S. Yang, H.P. Zhang, Y.Y. Zhou, A.Y. Zhang, Mater. Lett. 60 (2006) 2759.
- [9] T. Ding, J.J. Zhu, Mater. Sci. Engin. B 100 (2003) 307.
- [10] C. Gabriel, S. Gabriel, E.H. Grant, B.S.J. Halstead, D.M.P. Mingos, Chem. Soc. Rev. 27 (1998) 213.
- [11] Powder Diffract. File, JCPDS Internat. Centre Diffract. Data, PA 19073-3273, U.S.A., (2001).
- [12] T. Thongtem, S. Thongtem, Ceram. Internat. 31 (2005) 241.
- [13] S. Biswas, S. Kar, S. Chaudhuri, J. Cryst. Growth 299 (2007) 94.

- [14] Y.C. Zhang, X.Y. Hu, T. Qiao, Solid State Comm. 132 (2004) 779.
- [15] K. Sopunna, T. Thongtem, M. McNallan, S. Thongtem, Surf. Sci. 566-568 (2004) 810.
- [16] T. Thongtem, S. Kaowphong, S. Thongtem, J. Mater. Sci. 42 (2007) 3923.
- [17] A. Phuruangrat, T. Thongtem, S. Thongtem, Mater. Lett. 61 (2007) 3805.
- [18] T. Thongtem, A. Phuruangrat, S. Thongtem, Mater. Lett. 61 (2007) 3235.
- [19] C. Boudias, D. Monceau, CaRlne Crystallography 3.1, 17 rue du Moulin du Roy, F-60300 Senlis, France (1989-1998).
- [20] K.K. Nanda, S.N. Sahu, Phys. Rev. B 58 (1998) 15 405.
- [21] A.M. Qin, Y.P. Fang, W.X. Zhao, H.Q. Liu, C.Y. Su, J. Cryst. Growth 283 (2005) 230.
- [22] G.D. Smith, S. Firth, R.J.H. Clark, M. Cardona, J. Appl. Phys., 92 (2002) 4375.
- [23] R. Sherwin, R.J.H. Clark, R. Lauck, M. Cardona, Solid State Comm. 134 (2005) 565.

### Preparation of ear-like, hexapod and dendritic PbS using cyclic microwaveassisted synthesis

#### **Abstract**

Different morphologies of PbS were prepared using microwave-assisted synthesis of 1:4, 1:1 and 4:1 molar ratios of Pb(CH<sub>3</sub>COO)<sub>2</sub> to NH<sub>2</sub>CSNH<sub>2</sub> in propylene glycol. Cubic PbS was detected using X-ray diffraction (XRD) and selected area electron diffraction (SAED). Raman spectrometry revealed the presence of vibrations at 134, 275 and 431 cm<sup>-1</sup>. The product morphologies for different molar ratios of Pb(CH<sub>3</sub>COO)<sub>2</sub> to NH<sub>2</sub>CSNH<sub>2</sub> were also characterized using a scanning electron microscope (SEM) and a transmission electron microscope (TEM). The obtained morphologies changed with molar ratios used for the starting agents. The simulated diffraction pattern was also in accordance with the interpretation of the experimental results.

**Keywords**: Cyclic microwave-assisted synthesis; PbS; Ear-like structure; Hexapod; Dendrite

#### Introduction

PbS is one of luminescent materials which have novel semiconducting and optical properties [1]. It has a small band gap of 0.41 eV (for bulk at room temperature), large excitonic Bohr radius of 18 nm [2-4], and is very sensitive to the quantum-size effect [2,3]. Different morphologies can play the roles in the properties. They are nanocrystals [5], nanorods [6,7], nanotubes [6], nanocubes [8], star-shapes [9], dendrites [8,10] and flower-like crystals [11], which can be prepared by different methods, such as hydrothermal and solvothermal routes [4,8], electroless chemical deposition [12], microwave-assisted synthesis [11] and sonochemistry method [6].

Microwave-assisted synthesis [13] is a very attractive process for producing a variety of materials. When microwave radiation is applied to chemicals, at least one of the components is capable of coupling with the

radiation. It is able to promote the reaction rates, and consumes shorter reaction time, comparing to a conventional method. Temperature and concentration gradients are able to be solved by the vibration of microwave radiation. Due to a large amount of microwave energy focused onto solutions, the vibrating electric field applies a force on the charged particles to vibrate accordingly. The radiation can play the role in promoting the reaction kinetics with high efficiency.

To the best of our knowledge, there are not many reports on the preparation of ear-like, hexapod and dendritic PbS, and using only hydrothermal process [14,15]. In the present research, these PbS nanostructures were prepared from different molar ratios of Pb and S sources, using cyclic microwave-assisted synthesis. The final products were intensively analyzed for further discussion.

#### **Experiment**

Difference PbS morphologies were prepared from 1:4, 1:1 and 4:1 molar ratios of Pb(CH<sub>3</sub>COO)<sub>2</sub> to NH<sub>2</sub>CSNH<sub>2</sub> in propylene glycol, using 600 W cyclic microwave radiation for 9 cycles. A cyclic duration of 100 s, the radiation was on for 30 s every 70 s interval. At the conclusion of the process, the system naturally cooled down to room temperature. The products were washed with water and ethanol, and dried at 80 °C for 12 h. Then they were characterized by using X-ray diffraction (XRD), Raman spectrometry, scanning electron microscopy (SEM), transmission electron microscopy (TEM) as well as selected area electron diffraction (SAED) techniques. The electron diffraction patterns were simulated by CaRIne Crystallography 3.1 program [16] and compared with those of the experimental results.

#### **Results and Discussion**

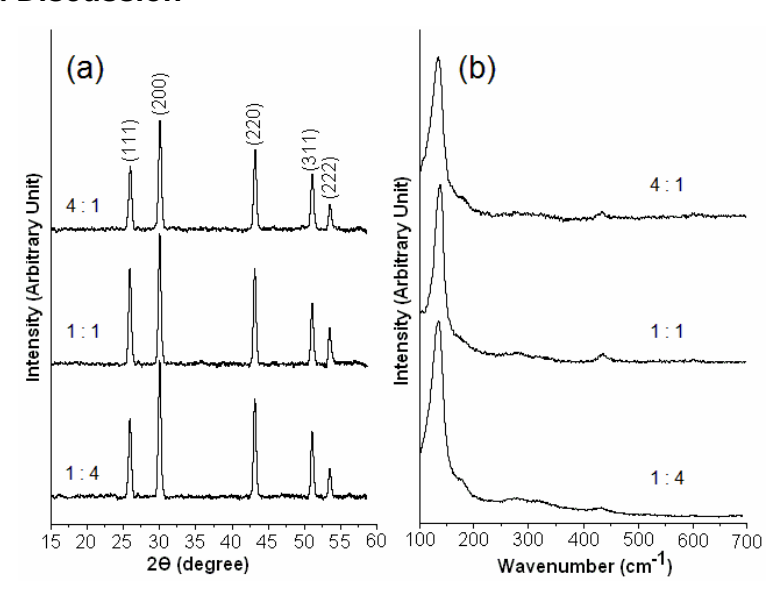


Fig 1. (a) XRD patterns and (b) Raman spectra of the products prepared using different molar ratios of Pb(CH<sub>3</sub>COO)<sub>2</sub> to NH<sub>2</sub>CSNH<sub>2</sub>.

XRD patterns (Fig 1a) were indexed by using ICDD-JCPDS database (card no. 05-0592) [17]. The examined products were cubic PbS, with the Fm-3m space group. No characteristic peaks of impurities were detected showing that each of the products is a pure phase. Their lattice parameters were calculated from the equation of plane spacing for cubic crystal system and Bragg's law for diffraction [18]. The averages and standard deviations are  $5.9476 \pm 0.0111$ ,  $5.9473 \pm 0.0096$  and  $5.9522 \pm 0.0119$  Å for the products prepared using 1:4,1:1 and 4:1 molar ratios of Pb(CH<sub>3</sub>COO)<sub>2</sub> to NH<sub>2</sub>CSNH<sub>2</sub>, respectively. They are very close to those of the ICDD-JCPDS reference data [17].

The chemical process leading to PbS formation is considered to proceed according to the following.

$$Pb(CH_3COO)_2 \rightarrow Pb^{2+} + 2(CH_3COO)^{-}$$
 (1)

$$NH_2CSNH_2 + H_2O \rightarrow NH_2CONH_2 + H_2S$$
 (2)

$$Pb^{2^{+}} + S^{2^{-}} \rightarrow PbS$$
 (3)

Theoretically, 1 mol  $Pb(CH_3COO)_2$  and 1 mol  $NH_2CSNH_2$  were used to produce 1 mol PbS. The products were able to be produced even when either of the reactants was excessive.

A definite existence of PbS was analyzed using Raman spectrometry. The Raman spectra (Fig 1b) contain prominent bands at the same wavenumbers. They are influenced by some parameters, such as atomic masses of Pb and S, and vibration constant of bonding between Pb and S atoms residing in the lattice. Among the different spectra, their peaks are at 134, 275 and 431 cm<sup>-1</sup>. The peak below 150 cm<sup>-1</sup> is tentatively attributable to the so-called plasma line of the excitation laser [1,19]. The 275 cm<sup>-1</sup> peak corresponds to two-phonon process [1]. The peak at 431 cm<sup>-1</sup> is allowed in the rock-salt structure [20]. It is specified as the first overtone of the longitudinal optical (2LO) mode at the center ( $\Gamma$ ) of Brillouin zone [19], which involves two phonons with equal but opposite wave vectors ( $\bar{k}$ ) [20]. The fundamental longitudinal optical (1LO) mode of the rock-salt structure at approximately 215.5 cm<sup>-1</sup> was unable to be detected due to the rising in intensity of baseline, caused by disordering in PbS lattice, at low wavenumbers. The baseline intensity covered the 1LO mode, which was forbidden [19,20].

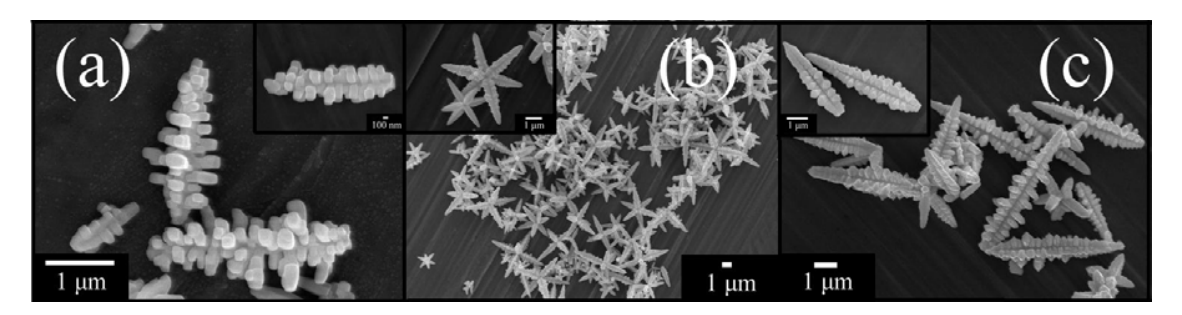


Fig 2. SEM images of the products prepared using (a-c) 1 : 4, 1 : 1, and 4 : 1 molar ratios of Pb(CH<sub>3</sub>COO)<sub>2</sub> to NH<sub>2</sub>CSNH<sub>2</sub>, respectively.

The SEM images from Fig 2 show that the products are ear-like structure, hexapod and dendrite for 1:4, 1:1 and 4:1 molar ratios of Pb(CH<sub>3</sub>COO)<sub>2</sub> to NH<sub>2</sub>CSNH<sub>2</sub>. The hexapods composed four coplanar pods, with the other two

pods at right angle with respect to the four-pod structure. One pod is on the top, and the other is at the bottom. The length of the trunk and the diameter of the branches of PbS dendrites are about 5–8 µm and 700–800 nm, respectively. The product morphologies were controlled by the different growth direction and rate [14,15]. Each arm of hexapod PbS is along the [100] direction. When NH<sub>2</sub>CSNH<sub>2</sub> is added excess, the independent arm of hexapod is broken from core to form a crystal dendrite. When Pb(CH<sub>3</sub>COO)<sub>2</sub> is in excess, it seems to favor the faster growth in [011] relative to [100] directions. The result is the formation of the earlike structure [14].

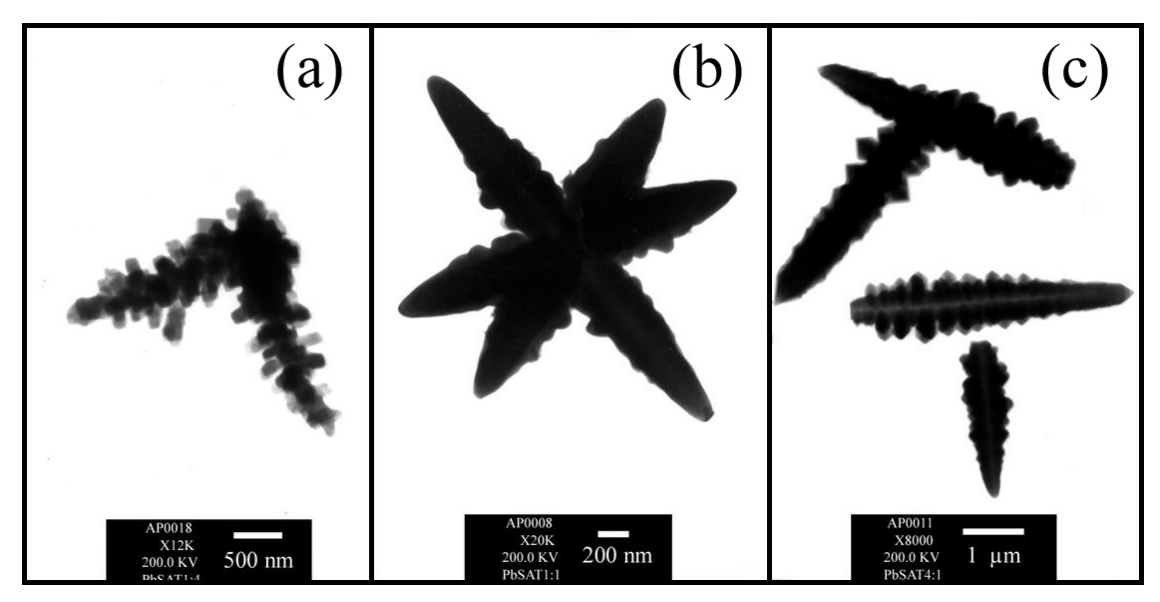


Fig 3. TEM images of the products prepared using (a-c) 1 : 4, 1 : 1, and 4 : 1 molar ratios of  $Pb(CH_3COO)_2$  to  $NH_2CSNH_2$ , respectively.

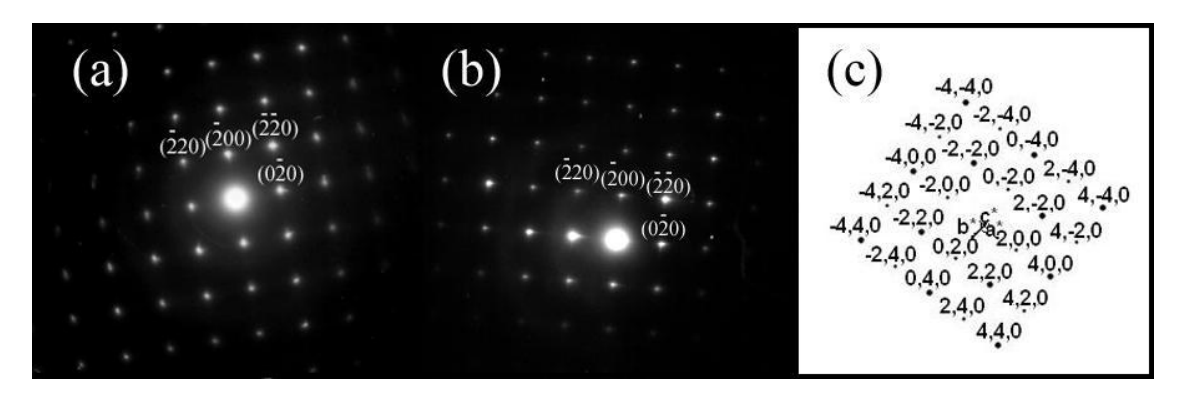


Fig 4. SAED patterns of the products prepared using (a) 4 : 1 and (b) 1 : 4 molar ratios of  $Pb(CH_3COO)_2$  to  $NH_2CSNH_2$ , and (c) simulated electron diffraction pattern.

TEM images (Fig 3) were used to specify the product morphologies. The results obtained using TEM are in accordance with those provided by SEM. For the present research, TEM images are 2D. But for SEM images, they are 3D. The SAED patterns from Figs 4a and 4b, for the products prepared using 4 : 1 and 1 : 4 molar ratios of Pb(CH<sub>3</sub>COO)<sub>2</sub> to NH<sub>2</sub>CSNH<sub>2</sub> appear as a symmetric and systematic array of bright spots showing that a number of atoms are arranged in respective crystalline structures. The patterns were interpreted [21], and specified as cubic PbS [17]. The electron beam used for the analysis was in the [001] direction. The electron diffraction simulated pattern (Fig 4c) is composed of systematic and symmetric array of bright spots as well. It is in good accordance with those obtained from the experiment.

#### **Conclusions**

Ear-like, hexapod and dendritic PbS nano-structures were successfully prepared from 1:4, 1:1 and 4:1 molar ratios of Pb(CH<sub>3</sub>COO)<sub>2</sub> to NH<sub>2</sub>CSNH<sub>2</sub> in propylene glycol, using cyclic microwave-assisted synthesis. XRD and SAED analyses revealed the presence of PbS with a cubic structure. The experimental and simulated patterns are in good accordance. Both SEM and TEM analyses revealed the presence of ear-like, hexapod and dendritic PbS which were prepared using different molar ratios of Pb and S sources. The 431 cm<sup>-1</sup> first

overtone mode was detected using Raman spectrometry, but the fundamental one was forbidden.

#### References

- 1. A.M. Qin, Y.P. Fang, W.X. Zhao, H.Q. Liu, and C.Y. Su, J. Cryst. Growth 2005;283:230-241.
- 2. L. Xu, W. Zhang, Y. Ding, W. Yu, J. Xing, F. Li, and Y. Qian, J. Cryst. Growth 2004;273:213-219.
- 3. Y.C. Zhang, T. Qiao, X.Y. Hu, G.Y. Wang, and X. Wu, J. Cryst. Growth 2005;277:518-523.
- 4. S. Wang, A. Pan, H. Yin, Y. He, Y. Lei, Z. Xu, and B. Zou, Mater. Lett. 2006;60:1242-1246.
- 5. U.K. Gautam and R. Seshadri, Mater. Res. Bull. 2004;39:669-676.
- 6. S.F. Wang, F. Gu, M.K. Lü, G.J. Zhou, and A.Y. Zhang, J. Cryst. Growth 2006;289: 621-625.
- 7. T. Saraidarov, R. Reisfeld, A. Sashchiuk, and E. Lifshitz, Physica E 2007;37:173-177.
- 8. W. Zhang, Q. Yang, L. Xu, W. Yu, and Y. Qian, Mater. Lett. 2005;59:3383-3388.
- 9. G. Zhou, M. Lü, Z. Xiu, S. Wang, H. Zhang, Y. Zhou, and S. Wang, J. Phys. Chem. B 2006;110:6543-6548.
- 10.Z. Zhang, S.H. Lee, J.J. Vittal, and W.S. Chin, J. Phys. Chem. B 2006;110:6649-6654.
- 11. Y. Ni, F. Wang, H. Liu, G. Yin, J. Hong, X. Ma, and Z. Xu, J. Cryst. Growth 2004;262:399-402.
- 12.B. Minceva-Sukarova, M. Najdoski, I. Grozdanov, and C.J. Chunnilall, J. Molec. Struct. 1997;410-411:267-270.

- 13. C. Gabriel, S. Gabriel, E.H. Grant, B.S.J. Halstead, and D.M.P. Mingos, Chem. Soc. Rev. 1998;27:213-223.
- 14.S. Shao, G. Zhang, H. Zhou, P. Sun, Z. Yuan, B. Li, D. Ding and T. Chen, Solid State Sci. 2007;9:725-731.
- 15.Y. Ji, X. Ma, H. Zhang, J. Xu and D. Yang, J. Phys.: Condens. Matter 2003;15:7611–7615.
- 16. C. Boudias, D. Monceau, CaRlne Crystallography 3.1, 17 rue du Moulin du Roy, F-60300 Senlis, France 1989-1998.
- 17. Powder Diffract. File, JCPDS Internat. Centre Diffract. Data, PA 19073-3273, U.S.A. 2001.
- 18.C. Suryanarayana and M.G. Norton, X-ray Diffract, A Practical Approach, Plenum Press, New York 1998.
- 19.G.D. Smith, S. Firth, R.J.H. Clark, and M. Cardona, J. Appl. Phys. 2002;92:4375-4380.
- 20.R. Sherwin, R.J.H. Clark, R. Lauck, and M. Cardona, Solid State Comm. 2005;134:565-570.
- 21.T. Thongtem, A. Phuruangrat, and S. Thongtem, Mater. Lett. 2007;61:3235-3238.

# Carboxymethyl cellulose-assisted hydrothermal synthesis of PbS with nano and microcrystals

#### Abstract

PbS with nano and microcrystals was hydrothermally synthesized from Pb(NO<sub>3</sub>)<sub>2</sub> and thiosemicarbazide using carboxymethyl cellulose (CMC) as a template at 140, 180 and 200 °C for 12 h. CMC, NaOH and hydrothermal temperatures have the influence on the product morphologies characterized using a scanning electron microscope (SEM) and a transmission electron microscope (TEM). PbS (cubic) composing of Pb and S was detected using an X-ray diffractometer (XRD), a selected area electron diffraction (SAED) technique and an energy dispersive X-ray (EDX) analyzer. The interpreted patterns are definitely true, and are in accord with those of the simulation. Raman spectrometer revealed the presence of the vibration modes at 136, 278, 432, 602 and 967 cm<sup>-1</sup>. Emission spectra of the products were detected at 384-388 nm using a photoluminescence (PL) spectrometer.

**Keywords:** Hydrothermal synthesis; Carboxymethyl cellulose (CMC); PbS with nano and microcrystals

#### Introduction

At present, nano and microcrystalline luminescent materials have become increasingly important. One of them is PbS which has a small band gap (0.41 eV) and a large exciton Bohr radius (18 nm).<sup>1-3</sup> It has novel semiconducting and optical properties influenced by different shapes and sizes.<sup>4</sup> It was synthesized using different methods, such as nanocubic and dendritic crystals by a complex

solvothermal synthetic route<sup>5</sup>, star-shaped dendrites, multipods, truncated nanocubes and nanocubes by a simple solution route<sup>6</sup>, nanorods, nanobelts, nanovelvet-flowers and dendritic nanostructures using aqueous solution at low temperature assisted by CTAB<sup>7</sup>, nanoclusters using a powder method on ionomers<sup>8</sup>, thin solid films by electroless chemical deposition<sup>9</sup>, magic-square structure by hydrothermal preparation<sup>10</sup>, and nanobelts by sonochemical synthesis<sup>11</sup>. The purpose of the research is to study the influence of carboxymethyl cellulose (CMC) and NaOH on PbS with nano and microcrystals synthesized using the home-made stainless steel autoclaves. Carboxymethyl cellulose, a non-toxic and inexpensive biomolecule, is used for modeling the morphologies of the products. It is a capping agent in the solutions as well.<sup>12</sup> The final products were intensively analyzed for further discussion.

#### **Experiment**

For the present research, 0.003 mol Pb(NO<sub>3</sub>)<sub>2</sub> in 15 ml water, and 0.05 g carboxymethyl cellulose (CMC) in 10 ml water were thoroughly mixed to form the CMC-Pb<sup>2+</sup> solution<sup>12</sup>. Subsequently, 0.003 mol thiosemicarbazide (NH<sub>2</sub>CSNHNH<sub>2</sub>) in 15 ml water and different molarities of NaOH were put in the CMC-Pb<sup>2+</sup> solution. To produce PbS with different morphologies, the reaction proceeded in the home-made stainless steel autoclaves at 140, 180 and 200 °C for 12 h. The precipitates were washed with water and 95 % ethanol, and dried at 80 °C for 24 h. The final products were analyzed using an X-ray diffractometer (XRD) operated at 20 kV, 15 mA and using Cu K<sub> $\alpha$ </sub> radiation in the 2 $\theta$  angular range of 15 - 60 deg, a transmission electron microscope (TEM) as well as the use of the selected area electron diffraction (SAED) technique operated at 200 kV, a scanning electron microscope (SEM) and an energy

dispersive X-ray (EDX) analyzer operated at 15 kV, a Raman spectrometer using 50 mW Ar laser with  $\lambda$  = 514.5 nm, and a luminescence spectrometer using 250 nm exciting wavelength.

#### **Results and Discussion**

XRD spectra (Fig 1) were indexed using Bragg's law for diffraction and compared with those of the JCPDS software (reference code : 05-0592)<sup>13</sup>. They were specified as cubic PbS with Fm-3m space group. The spectra are very sharp showing that well-crystallized PbS was successfully synthesized.<sup>14</sup> The products compose of a number of atoms aligning in a periodic lattice. The strongest intensity is at  $2\theta = 30.08$  deg and diffracts from (200) plane of the crystalline products. No other characteristic peaks of impurities such as different oxide-sulfates were detected showing that the products are pure phase.

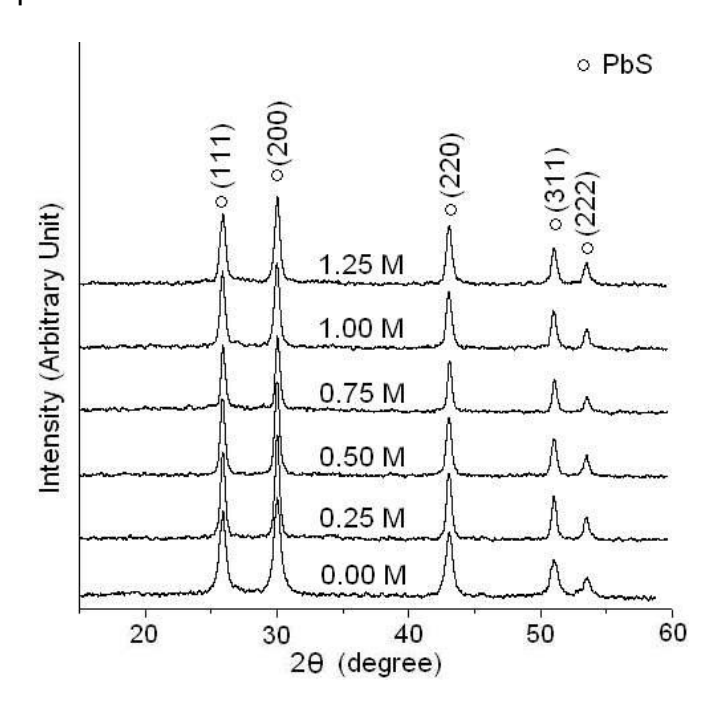


Fig 1. XRD spectra of the products synthesized in the solutions containing 0.05 g CMC and different molarities of NaOH by 140 °C hydrothermal reaction for 12 h.

A definite existence of the products was analyzed using a Raman spectrometer. The spectra (Fig 2) contain prominent bands at the same wavenumbers although the products were synthesized using different conditions. Among the different spectra, their peaks are at 136, 278, 432, 602 and 967 cm<sup>-1</sup>. The peak below 150 cm<sup>-1</sup> is tentatively attributable to the so-called plasma line of the excitation laser. The 278 cm<sup>-1</sup> peak was caused by the two-phonon process. Those at 432 and 602 cm<sup>-1</sup> are specified as the first and second overtone modes, respectively. The peak above 960 cm<sup>-1</sup> is attributable to oxide-sulfates. Their constituents were also characterized using EDX. The spectra (Fig 3) reveal the presence of Pb and S.

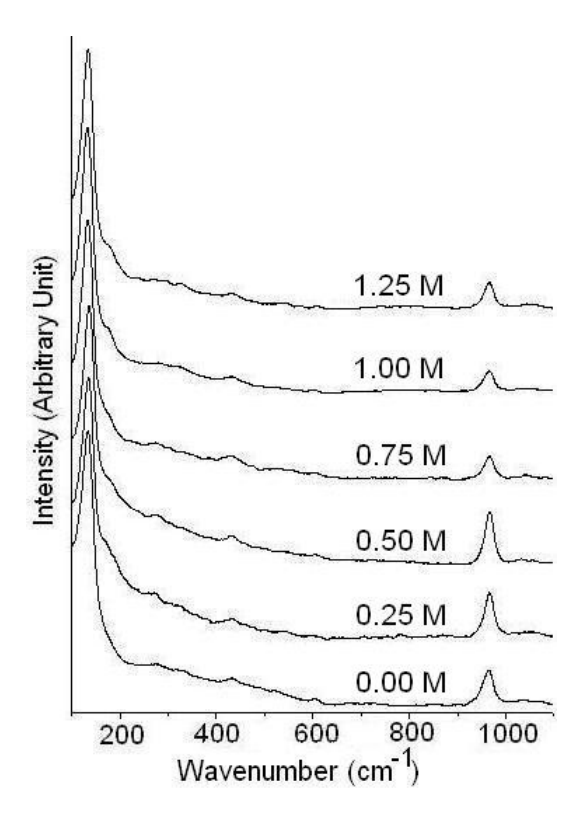


Fig 2. Raman spectra of the products synthesized in the solutions containing 0.05 g CMC and different molarities of NaOH by 140 °C hydrothermal reaction for 12 h.

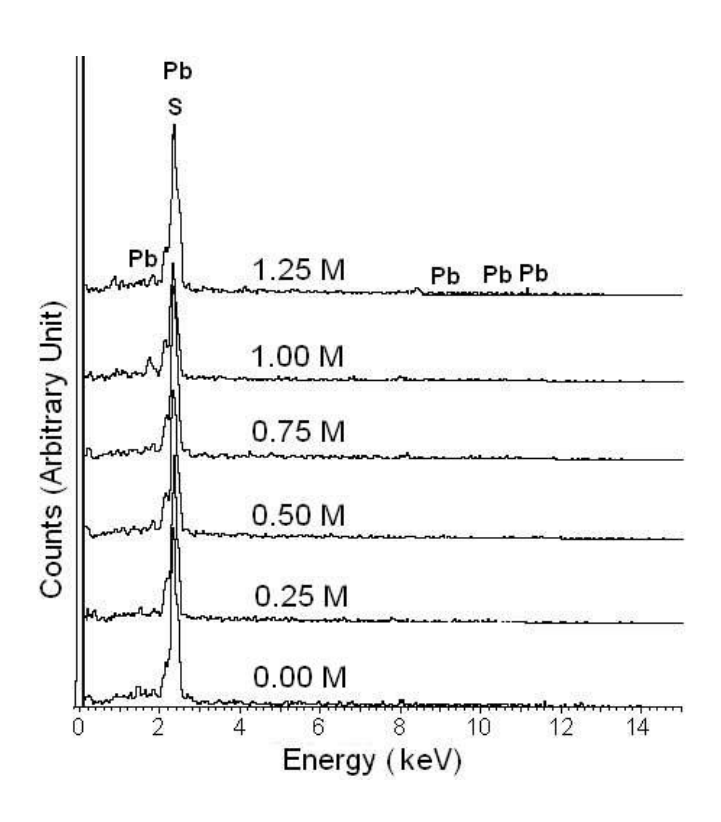


Fig 3. EDX spectra of the products synthesized in the solutions containing 0.05 g CMC and different molarities of NaOH by 140 °C hydrothermal reaction for 12 h.

TEM images and SAED patterns (Fig 4) are used to specify the morphologies and phases of the products. In NaOH-free solution containing 0.05 g CMC (pH = 4.7), the product is flower-like at 140 °C hydrothermal reaction (Fig 4a). At 180 and 200 °C (Figs 4b and 4c), the flower becomes larger and more complete. Their SAED patterns (Figs 4a-4c) appear as systematic array of bright spots showing that a number of atoms are aligned in their normal lattice. The patterns were interpreted <sup>16</sup>, and specified as cubic PbS crystal <sup>13</sup>. Calculated electron beams (zone axes) <sup>16</sup> are in the [013], [112] and [101] directions for the products produced at 140, 180 and 200 °C hydrothermal reactions, respectively. They are the directions that the beams of electrons were sent to the corresponding crystalline facets. To show whether the diffraction patterns are definitely true, simulated patterns (Figs 4a-4c) were created <sup>17</sup> using the corresponding zone axes. They are systematic and symmetric, and are in

good accord with the corresponding interpreted patterns. The a\*, b\* and c\* lattice vectors of the simulated patterns are in the [100], [010] and [001] directions, respectively. For one crystal structure, the corresponding lattice vectors are the same although their zone axes are different. In the solution containing 0.05 g CMC and 1.00 M NaOH, a tubular cluster of nano-particles at 140 °C hydrothermal reaction (Fig 4d) is shown. SAED pattern composes of several concentric rings characterized as polycrystals. Interplanar spaces were calculated 18,19 using their diffraction ring diameters, and compared with those of the JCPDS software 13. They correspond to (111), (200), (220) and (311) crystallographic planes of the products and were specified as PbS. When NaOH concentration was increased to 1.25 M, a tubular cluster of nano-particles (Fig 4e) was in evidence. The cluster has the dark and light contrast bands showing that it is a tube with 220 nm outside diameter. Its external surface is not even showing that it composes of a number of nano-particles. The SAED pattern composes of (111), (200), (220), (311) and (222) planes and were specified as PbS as well.

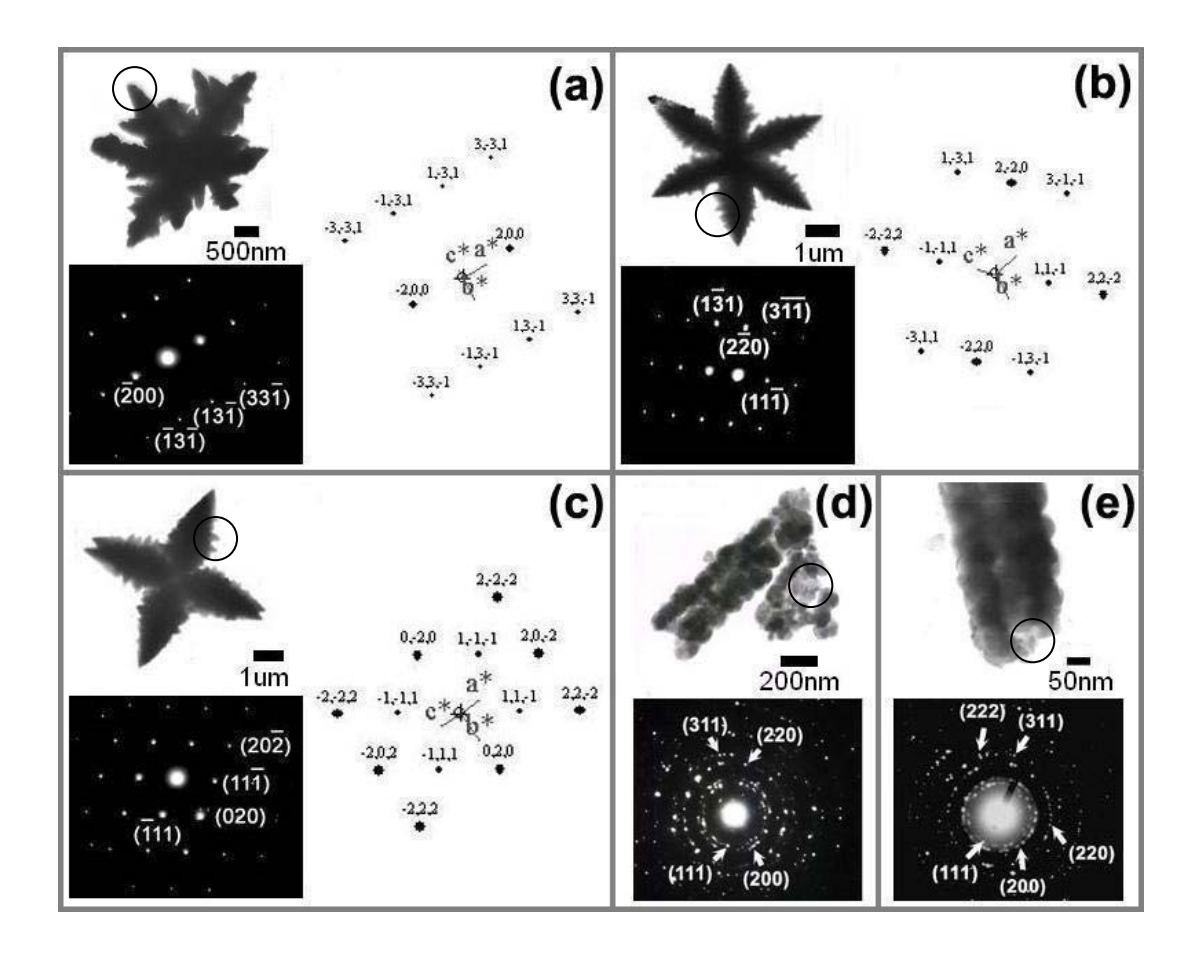


Fig 4. TEM images and SAED patterns of PbS synthesized in (a-c) NaOH-free solution containing 0.05 g CMC at 140, 180 and 200  $^{\circ}$ C, and (d, e) 1.00 M and 1.25 M NaOH solutions containing 0.05 g CMC at 140  $^{\circ}$ C, respectively. The corresponding simulated patterns are also shown in (a) – (c). The products marked with the circles on the corresponding images were used for SAED analysis.

SEM images or surface morphologies (Fig 5) show that the products were successfully synthesized in a variety of shapes and sizes which were influenced by CMC, NaOH and hydrothermal temperatures. At 140 °C, and in CMC and NaOH – free solution (Fig 5a), Pb(NO<sub>3</sub>)<sub>2</sub> reacted with thiosemicarbazide (NH<sub>2</sub>CSNHNH<sub>2</sub>) to produce PbS with submicro-sized particles in irregular clusters. When 0.05 g CMC was used in the process (NaOH-free solutions), Pb(NO<sub>3</sub>)<sub>2</sub> reacted with CMC to form

CMC-Pb<sup>2+</sup> solutions<sup>12</sup>. Following the addition of thiosemicarbazide in the CMC-Pb<sup>2+</sup> solution, H<sub>2</sub>S gradually evolved and further combined with lead ions to produce PbS. 12 CMC is rich in carboxylate groups which can play a key role in the formation of nanostructured flowers by coordinating with Pb<sup>2+</sup>. The process determined the nucleation sites and growth of the products<sup>12</sup>, composing of nanostructured flower (Fig 5b). It is more complete and becomes larger at 200 °C hydrothermal reaction (Fig 5c). The flower is made up of several petals. A distance between two apices of the two petals across the center of the flower is approximately 8.4 µm long. Each of the petals is composed of a number of small plates arranged in systematic order. For 0.05 g CMC, 0.5 M NaOH and 140 °C (Fig 5d), the product composes of nano-sized particles in clusters. When 1.00 M NaOH was used (Fig 5e), some clusters (marked with arrows) are similar to the tubes. The added NaOH coordinated with carboxylate groups which resulted to the decrease in the efficiency of CMC-Pb<sup>2+</sup> coordination. Nucleation and growth processes were changed. OH ions seemed to limit the growth of particles in all directions. The nano-particles were assembled in the perfectly tubular structure in 0.05 g CMC and 1.25 M NaOH solution (Fig 5f). The diameters of the tubes are 162-387 nm.

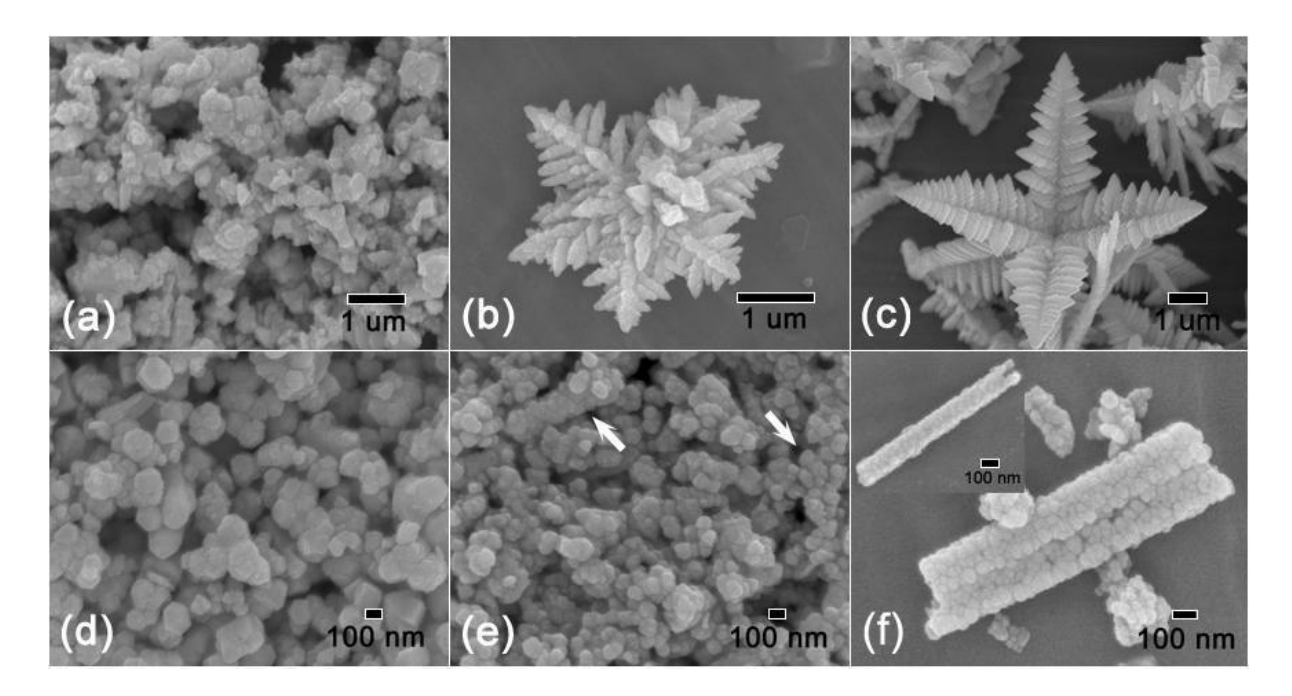


Fig 5. Surface morphologies of PbS synthesized using different conditions (0 or 0.05 g CMC / 0-1.25 M NaOH / 140 or 200 °C). (a) (0/0/140), (b) (0.05/0/140), (c) (0.05/0/200), (d) (0.05/0.5/140), (e) (0.05/1.00/140) and (f) (0.05/1.25/140).

Photoluminescence (PL) property of the products (Fig 6) was characterized using a 250 nm exciting wavelength. The maximum intensities were detected over the range 384-388 nm although their intensities are different. Their PL emission is in accord with other result.<sup>20</sup> Morphologies have the influence on the intensities, which were increased with the decreasing in the NaOH molarities (acidity increase). At a constant hydrothermal temperature and time, and different NaOH molarities, PL intensity of nanostructured flower (NaOH-free solution) is at the highest. In general, the intensities are also very sensitive to the number of electronic transfers and defects in the products.<sup>21</sup>

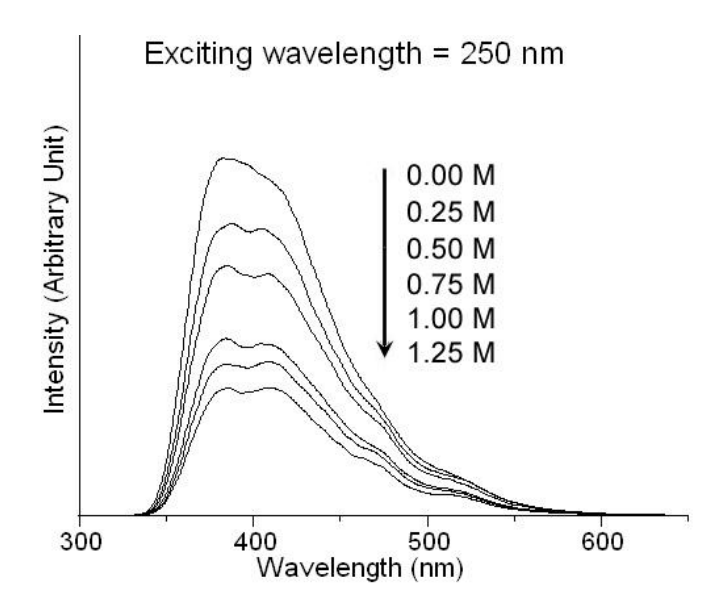


Fig 6. PL spectra of the products synthesized in the solutions containing 0.05 g CMC and different molarities of NaOH by 140 °C hydrothermal reaction for 12 h.

#### **Conclusions**

PbS with nano and microcrystals was successfully synthesized using hydrothermal reaction at different temperatures. Both CMC and NaOH can play the role in the reaction by producing a variety of product morphologies. XRD, SEM, EDX, TEM, SAED and Raman analyses revealed the presence of nano and micro-crystalline PbS (cubic) composing of Pb and S with the first and second overtone modes at 432 and 602 cm<sup>-1</sup>, respectively. The interpreted and simulated patterns are in good accordance. PL emission spectra of the products were detected at 384-388 nm, and PL intensity of the nanostructured flowers is the highest.

#### References

- 1. L. Xu, W. Zhang, Y. Ding, W. Yu, J. Xing, F. Li, Y. Qian, J. Cryst. Growth 273, 213 (2004).
- 2. Y.C. Zhang, T. Qiao, X.Y. Hu, G.Y. Wang, X. Wu, J. Cryst. Growth 277, 518 (2005).
- 3. S. Wang, A. Pan, H. Yin, Y. He, Y. Lei, Z. Xu, B. Zou, Mater. Lett. 60, 1242 (2006).
- 4. A.M. Qin, Y.P. Fang, W.X. Zhao, H.Q. Liu, C.Y. Su, J. Cryst. Growth 283, 230 (2005).
- 5. W. Zhang, Q. Yang, L. Xu, W. Yu, Y. Qian, Mater. Lett. 59, 3383 (2005).
- G. Zhou, M. Lü, Z. Xiu, S. Wang, H. Zhang, Y. Zhou, S. Wang, J. Phys. Chem. B 110, 6543 (2006).
- 7. L. Dong, Y. Chu, Y. Liu, M. Li, F. Yang, L. Li, J. Coll. Interf. Sci. 301, 503 (2006).
- 8. G.R. Deen, M. Hara, Polymer 46, 10883 (2005).
- 9. B. Minceva-Sukarova, M. Najdoski, I. Grozdanov, C.J. Chunnilall, J. Molec. Struct. 410-411, 267 (1997).
- 10. Y. Ni, X. Wei, J. Hong, X. Ma, Mater. Res. Bull. 42, 17 (2007).
- 11. S.M. Zhou, X.H. Zhang, X.M. Meng, X. Fan, S.T. Lee, S.K. Wu, J. Solid State Chem. 178, 399 (2005).
- 12. M. Wu, X. Pan, X. Qian, J. Yin, Z. Zhu, Inorg. Chem. Comm. 7, 359 (2004).
- 13. Powder Diffract. File, JCPDS Internat. Centre Diffract. Data, PA 19073-3273, U.S.A., (2001).
- 14. T. Thongtem, S. Thongtem, Ceram. Internat. 30, 1463 (2004).
- 15. G.D. Smith, S. Firth, R.J.H. Clark, M. Cardona, J. Appl. Phys. 92, 4375 (2002).
- 16. T. Thongtem, A. Phuruangrat, S. Thongtem, Mater. Lett. 61, 3235 (2007).

- 17. C. Boudias, D. Monceau, CaRlne Crystallography 3.1, 17 rue du Moulin du Roy, F-60300 Senlis, France, (1989-1998).
- 18. A. Phuruangrat, T. Thongtem, S. Thongtem, Mater. Lett 61, 3805 (2007).
- 19. T. Thongtem, S. Kaowphong, S. Thongtem, J. Mater. Sci. 42, 3923 (2007).
- 20. S. Ye, Y. Ye, Y. Ni, Z. Wu, J. Cryst. Growth 284, 172 (2005).
- 21. M. Alonso, E.J. Finn, Fundamental University Phys., Vol.3, Addison-Wesley Publ. Co., MA, (1968).

## Output ที่ได้จากโครงการวิจัย ฯ

- 1. เผยแพร่ผลงานวิจัยในวารสารต่าง ๆ จำนวน 7 เรื่อง ดังนี้ คือ
- [1] Titipun Thongtem\*, Anukorn Phuruangrat, Somchai Thongtem, Characterization of nano- and micro-crystalline CdS synthesized using cyclic microwave radiation, J. of Physics and Chemistry of Solids, 69 (2008) 1346-1349.(IF-2009 = 1.189)
- [2] Titipun Thongtem\*, Anukorn Phuruangrat, Somchai Thongtem, Formation of CuS with flower-like, hollow spherical, and tubular structures using the solvothermal-microwave process, Current Applied Physics, 9 (2009) 195-200. (IF-2009 = 1.586)
- [3] Titipun Thongtem\*, Sulawan Kaowphong, Somchai Thongtem, Influence of cetyltrimethylammonium bromide on the morphology of  $AWO_4$  (A = Ca, Sr) prepared by cyclic microwave irradiation, Applied Surface Science, 254 (2008) 7765-7769. (IF-2009 = 1.616)
- [4] Titipun Thongtem\*, Anukorn Phuruangrat, Somchai Thongtem, Characterization of  $MeWO_4$  (Me = Ba, Sr and Ca) nanocrystallines prepared by sonochemical method, Applied Surface Science, 254 (2008) 7581-7585. (IF-2009 = 1.616)
- [5] Anukorn Phuruangrat, Titipun Thongtem\*, Somchai Thongtem, Characterization of PbS with different morphologies produced using a cyclic microwave radiation, Applied Surface Science, 254 (2008) 7553-7558. (IF-2009 = 1.616)
- [6] Anukorn Phuruangrat\*, Titipun Thongtem\*, Somchai Thongtem, Preparation of ear-like, hexapod and dendritic PbS using cyclic microwave-assisted synthesis, Materials Letters, 63 (2009) 667-669. (IF-2009 = 1.94)
- [7] Titipun Thongtem\*, Sulawan Kaowphong, Somchai Thongtem, Carboxymethyl cellulose-assisted hydrothermal synthesis of PbS with nano- and micro-crystals, Journal of Nanoscience and Nanotechnology, 10 (2010) 2853-2857. (IF-2009 = 1.435)
  - 2. ผลิตดุษฎีบัณฑิตได้จำนวน 2 คน
  - ผลิตมหาบัณฑิตได้จำนวน 7 คน
  - 4. เสนอผลงานวิจัยในการประชุมต่าง ๆ ดังนี้ คือ

- Titipun Thongtem, Chalermchai Pilapong and Somchai Thongtem, Silica gel-assisted solvothermal production of CdS,  $Cu_xS$  (x=1,2) and ZnS with different morphologies, The 1<sup>st</sup> International Symposium on Hybrid Materials and Processing (HyMaP 2008), October 27-29, 2008, Grand Hotel, Busan, Korea, PA2-056.
- Titipun Thongtem, Sulawan Kaowphong and Somchai Thongtem, Carboxymethyl cellulose-assisted hydrothermal synthesis of PbS with nano and microcrystals, 2<sup>nd</sup> International Conference on Advanced Nano Materials (ANM 2008), June 22-25, 2008, Aveiro, Portugal, Abstract No. 41.
- Anukorn Phuruangrat, Titipun Thongtem and Somchai Thongtem, Effect of Cd and S sources on the aspect ratios of CdS synthesized by solvothermal reactions in mixed solvents, The 1<sup>st</sup> International Symposium on Hybrid Materials and Processing (HyMaP 2008), October 27-29, 2008, Grand Hotel, Busan, Korea, PD2-121.
- Titipun Thongtem, Anukorn Phuruangrat and Somchai Thongtem, Sonochemical synthesis of  $MMoO_4$  (M = Ca, Sr and Ba) nanocrystals, The  $9^{th}$  International Symposium on Ecomaterials Processing and Design, 7-9 Jan 2008, Changwon, Korea, B-P-012.
- Titipun Thongtem, Anukorn Phuruangrat and Somchai Thongtem, Synthesis of CaWO<sub>4</sub>, SrWO<sub>4</sub> and BaWO<sub>4</sub> with nanosized particles using a cyclic microwave radiation, The 9<sup>th</sup> International Symposium on Eco-materials Processing and Design, 7-9 Jan 2008, Changwon, Korea, B-P-013.
- Titipun Thongtem, Anukorn Phuruangrat and Somchai Thongtem, Characterization of CdS nanowires produced using solvothermal reactions, 2<sup>nd</sup> International Conference on Advanced Nano Materials (ANM 2008), June 22-25, 2008, Aveiro, Portugal, Abstract Nos. 40 and 308.
- Chalermchai Pilapong, Somchai Thongtem, Titipun Thongtem\*, Large-scale synthesis of CuS nano-hexaplate using the mixed solvent solvothermal method, The 3<sup>rd</sup> International Symposium on Functional Materials (ISFM2009), June 15-18, 2009, Jinju, Korea, T0096, p. 81.
- Titipun Thongtem, Anukorn Phuruangrat and Somchai Thongtem, Characterization of CdS nanorods produced using solvothermal reaction, 15<sup>th</sup> International Symposium on Intercalation Compounds, May 11-15, 2009, Tsinghua University, Beijing, China, P134.

- Anukorn Phuruangrat, Titipun Thongtem and Somchai Thongtem, Characterization of  $Bi_2S_3$  with different morphologies produced using a microwave radiation, The  $3^{rd}$  International Symposium on Functional Materials (ISFM2009), June 15-18, 2009, Jinju, Korea, T0081, p. 319.
- Chalermchai Pilapong, Titipun Thongtem and Somchai Thongtem, Fabrication of novel  $ZnS/ZnAl_2S_4$  nanocomposite using a facile solvothermal route, IEEE International NanoElectronics Conference (INEC) 2010, Jan. 3-8, 2010, City University of Hong Kong, China, FP239.
- Titipun Thongtem, Narongrit Tipcompor and Somchai Thongtem, Characterization of nanostrucured dendritic silver bismuth sulfide produced by solvothermal reactions, IEEE International NanoElectronics Conference (INEC) 2010, Jan. 3-8, 2010, City University of Hong Kong, China, FP459.
- Chalermchai Pilapong, Titipun Thongtem and Somchai Thongtem, Large-scale synthesis of  $Sb_2S_3$  spikes by hydrothermal reaction, IEEE International NanoElectronics Conference (INEC) 2010, Jan. 3-8, 2010, City University of Hong Kong, China, FP261.
- Titipun Thongtem, Siriprapha Jattukul and Somchai Thongtem, Characterization of nanostructured ZnO synthesized using sonochemical method, 11<sup>th</sup> International Symposium on Ecomaterials Processing & Design (ISEPD2010), Jan. 9-12, 2010, Osaka Prefecture University, Japan, C-P36.
- Somchai Thongtem, Kamonwan Aup-Ngoen and Titipun Thongtem, Bio-molecule and cyclic microwave radiation-assisted synthesis of Cu<sub>3</sub>BiS<sub>3</sub> nanostructured crystals, 11<sup>th</sup> International Symposium on Ecomaterials Processing & Design (ISEPD2010), Jan. 9-12, 2010, Osaka Prefecture University, Japan, C-P34.
- Somchai Thongtem, Prem Thongchai and Titipun Thongtem, Microwave-assisted synthesis of diamond-like carbon on glass substrates, 11<sup>th</sup> International Symposium on Ecomaterials Processing & Design (ISEPD2010), Jan. 9-12, 2010, Osaka Prefecture University, Japan, C-P53.
- Jutarat Kavinchan, Somchai Thongtem and Titipun Thongtem, Characterization of straw-tied-like architecture Sb<sub>2</sub>S<sub>3</sub> synthesized by a cyclic microwave radiation, 11<sup>th</sup> International Symposium on Ecomaterials Processing & Design (ISEPD2010), Jan. 9-12, 2010, Osaka Prefecture University, Japan, D-P22.

- Anukorn Phuruangrat\*, Titipun Thongtem, Pimsuda Pongphab, Somchai Thongtem, Solvothermal synthesized high aspect ratio of CdS nanowires and its optical properties, The 3<sup>rd</sup> International Symposium on Organic and Inorganic Electronic Materials and Related Nanotechnologies (EM-NANO 2010), June 22-25, 2010, Toyama International Conference Center, Toyama, Japan, P3-8.
- Wonchai Promnopas, Somchai Thongtem, Titipun Thongtem, Characterization of purified nanostructured ZnTe (cubic) synthesized by solid state microwave-plasma process, The 12<sup>th</sup> International Symposium on Eco-materials Processing and Design, January 8-11, 2011, The Empress Hotel, Chiang Mai, Thailand, P-A05.
- Hathai Sinim, Titipun Thongtem, Dong Jin Ham, Jae Sung Lee, Anukorn Phuruangrat, Somchai Thongtem, Facial hydrothermal synthesis of  $\mathbf{C}$ -MoO $_3$  nanobelts with free controlling morphology and its electrochemical for hydrogen evolution reaction and optical properties, The 12<sup>th</sup> International Symposium on Eco-materials Processing and Design, January 8-11, 2011, The Empress Hotel, Chiang Mai, Thailand, P-A23.
- Jirapong Arin, Titipun Thongtem, Anukorn Phuruangrat, Somchai Thongtem, Sonochemical synthesis and characterization of La-doped ZnO nanostructures, The 12<sup>th</sup> International Symposium on Eco-materials Processing and Design, January 8-11, 2011, The Empress Hotel, Chiang Mai, Thailand, P-A41.
- Oranuch Yayapao, Titipun Thongtem, Anukorn Phuruangrat, Somchai Thongtem, Hydrothermal synthesis of orthorhombic tungsten oxide microflowers using CTAB as a surfactant, The 12<sup>th</sup> International Symposium on Eco-materials Processing and Design, January 8-11, 2011, The Empress Hotel, Chiang Mai, Thailand, P-F05.
- Nuengruethai Ekthammathat, Titipun Thongtem, Anukorn Phuruangrat, Somchai Thongtem, Microwave-assisted synthesis of CePO<sub>4</sub> nonorods phosphor with violet emission, The 12<sup>th</sup> International Symposium on Eco-materials Processing and Design, January 8-11, 2011, The Empress Hotel, Chiang Mai, Thailand, P-F06.
- Chaned Wichasilp, Titipun Thongtem, Somchai Thongtem, Effect of p-type semiconductor polymer-composited electrolyte on the photovoltaic performance for using as solid-

state dye-sensitized solar cells, The 12<sup>th</sup> International Symposium on Eco-materials Processing and Design, January 8-11, 2011, The Empress Hotel, Chiang Mai, Thailand, P-G02.

- Surangkana Wannapop, Somchai Thongtem, Titipun Thongtem, Analysis of strontium tungstate nanofibers synthesized by electrospinning, The 12<sup>th</sup> International Symposium on Ecomaterials Processing and Design, January 8-11, 2011, The Empress Hotel, Chiang Mai, Thailand, P-J03.
- Yanee Keereeta, Titipun Thongtem, Somchai Thongtem, Characterization of zinc tungstate nanofibers synthesized by electrospinning, The 12<sup>th</sup> International Symposium on Ecomaterials Processing and Design, January 8-11, 2011, The Empress Hotel, Chiang Mai, Thailand, P-J04.
- Kamonwan Aup-Ngoen, Somchai Thongtem, Titipun Thongtem, Cyclic microwave-assisted synthesis and characterization of flower-like Cu<sub>3</sub>SbS<sub>4</sub>, The 12<sup>th</sup> International Symposium on Eco-materials Processing and Design, January 8-11, 2011, The Empress Hotel, Chiang Mai, Thailand, P-J05.
- Jarupat Sungpanich, Somchai Thongtem, Titipun Thongtem, Synthesis of tungsten trioxide polyvinyl alcohol nanofiber composites using a home-made electrospinning equipment, The 12<sup>th</sup> International Symposium on Eco-materials Processing and Design, January 8-11, 2011, The Empress Hotel, Chiang Mai, Thailand, P-J22.
  - ได้รับเชิญจาก ให้เป็น International Advisory Committee ในการประชุม 12<sup>th</sup> International Symposium on Eco-Materials Processing and Design (ISEPD 2011) 8 – 11 January 2011, Chiang Mai, Thailand
  - 6. ได้รับแต่งตั้งให้เป็นกรรมการบริหารหลักสูตรบัณฑิตศึกษา สาขาวิชาเคมี คณะวิทยาศาสตร์ มหาวิทยาลัยเชียงใหม่ ประจำปีการศึกษา 2551-2553
  - 7. ได้รับแต่งตั้งให้เป็นกรรมการประเมินการปฏิบัติงานของพนักงานมหาวิทยาลัย ตำแหน่งอาจารย์ จาก คณะวิทยาศาสตร์ มหาวิทยาลัยเชี่ยงใหม่
  - 8. ได้รับเชิญให้เป็น reviewer เพื่อตรวจสอบ manuscript ที่จะตีพิมพ์ใน Applied Surface Science, Materials Letters, Journal of Materials Processing Technology, Solid State Phenomena, Journal of Alloys and Compounds

- 9. ได้รับแต่งตั้งให้เป็นกรรมการและคณะทำงานจัดประชุมวิชาการระดับทวิภาคีระหว่างสหพันธ์ สาธารณรัฐเยอรมนีและประเทศไทย ด้านนาในวิทยาและนาในเทคในโลยี
- 10. ได้รับแต่งตั้งให้เป็นกรรมการบริหารโครงการศูนย์วิจัยนาโนวิทยาและนาโนเทคโนโลยีคณะ วิทยาศาสตร์ มหาวิทยาลัยเชียงใหม่ ประจำปี 2552-2553
- 11. การเชื่อมโยงทางวิชาการกับนักวิชาการอื่น ๆ ทั้งในและต่างประเทศ
  - Professor Dr. Masato Kakihana, Tohoku University, Japan
  - Professor Dr. Ken Kurosaki, Osaka University, Japan
  - Professor Dr. Jae Sung Lee, Pohang University of Science and Technology, Korea
  - Professor Dr. Dejian Zhou School of Chemistry and the Astbury Centre University of
  - ดร. อนุกร ภู่เรื่องรัตน์ คณะวิทยาศาสตร์ มหาวิทยาลัยสงขลานครินทร์
  - ผู้ช่วยศาสตราจารย์ ดร. ยุทธนา ตันติรุ่งโรจน์ชัย ศูนย์นาโนเทคโนโลยีแห่งชาติ สำนักงาน พัฒนาวิทยาศาสตร์และเทคโนโลยีแห่งชาติ
- 12. การเชื่อมโยงทางวิชาการกับนักวิชาการในสถาบันเดียวกัน
  - รองศาสตราจารย์ ดร. พิศิษฐ์ สิงห์ใจ ภาควิชาฟิสิกส์และวัสดุศาสตร์ คณะวิทยาศาสตร์ มหาวิทยาลัยเชียงใหม่
  - รองศาสตราจารย์ ดร. Yu Liandeng ภาควิชาฟิสิกส์และวัสดุศาสตร์ คณะวิทยาศาสตร์ มหาวิทยาลัยเชียงใหม่
- 13. รางวัลที่ได้รับ : ได้รับรางวัลชนะเลิศอันดับสองที่มีผลงานวิจัยตีพิมพ์ในวารสารที่มี impact factor จากคณะวิทยาศาสตร์ มหาวิทยาลัยเชียงใหม่ (ธันวาคม 2553)

ผลงานวิจัยที่เผยแพร่ในวารสารต่าง ๆ





Journal of Physics and Chemistry of Solids 69 (2008) 1346-1349

JOURNAL OF PHYSICS AND CHEMISTRY OF SOLIDS

www.elsevier.com/locate/jpcs

## Characterization of nano- and micro-crystalline CdS synthesized using cyclic microwave radiation

Titipun Thongtem<sup>a,\*</sup>, Anukorn Phuruangrat<sup>b</sup>, Somchai Thongtem<sup>b</sup>

<sup>a</sup>Department of Chemistry, Faculty of Science, Chiang Mai University, Chiang Mai 50200, Thailand <sup>b</sup>Department of Physics, Faculty of Science, Chiang Mai University, Chiang Mai 50200, Thailand

Received 27 June 2007; received in revised form 1 October 2007; accepted 30 October 2007

#### **Abstract**

Nano- and micro-crystalline CdS was synthesized from cadmium  $[CdCl_2 \cdot 2H_2O, Cd(NO_3)_2 \cdot 4H_2O, Cd(CH_3COO)_2 \cdot 2H_2O]$  and sulfur  $[CH_3CSNH_2, CH_5N_3S, CH_6N_4S]$  sources in ethylene glycol assisted by cyclic microwave radiation at different conditions. Phases (hcp and cubic) and morphologies (rose-shaped particles, spikes in cluster, cauliflowers, and nano-particles in cluster) were detected using XRD, SAED, TEM, and SEM, and influenced by Cd and S sources. The crystalline products are aligned in a systematic array and analyzed by HRTEM. A Raman spectrometer revealed the presence of fundamental and overtone modes at 298 and 597 cm<sup>-1</sup>, respectively. Exposure times and microwave powers also play a role in the crystallinity and size of the products. © 2007 Elsevier Ltd. All rights reserved.

Keywords: A. Nanostructures; B. Crystal growth; C. X-ray diffraction; D. Crystal structure

CdS is one of the II–VI compounds having unique properties [1]. It has promising applications for light-emitting diodes [2], solar cells [2], optoelectronics [3], catalysts [3], and others. There are different methods used to synthesize CdS such as solvothermal synthesis [2], hydrothermal process [3], and microwave irradiation [4]. Among the products with the same phase, different morphologies such as nanowires [2], nanorods [3], nanoparticles [4], flower-like particles [5], and hexagonal and triangular plates [6] were synthesized.

To synthesize CdS with different phases and morphologies,  $0.005\,\mathrm{mol}$  each of cadmium [CdCl<sub>2</sub>·2H<sub>2</sub>O, Cd(NO<sub>3</sub>)<sub>2</sub>·4H<sub>2</sub>O, Cd(CH<sub>3</sub>COO)<sub>2</sub>·2H<sub>2</sub>O] and sulfur [CH<sub>3</sub>CSNH<sub>2</sub>, CH<sub>5</sub>N<sub>3</sub>S, CH<sub>6</sub>N<sub>4</sub>S] sources were dissolved in 30 ml ethylene glycol. Each mixture was stirred for 30 min and left for the reaction to proceed by cyclic microwave radiation at different powers and exposure times. Each cycle was 100 s long, and composed of 30 and 70 s for the on and off periods, respectively.

The precipitates were washed with water and ethanol, dried at 80 °C for 24 h and further analyzed.

XRD spectra (Figs. 1 and 2) were compared with those of the JCPDS software (reference codes 06-0314 and 80-0019) [7]. The products synthesized using CdCl<sub>2</sub>·2H<sub>2</sub>O and CH<sub>3</sub>CSNH<sub>2</sub> at different exposure times and microwave powers (Fig. 1) were identified as CdS (hcp). The spectra are very sharp, showing that the products are composed of crystalline particles. The degree of crystallinity was increased on increasing the exposure time and microwave power. The effects of Cd and S sources on the phase were studied (Fig. 2). The products synthesized using CdCl<sub>2</sub>·2H<sub>2</sub>O and one of the sulfur sources [CH<sub>3</sub>CSNH<sub>2</sub>, CH<sub>5</sub>N<sub>3</sub>S, CH<sub>6</sub>N<sub>4</sub>S] are CdS (hcp). Those synthesized using Cd(NO<sub>3</sub>)<sub>2</sub>.4H<sub>2</sub>O or Cd(CH<sub>3</sub>COO)<sub>2</sub>.2H<sub>2</sub>O and CH<sub>3</sub>CSNH<sub>2</sub> are CdS (cubic). These show that Cd sources have an influence on the crystal structure. Two peaks at  $2\theta = 36.65^{\circ}$  and  $47.88^{\circ}$  are the characteristics of hcp phase [8]. They are diffracted from the (102) and (103) planes of the products. Other two peaks diffracting from the (002) and (110) planes of the hcp phase are almost at the same Bragg's angles as those diffracting from the (111) and (220) planes of the cubic phase, respectively. Their planar

<sup>\*</sup>Corresponding author. *E-mail addresses:* ttpthongtem@yahoo.com, ttpthongtem@hotmail.com (T. Thongtem).

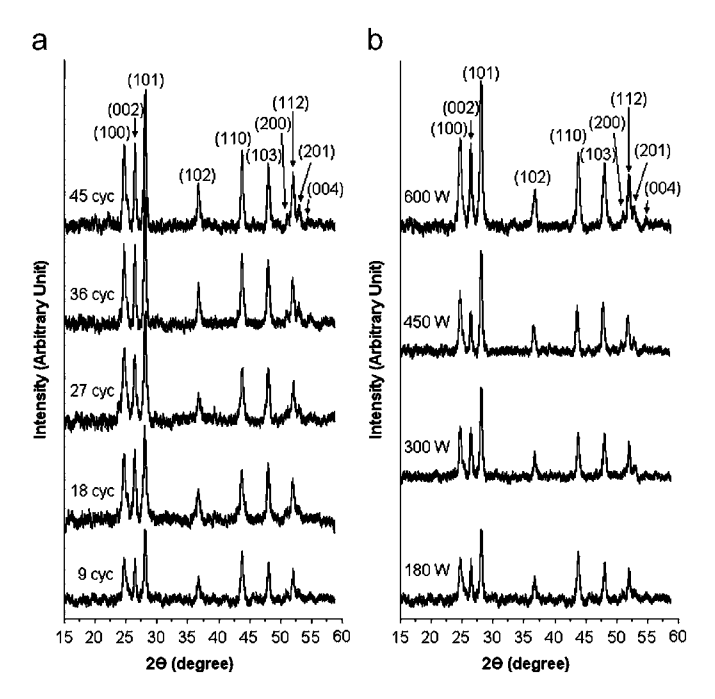


Fig. 1. XRD spectra of the products prepared using  $CdCl_2 \cdot 2H_2O$  and  $CH_3CSNH_2$  at (a) 180W for different cycles (cyc.) and (b) different microwave powers for nine cycles.

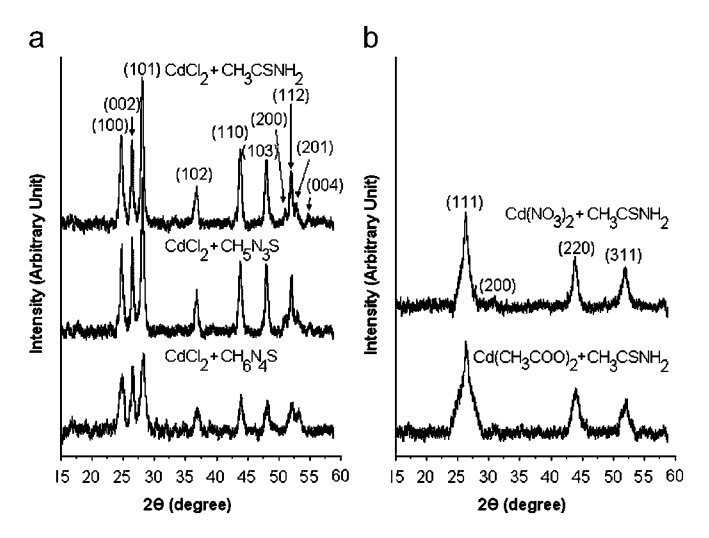


Fig. 2. XRD spectra of the products prepared using different Cd and S sources at 600 W for nine cycles. (a) and (b) are hcp and cubic phases, respectively.

spaces with the corresponding Bragg's angles are almost at the same values as well. XRD peaks of different structures are able to diffract from the same Bragg's angle, but the diffraction planes are different. Generally, CdS (hcp) is more thermodynamically stable than CdS (cubic) [9]. For the present research, no other characteristic peaks of impurity were detected, showing that the products (Figs. 1 and 2) are in pure phase.

The Raman spectra (Fig. 3) are almost identical to each other although the products have different phases (hcp and cubic). Two peaks were detected for both crystal structures.

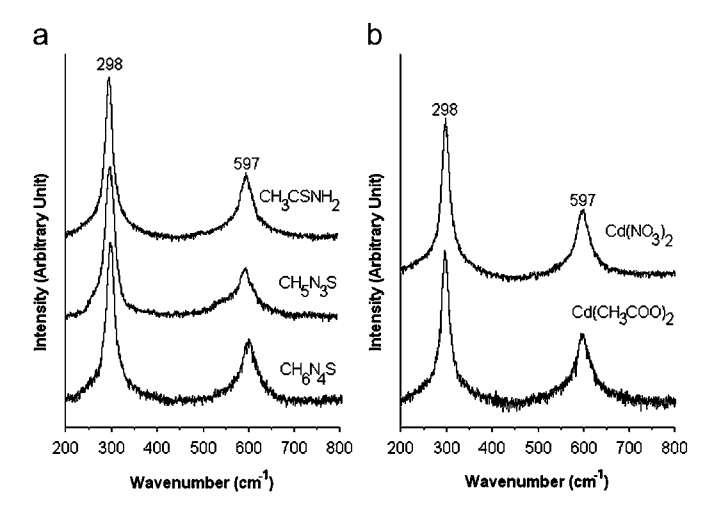


Fig. 3. Raman spectra of the products prepared at 600 W for nine cycles by using (a)  $CdCl_2 \cdot 2H_2O$  and one of the S sources  $[CH_3CSNH_2, CH_5N_3S, CH_6N_4S]$ , and (b) one of the Cd sources  $[Cd(NO_3)_2 \cdot 4H_2O, Cd(CH_3COO)_2 \cdot 2H_2O]$  and  $CH_3CSNH_2$ .

They are the first and second longitudinal optical (LO) phonon modes. The strong 1LO and weak 2LO correspond to the fundamental and overtone modes, respectively [10]. The vibrations of both phases, coinciding with each other [11], are at 298 and 597 cm<sup>-1</sup>, respectively. Some defects can play a role in the spectra as well.

SEM images (Fig. 4) show that the product morphologies are in the shapes of roses, spikes in cluster, and cauliflowers, respectively, using CH<sub>3</sub>CSNH<sub>2</sub>, CH<sub>5</sub>N<sub>3</sub>S, and CH<sub>6</sub>N<sub>4</sub>S as S sources, and CdCl<sub>2</sub>·2H<sub>2</sub>O as a Cd source, although they have the same hcp structure. The roses are composed of a number of nano-flakes in clusters, but the spikes and cauliflowers are fundamentally composed of round nano-particles. The spikes grew by a rapid assemblage of nano-particles in some specified directions, the cauliflowers by the assemblage of nano-particles in all directions at almost the same rates. These show that S sources dominated CdCl<sub>2</sub>·2H<sub>2</sub>O. Different product morphologies were influenced by S sources which have different structure formulas. Nucleation and growth of the particles can play roles in the morphologies. The crystal growth of some preferred structure or planes relates to the surface energy of the planes in the specified condition. The planes with lower surface energy dominate those with higher surface energy. This is described as a shape selective surface absorption process [12]. The amount of starting agents in the solution also has an influence on different orientations of the particles which reflects nucleation and growth of the crystals. The orientation was increased by increasing the amount of starting agents [13]. Apart from the above, crystal growth is influenced by the solubility of the precursors in the particular solvent and the synthesis temperature which have influences on the morphologies [12]. Polarities and boiling points of solvents [14], pH values of the solutions, and others can play a role on the shapes and sizes due to the different rates of nucleation and growth. The products with different morphologies were

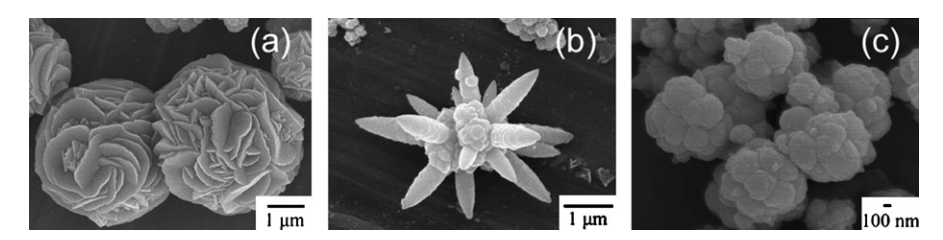


Fig. 4. SEM images of the products prepared using (a)  $CdCl_2 \cdot 2H_2O + CH_3CSNH_2$ , (b)  $CdCl_2 \cdot 2H_2O + CH_5N_3S$ , and (c)  $CdCl_2 \cdot 2H_2O + CH_6N_4S$  at 600 W for nine cycles.

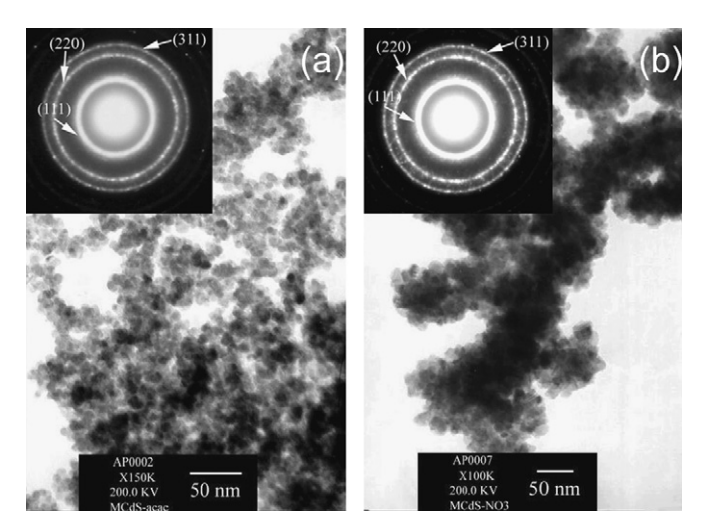


Fig. 5. TEM images and SAED patterns of the products prepared using (a) Cd(CH<sub>3</sub>COO)<sub>2</sub>  $\cdot$  2H<sub>2</sub>O + CH<sub>3</sub>CSNH<sub>2</sub> and (b) Cd(NO<sub>3</sub>)<sub>2</sub>  $\cdot$  4H<sub>2</sub>O + CH<sub>3</sub>CSNH<sub>2</sub> at 600 W for nine cycles.

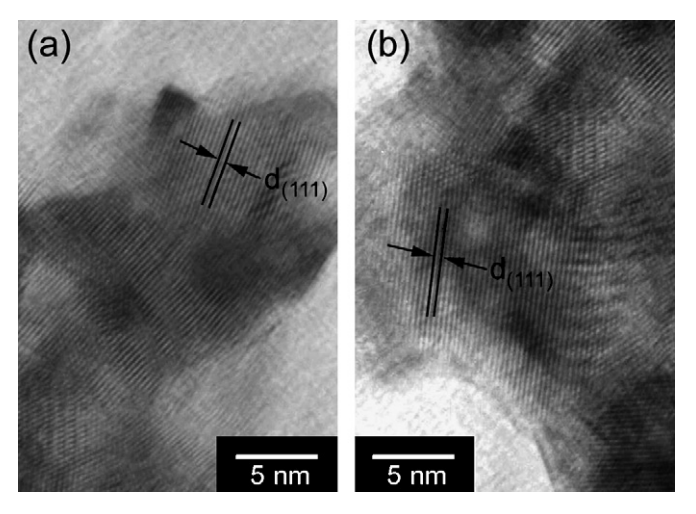


Fig. 6. Interplanar space  $(d_{111})$  of the products prepared using (a)  $Cd(CH_3COO)_2 \cdot 2H_2O + CH_3CSNH_2$  and (b)  $Cd(NO_3)_2 \cdot 4H_2O + CH_3CSNH_2$  at 600 W for nine cycles.

also produced when different Cd sources reacted with CH<sub>3</sub>CSNH<sub>2</sub>. TEM images (Fig. 5) show that the products are composed of a number of nano-particles clustered together at random. At present, nano-flakes and nano-particles are the fundamental particles of the products. The nano-flakes were formed by stacking hcp unit cells aside. There were some hcp unit cells stacked up as well, but its rate was slower. The nano-particles were formed by the assemblage of unit cells (hcp for the spikes and cauliflowers, cubic for nano-particles in clusters). Growth of the nano-particles in all directions are at the same rates. The fundamental particles may contain some defects, due to the microwave vibration frequency, internal stress, and others.

SAED patterns (Fig. 5) show bright concentric rings corresponding to the diffraction planes of the crystalline products. The rings are diffuse and hollow, showing that the products are composed of very fine particles. The values of interplanar spaces were calculated [15] using diameters of the diffraction rings measured from the patterns on the films, and compared with those of the JCPDS software [7]. The diffraction patterns correspond to CdS (cubic). HRTEM images (Fig. 6) show the (111) plane of CdS (cubic) which are aligned in a systematic array. There are several domains in the images. Each of them, belonging to a cluster of nano-particles, is composed

of a number of planes aligning in the same direction. By using XRD spectra in Fig. 2(b) and Bragg's law for diffraction, calculated interplanar spaces of (111) plane  $[0.3476\,\mathrm{nm}$  for  $Cd(CH_3COO)_2\cdot 2H_2O+CH_3CSNH_2$ , and  $0.3469\,\mathrm{nm}$  for  $Cd(NO_3)_2\cdot 4H_2O+CH_3CSNH_2]$  are very close to the corresponding values (0.3521 and 0.3424 nm) measured from Fig. 6.

For the present research, Cd and S sources have an influence on the nucleation and growth of the crystals. The phase with the lowest Gibbs free energy is thermodynamically stable, and has more chance to exist in the process [16]. These reflect the product morphologies. Apart from the above, crystal growth is influenced by the solubility of the precursors in the particular solvent and synthesis conditions which reflect the morphologies [12]. Higher microwave powers and exposure times also play a role in the product morphologies by enlarging the size of the roses synthesized using CdCl<sub>2</sub>·2H<sub>2</sub>O and CH<sub>3</sub>CSNH<sub>2</sub>. Microwave radiation is able to reduce time scales of the reactions, and can rapidly lead to very high temperatures which have the influence of accelerating the reaction process.

We would like to thank the Thailand Research Fund, Bangkok, Thailand, for funding the research.

- A.V. Murugan, R.S. Sonawane, B.B. Kale, S.K. Apte, A.V. Kulkarni, Microwave-solvothermal synthesis of nanocrystalline cadmium sulfide, Mater. Chem. Phys. 71 (2001) 98–102.
- [2] W. Qingqing, X. Gang, H. Gaorong, Solvothermal synthesis and characterization of uniform CdS nanowires in high yield, J. Solid State Chem. 178 (2005) 2680–2685.
- [3] Q. Zhao, L. Hou, R. Huang, S. Li, Surfactant-assisted growth and characterization of CdS nanorods, Inorg. Chem. Commun. 6 (2003) 1459–1462.
- [4] H. Yang, C. huang, X. Li, R. Shi, K. Zhang, Luminescent and photocatalytic properties of cadmium sulfide nanoparticles synthesized via microwave irradiation, Mater. Chem. Phys. 90 (2005) 155–158.
- [5] L. Wang, L. Chen, T. Luo, Y. Qian, A hydrothermal method to prepare the spherical ZnS and flower-like CdS microcrystallites, Mater. Lett. 60 (2006) 3627–3630.
- [6] T. Thongtem, A. Phuruangrat, S. Thongtem, Free surfactant synthesis of microcrystalline CdS by solvothermal reaction, Mater. Lett. 61 (2007) 3235–3238.
- [7] Powder Diffract. File, JCPDS Internat. Centre Diffract. Data, PA 19073-3273, USA, 2001.
- [8] V. Sivasubramanian, A.K. Arora, M. Premila, C.S. Sundar, V.S. Sastry, Optical properties of CdS nanoparticles upon annealing, Physica E 31 (2006) 93–98.

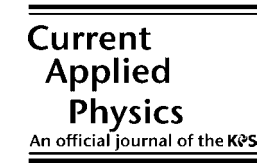
- [9] J. Lee, Raman scattering and photoluminescence analysis of B-doped CdS thin films, Thin Solid Films 451–452 (2004) 170–174.
- [10] C. Li, X. Yang, B. Yang, Y. Yan, Y. Qian, Growth of microtubular complexes as precursors to synthesize nanocrystalline ZnS and CdS, J. Cryst. Growth 291 (2006) 45–51.
- [11] O. Zelaya-Angel, F. de L. Castillo-Alvarado, J. Avendaño-López, A. Escamilla-Esquivel, G. Contreras-Puente, R. Lozada-Morales, G. Torres-Delgado, Raman studies in CdS thin films in the evolution from cubic to hexagonal phase, Solid State Commun. 104 (1997) 161–166.
- [12] S. Biswas, S. Kar, S. Chaudhuri, Growth of different morphological features of micro and nanocrystalline manganese sulfide via solvothermal process, J. Cryst. Growth 299 (2007) 94–102.
- [13] Y.C. Zhang, X.Y. Hu, T. Qiao, Shape-controlled synthesis of CuS nanocrystallites via a facile hydrothermal route, Solid State Commun. 132 (2004) 779–782.
- [14] J. Lu, Q. Han, X. Yang, L. Lu, X. Wang, Microwave-assisted synthesis and characterization of 3D flower-like Bi<sub>2</sub>S<sub>3</sub> superstructures, Mater. Lett. 61 (2007) 2883–2886.
- [15] T. Thongtem, S. Kaowphong, S. Thongtem, Malic acid complex method for preparation of LiNiVO $_4$  nano-crystallites, J. Mater. Sci. 42 (2007) 3923–3927.
- [16] K. Sopunna, T. Thongtem, M. McNallan, S. Thongtem, Formation of titanium nitride on γ-TiAl alloys by direct metal–gas reaction, J. Mater. Sci. 41 (2006) 4654–4662.



Available online at www.sciencedirect.com



Current Applied Physics 9 (2009) 195-200



www.elsevier.com/locate/cap www.kps.or.kr

# Formation of CuS with flower-like, hollow spherical, and tubular structures using the solvothermal-microwave process

Titipun Thongtem a,\*, Anukorn Phuruangrat b, Somchai Thongtem b

<sup>a</sup> Department of Chemistry, Faculty of Science, Chiang Mai University, Chiang Mai 50200, Thailand <sup>b</sup> Department of Physics, Faculty of Science, Chiang Mai University, Chiang Mai 50200, Thailand

Received 17 October 2007; received in revised form 17 January 2008; accepted 18 January 2008 Available online 2 February 2008

#### Abstract

 $\text{CuCl}_2 \cdot 2\text{H}_2\text{O}$  and  $\text{CH}_3\text{CSNH}_2$  were dissolved in ethylene glycol, and followed by the addition of NaOH to form solutions with different pH values. Reactions proceeded in surfactant-free solutions contained in an acid digestion bomb using a microwave irradiation at different conditions. Pure CuS (hcp) with flower-like, hollow spherical, and tubular structures were detected, and had the same vibration wavenumber at 474 cm<sup>-1</sup>. They displayed two emission peaks at 411, and 432 nm. The formation of CuS with different morphologies was proposed according to the analytical results. © 2008 Elsevier B.V. All rights reserved.

PACS: 81.07.-b

Keywords: Surfactant-free solutions; Solvothermal-microwave process; CuS; Flower-like structure; Hollow spheres; Tubular structure

### 1. Introduction

CuS with flower-like, hollow spherical, and tubular structures in nanometer and micrometer sizes is a very attractive material due to its specific structures and novel properties. It has a wide variety of applications, such as solar cells, superionic materials, and optical filters [1]. CuS was produced by different methods, such as spray pyrolysis [2], solvothermal process [3], sonochemistry [4], and microwave synthesis [5]. Surfactants, templates, and other additives were used to control the morphologies in most processes. For solution in a digestion bomb, microwave heating is a very attractive method due to focusing a large amount of energy into the chemicals under high pressure. The purpose of this research is to produce CuS with flower-like, hollow spherical, and tubular structures

in surfactant-free solutions with different pH values using the solvothermal-microwave process in an acid digestion bomb.

#### 2. Experiment

The 5 mmol each of  $CuCl_2 \cdot 2H_2O$  and  $CH_3CSNH_2$  was dissolved in 40 mL ethylene glycol. The pH was adjusted using NaOH. The solutions were stirred at ambient temperature. The reactions proceeded in an acid digestion bomb using 180 W cyclic microwave irradiation for 24 and 72 cycles (1200 and 3600 s). Each cycle was 50 s long. It was on for x s and off for 50 - x s. The irradiation percents for every cycle were 2x = 20%, 30%, 50%, and 60%. An increase in the irradiation percent of each cycle had an influence on the system by raising its temperature. The number of cycles is the time that the reaction proceeded in both the on and off states. At the conclusion of the test, the products were washed with water and ethanol, dried at 80 °C for 12 h, and intensively analyzed.

*E-mail addresses:* ttpthongtem@yahoo.com, ttpthongtem@hotmail.com (T. Thongtem).

<sup>\*</sup> Corresponding author.

#### 3. Results and discussion

To determine the phase of the products, their XRD spectra (Fig. 1) were compared with that of the JCPDS software (reference code: 78-0876) [6], and specified as CuS (hcp). No other characteristic peaks of impurities were detected although they were produced using different conditions. The degrees of crystallinity were increased with the increase in the irradiation percents of each cycle, and numbers of the heating cycles (Fig. 1a), identified by the narrower and higher peaks. When more energy was supplied to the system, atoms violently vibrated and aligned in a periodic array in the lattice. Different pH values (Fig. 1b) did not play a significant role in the diffraction peaks, and degree of crystallinity.

To produce CuS in an acid digestion bomb,  $CuCl_2 \cdot 2H_2O$  and  $CH_3CSNH_2$  were mixed in ethylene glycol and stirred at ambient temperature. The existence of precipitates (copper–thioacetamide complex) which were subsequently decomposed by the microwave irradiation [7], is shown

$$\begin{split} CuCl_2 + 2CH_3CSNH_2 &\overset{Ethylene\ glycol}{\to} [Cu(CH_3CSNH_2)_2]^{2+} + 2Cl^- \\ &[Cu(CH_3CSNH_2)_2]^{2+\ microwave irradiation} &\overset{CuS(black)}{\to} \end{split}$$

To show that copper–thioacetamide complex was definitely produced, FTIR spectra (Fig. 2) of CH<sub>3</sub>CSNH<sub>2</sub> and the precipitates (copper–thioacetamide complex, [Cu(CH<sub>3</sub>CSNH<sub>2</sub>)<sub>2</sub>]Cl<sub>2</sub>) were analyzed. For CH<sub>3</sub>CSNH<sub>2</sub>, C=S stretching vibrations were detected at 735 and 984 cm<sup>-1</sup>, and N-H stretching vibrations at 3178 and 3443 cm<sup>-1</sup>. Corresponding vibrations of the complex were at 710 and 978 cm<sup>-1</sup> for C=S stretching, and 3153 and

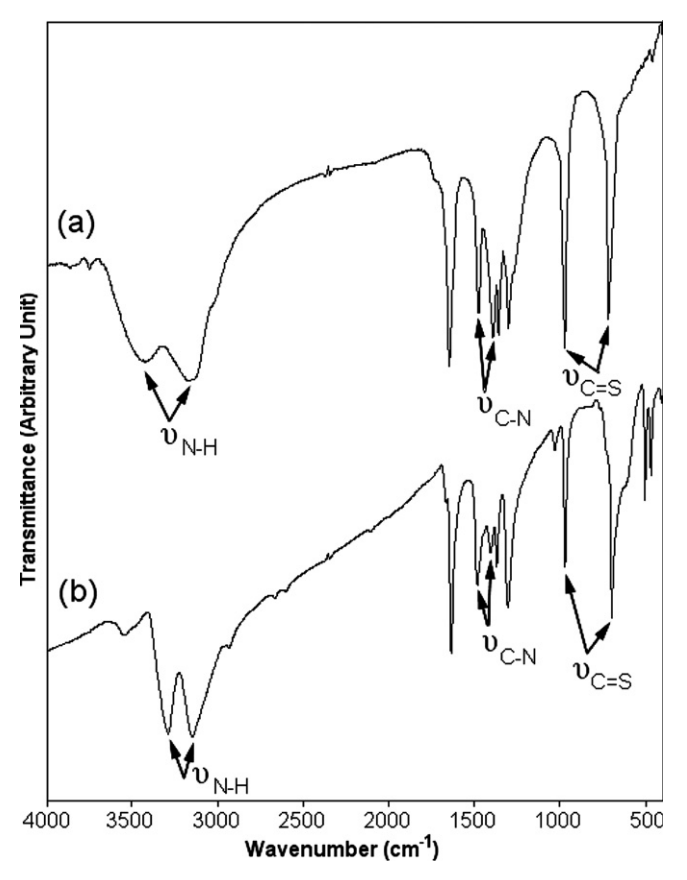


Fig. 2. FTIR spectra of (a) CH<sub>3</sub>CSNH<sub>2</sub> and (b) [Cu(CH<sub>3</sub>CSNH<sub>2</sub>)<sub>2</sub>]Cl<sub>2</sub>.

3305 cm<sup>-1</sup> for N–H stretching. The two C=S peaks of CH<sub>3</sub>CSNH<sub>2</sub> became weakened. The 710 cm<sup>-1</sup> C=S vibration tended to split into two peaks. Both C=S and N–H peaks shifted to the lower wavenumbers due to the reduc-

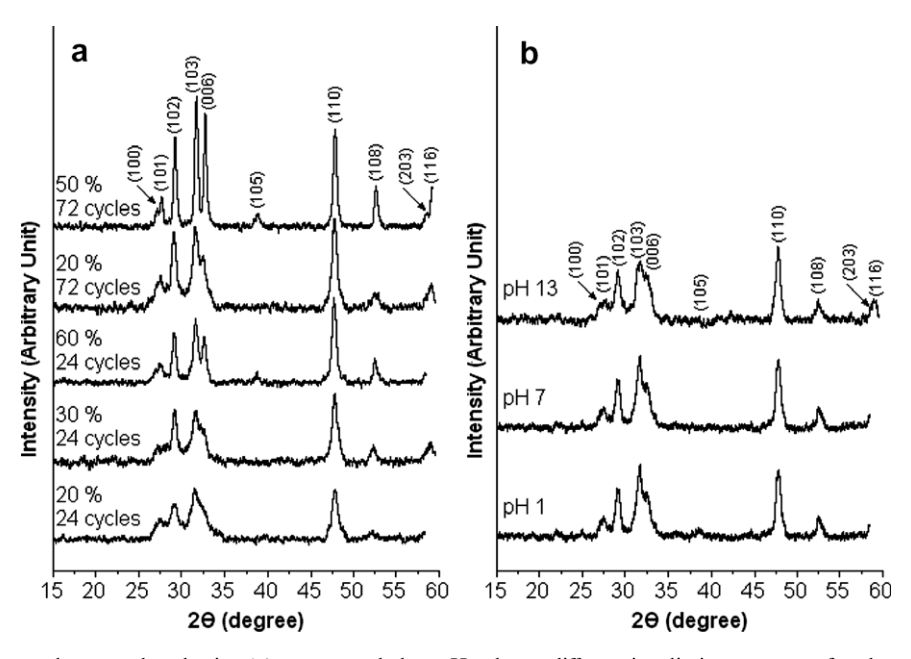


Fig. 1. XRD spectra of the products produced using (a) an extremely low pH value at different irradiation percents of each cycle and numbers of heating cycles, and (b) different pH values at 50% irradiation for 24 cycles.

tion in the vibration constants and bonding energies of C=S and N-H. These were caused by the reduction in the electronegativities of N and S atoms which were the result of the partial donation of lone pair electrons of N and S atoms to the vacant d orbital of Cu<sup>2+</sup> ions [8]. C-N peaks of CH<sub>3</sub>CSNH<sub>2</sub> and the complex were detected at the same wavenumbers [8] of 1411 and 1496 cm<sup>-1</sup>. The peaks remained stationary but became weakened and broadened, when they were in the complex. Changes in the nature of C=S, C-N, and N-H bonds are the evidence of the complex formation [8,9]. In addition, the complex was analyzed using CHON/S analyzer and AAS. It is composed of 27.01 wt% Cu, 14.28 wt% C, 3.04 wt% H, 22.29 wt% S, and 8.21 wt% N. For 100 wt% complex, mole ratios of Cu:C:H:S:N:Cl are 1.42:3.96:10.05:2.32:1.95:2.37, which are in accordance with its formula.

Alternatively,  $CH_3CSNH_2$  reacted with  $H_2O$  (crystal water in  $CuCl_2 \cdot 2H_2O$  and trace water in ethylene glycol) to form  $H_2S$  [10]. Subsequently,  $H_2S$  combined with  $CuCl_2$  to produce CuS. The reactions proceeded by the assistance of the microwave irradiation

After the starting agents were mixed and stirred, the solution has the characteristic of strong acid that the pH was extremely low (very close to zero). Once CuS nuclei formed in the digestion bomb by the assistance of the microwave irradiation, they were not fully developed (nascent). They grew very rapidly via the diffusion process. When NaOH was slowly added into the solutions, different pH values can play a role in the nucleation and growth processes.

At extremely low pH value, the morphologies (Fig. 3) were influenced by the irradiation percents and cycles. At 20% irradiation and 24 cycles (Fig. 3a), the product composed of a number of nano-plates in clusters shaped like flowers, and became larger when the irradiation time was prolonged to 72 cycles (Fig. 3b). Their particle-sized distributions will be discussed in more detail later in this section. To form plate-like particles, the stacking rate of hcp

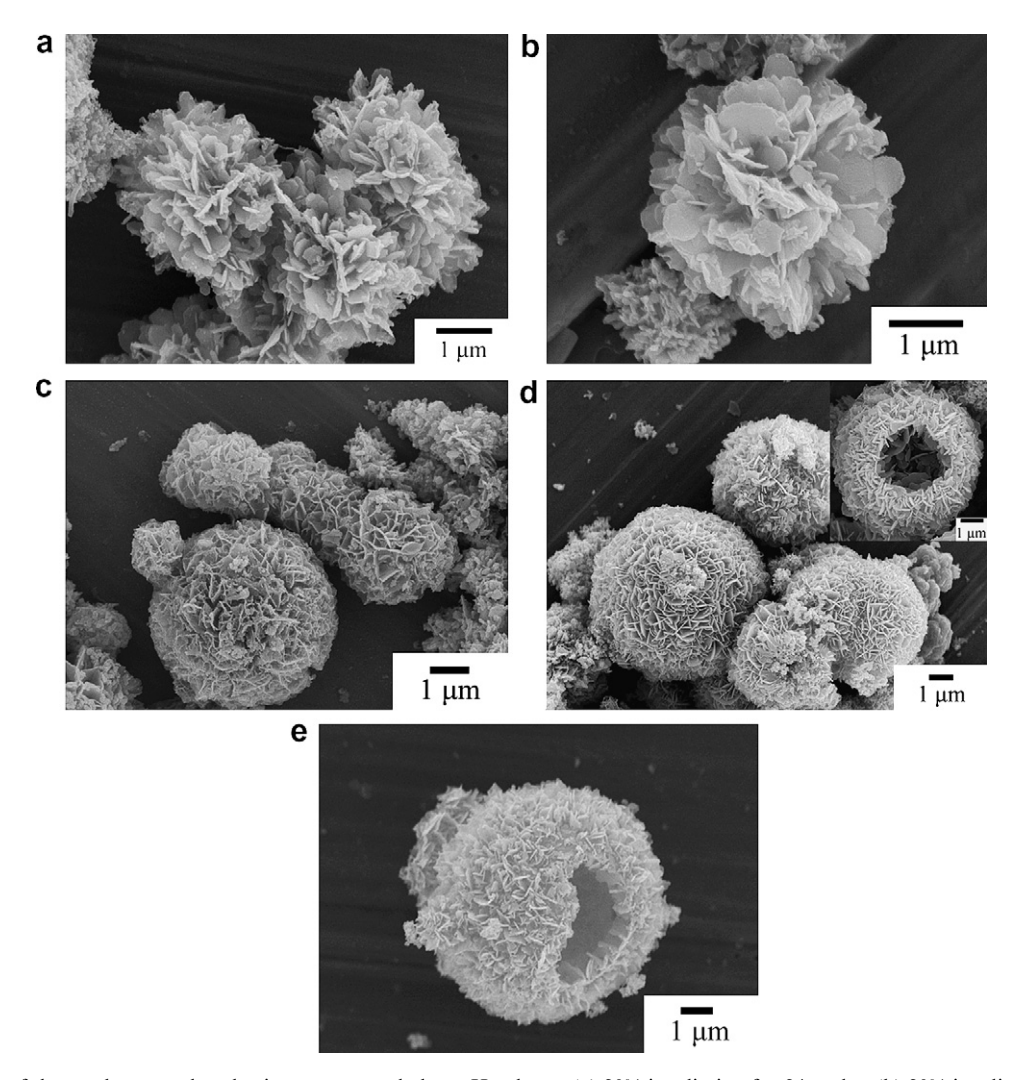


Fig. 3. SEM images of the products produced using an extremely low pH value at (a) 20% irradiation for 24 cycles, (b) 20% irradiation for 72 cycles, (c) 30% irradiation for 24 cycles, (d) 60% irradiation for 24 cycles, and (e) 50% irradiation for 72 cycles.

structure in the normal direction to the plates was the slowest. Plate-like formation and clustering simultaneously proceeded to produce flower-like products. At 30% and 60% irradiations for 24 cycles (Fig. 3c and d), and 50% irradiation for 72 cycles (Fig. 3e), the flowers are very similar to spheres. They were produced in different sizes showing that their initiation was different. There are more pores on the spheres at higher irradiation percents and cycles. Some spheres were broken. During processing, the irradiation percents of each cycle were long enough to heat up the products to be at higher temperatures. The spheres became larger due to the growth process. More gas was produced inside. There was some gas diffused out of the spheres as well. The evolution of the gas seems to be from the following. (1) Decomposition of ethylene glycol and acetamide (CH<sub>3</sub>(NH<sub>2</sub>)C=O). (2) Dehydration of ethylene glycol with acid served as a catalyst. Acetaldehyde developed [11], and further combined with oxygen to form CO<sub>2</sub> and water. When the pressure inside the spheres was high enough, fracture ultimately occurred and holes appeared. Some spheres were broken but some were not, depending on

the number of defects in their shells, initiation time, pressure inside the spheres and others. Both the irradiation percents and cycles can play important roles in the gas formation leading to the explosion process.

When NaOH was slowly added into the solutions (Fig. 4), the pH values slowly increased. At a pH of 1, 50% irradiation, and 24 cycles (Fig. 4a), the products were clusters of nano-sized particles. OH- ions seem to have the influence on their nucleation and growth. No flower-like product existed, but some plates were left in the solution. At higher pH values (Fig. 4b and c), more nano-sized and less plate-like particles existed. Simultaneously, the nano-sized particles began to assemble into a hollow object in the shape of a tube. The degree of roughness on the side walls is higher than that at the ends. At the present stage, there are a number of sites for OH<sup>-</sup> ions to adsorb on the outside walls. It implies that the concentration of OH<sup>-</sup> ions adsorbing on outside walls is the highest. OH<sup>-</sup> layer shields the tubular wall from the deposition of nano-sized particles. Therefore, clustering in the radial direction of the tubes is limited to some range. Growth pro-

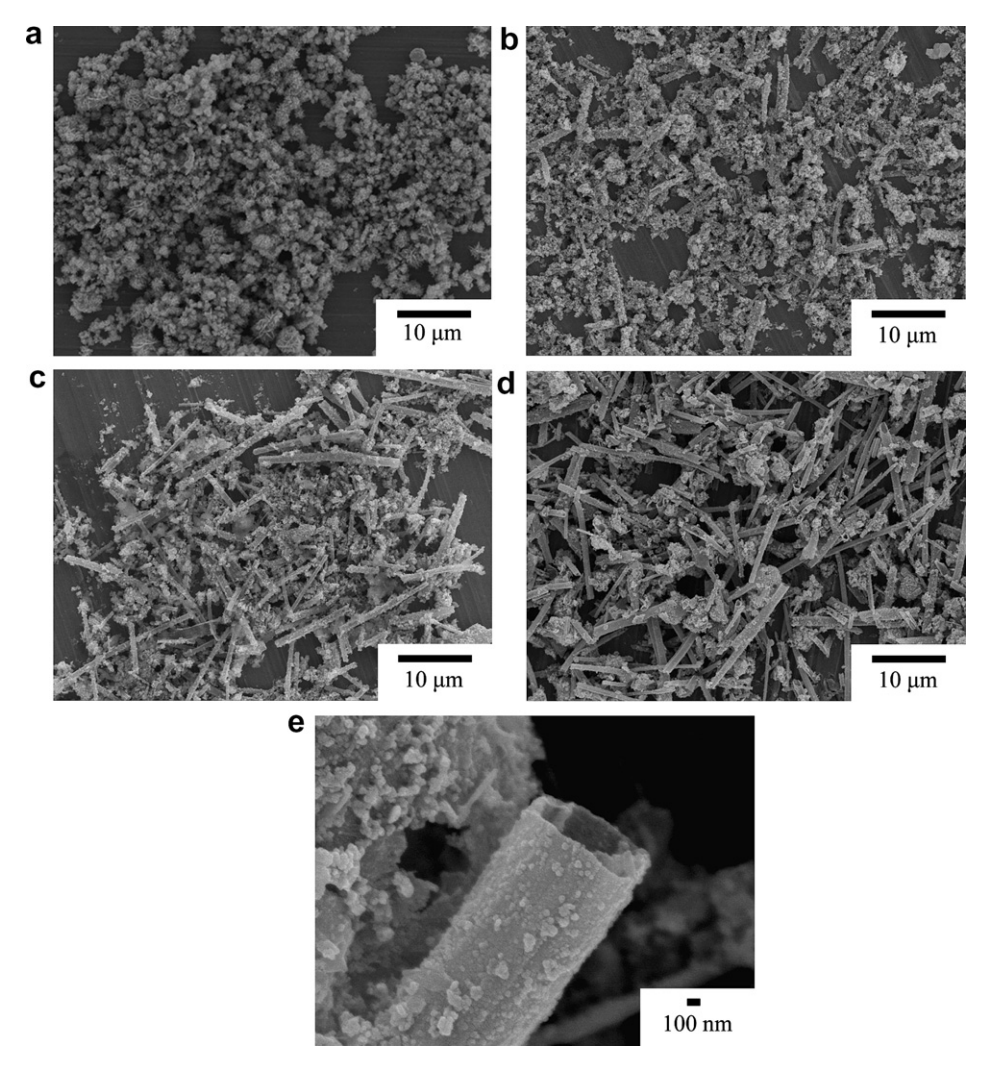


Fig. 4. SEM images of the products produced using a pH of (a-d) 1, 5, 9 and 13 at 50% irradiation for 24 cycles, respectively. [(e) is the enlarged image of (d).]

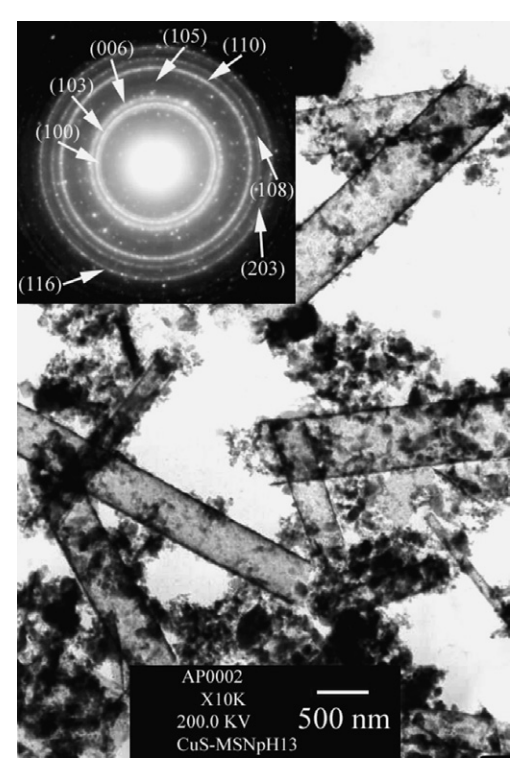


Fig. 5. TEM image and SAED pattern of the product produced using a pH of 13 at 50% irradiation for 24 cycles.

ceeded only in the axial direction. A number of the tubes were produced. They were increased with the increase in the pH values. At a pH of 13 (Fig. 4d), a great number of the tubes were detected. Its enlarged SEM image (Fig. 4e) shows the nano-size particles assembling as tubular structure.

TEM image (Fig. 5) shows different sizes of tubular structure composing of nano-sized particles. Some particles existed as clusters. The tubes are 82–574 nm in diameter, and are as long as 6420 nm (result not shown). Some irregular shapes and sizes of defects were detected on the tubular surfaces. SAED pattern (Fig. 5) shows eight concentric rings. They are diffuse showing that the tubes composed of nano-sized particles. Interplanar spaces were calculated [12,13] and compared with those of the JCPDS software

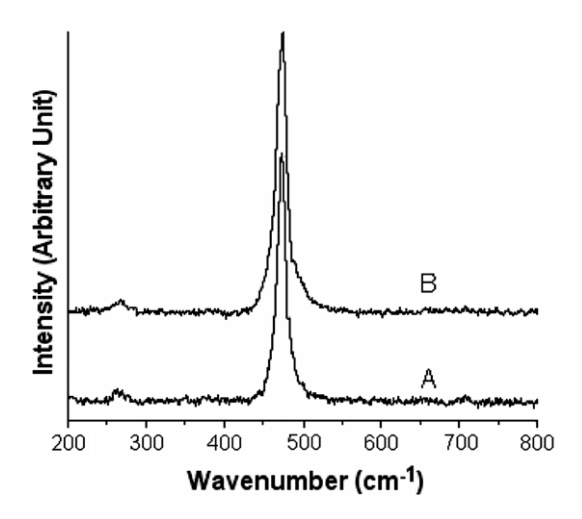


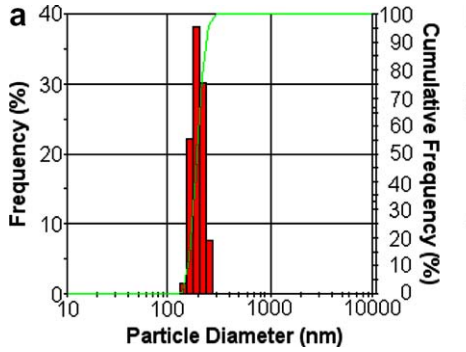
Fig. 7. Raman spectra of the products produced using (A) an extremely low pH value at 50% irradiation for 72 cycles, and (B) a pH of 13 at 50% irradiation for 24 cycles.

[6]. The rings correspond to (100), (103), (006), (105), (110), (108), (203), and (116) planes, and reveal the presence of CuS (hcp).

Particle-sized distributions of the flower-like products produced using an extremely low pH value at 20% irradiation for 24 and 72 cycles are shown in Fig. 6. The average sizes are  $198 \pm 32$  nm and  $775 \pm 167$  nm for 24 and 72 cycles, respectively. Size distributions of the flower-like particles are over the range 142–295 nm for 24 cycles, and 459– 1281 nm for 72 cycles. Numbers of the cycles can play a role in the range of size distributions. Cumulative frequency (S curve) shows that the particles were counted and arranged from the smallest value. It increased in a smooth monotone, showing that the particle-sized distribution shapes like a bell.

Raman spectra (Fig. 7) are very sharp, showing that the lattice atoms are aligned in the periodic array. Their vibrations are in the same wavenumbers at 474 cm<sup>-1</sup>, corresponding to lattice vibrations. The present results are in accordance with those of the CuS thin films [14].

Photoluminescent (PL) emission of CuS dispersed in absolute ethanol (0.2 mg/mL) was determined at ambient



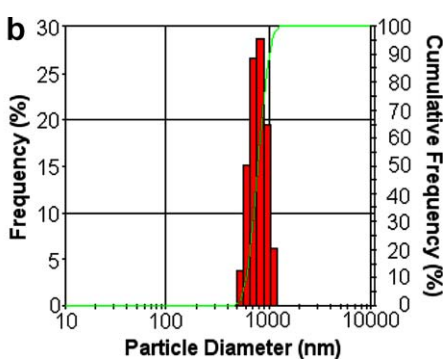


Fig. 6. Particle-sized distributions of the flower-like products produced using an extremely low pH value at 20% irradiation for (a) 24 cycles, and (b) 72 cycles.

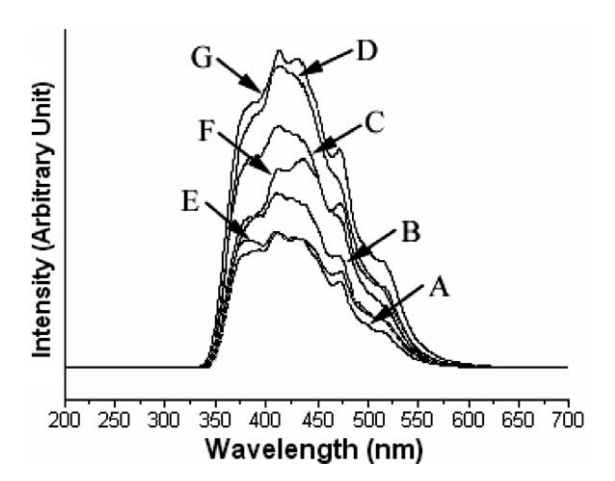


Fig. 8. PL emission of the products produced using (A–D) an extremely low pH value at 20% irradiation for 24 cycles, 60% irradiation for 24 cycles, 20% irradiation for 72 cycles, and 50% irradiation for 72 cycles, and (E–G) the pH of 1, 7 and 13 at 50% irradiation for 24 cycles, respectively.

temperature using an excitation wavelength of 202 nm, and is shown in Fig. 8. The spectra are broad and the two emission peaks are at 411 and 432 nm. The results are in accordance with the emission peaks of CuS at 414 and 437.5 nm [3]. Their intensities are influenced by several parameters such as shapes, sizes, and crystallinities, which were controlled by synthesis conditions. For an extremely low pH value (A-D), PL intensities were increased with the increase in the irradiation percents of each cycle and the numbers of heating cycles. The intensity was the highest at 50% irradiation, and 72 cycles (D). For the pH of 1, 7 and 13, at 50% irradiation for 24 cycles (E-G), PL intensities were increased with the increase in the pH values, until to the highest at the pH of 13 (G). For the present analysis, the tubular product (at the pH of 13, 50% irradiation, and 24 cycles) displayed the most efficient PL.

#### 4. Conclusions

CuS with flower-like, hollow spherical, and tubular structures was successfully produced by solvothermal-

microwave process at different conditions in an acid digestion bomb. CuS (hcp) was detected using XRD and SAED. Its Raman wavenumber is at 474 cm<sup>-1</sup>. Different morphologies were characterized using SEM and TEM, ranging from flower-like in a solution with extremely low pH to tubular in a pH of 13. PL emission peaks are at 411 and 432 nm. Their intensities are influenced by several parameters such as shapes, sizes, and crystallinities, controlled by synthesis conditions. The product with tubular structure exhibits the best PL efficiency. The formation of CuS with different morphologies was also proposed.

# Acknowledgement

This research was supported by the Thailand Research Fund, Bangkok, Thailand

- [1] Y. Ni, R. Liu, X. Cao, X. Wei, J. Hong, Mater. Lett. 61 (2007) 1986– 1989
- [2] J. Madarász, M. Okuya, S. Kaneko, J. Europ. Ceram. Soc. 21 (2001) 2113–2116
- [3] S. Ou, Q. Xie, D. Ma, J. Liang, X. Hu, W. Yu, Y. Qian, Mater. Chem. Phys. 94 (2005) 460–466.
- [4] J.Z. Xu, S. Xu, J. Geng, G.X. Li, J.J. Zhu, Ultrason. Sonochem. 13 (2006) 451–454.
- [5] X.H. Liao, J.J. Zhu, H.Y. Chen, Mater. Sci. Eng. B 85 (2001) 85–89.
- [6] Powder Diffract. File, JCPDS Internat. Centre Diffract. Data, PA 19073-3273, USA, 2001.
- [7] D. Chen, K. Tang, G. Shen, J. Sheng, Z. Fang, X. Liu, H. Zheng, Y. Qian, Mater. Chem. Phys. 82 (2003) 206–209.
- [8] J.Y. Gong, S.H. Yu, H.S. Qian, L.B. Luo, X.M. Liu, Chem. Mater. 18 (2006) 2012–2015.
- [9] T. Thongtem, A. Phuruangrat, S. Thongtem, J. Mater. Sci. 42 (2007) 9316–9323.
- [10] J. Zhu, M. Zhou, J. Xu, X. Liao, Mater. Lett. 47 (2001) 25-29.
- [11] W.B. Smith, Tetrahedron 58 (2002) 2091–2094.
- [12] T. Thongtem, A. Phuruangrat, S. Thongtem, Mater. Lett. 60 (2006) 3776–3781.
- [13] T. Thongtem, S. Kaowphong, S. Thongtem, J. Mater. Sci. 42 (2007) 3923–3927.
- [14] S.Y. Wang, W. Wang, Z.H. Lu, Mater. Sci. Eng. B 103 (2003) 184–188



Available online at www.sciencedirect.com





applied surface science

Applied Surface Science 254 (2008) 7765-7769

# Influence of cetyltrimethylammonium bromide on the morphology of $AWO_4$ (A = Ca, Sr) prepared by cyclic microwave irradiation

Titipun Thongtem a,\*, Sulawan Kaowphong b, Somchai Thongtem b

<sup>a</sup> Department of Chemistry, Faculty of Science, Chiang Mai University, Chiang Mai 50200, Thailand <sup>b</sup> Department of Physics, Faculty of Science, Chiang Mai University, Chiang Mai 50200, Thailand

Available online 14 February 2008

#### Abstract

AWO<sub>4</sub> (A = Ca, Sr) was prepared from metal salts  $[Ca(NO_3)_2 \cdot 4H_2O \text{ or } Sr(NO_3)_2]$ ,  $Na_2WO_4 \cdot 2H_2O$  and different moles of cetyltrimethy-lammonium bromide (CTAB) in water by cyclic microwave irradiation. The structure of AWO<sub>4</sub> was characterized by X-ray diffraction (XRD) and selected area electron diffraction (SAED). Transmission electron microscopy (TEM) and scanning electron microscopy (SEM) revealed the presence of nanoparticles in clusters with different morphologies; spheres, peaches with notches, dumb-bells and bundles, influenced by CTAB. Six Raman vibrational peaks of scheelite structure were detected at 908, 835, 793, 399, 332 and 210 cm<sup>-1</sup> for CaWO<sub>4</sub> and 917, 833, 795, 372, 336 and 192 cm<sup>-1</sup> for SrWO<sub>4</sub>, which are assigned as  $\nu_1(A_g)$ ,  $\nu_3(B_g)$ ,  $\nu_3(E_g)$ ,  $\nu_4(B_g)$ ,  $\nu_2(A_g)$  and  $\nu_{f.r.}(A_g)$ , respectively. Fourier transform infrared (FTIR) spectra provided the evidence of W–O stretching vibration in  $[WO_4]^2$  tetrahedrons at 793 cm<sup>-1</sup> for CaWO<sub>4</sub> and 807 cm<sup>-1</sup> for SrWO<sub>4</sub>. The peaks of photoluminescence (PL) spectra were at 428–434 nm for CaWO<sub>4</sub>, and 447–451 nm for SrWO<sub>4</sub>.

PACS: 81.07.-b

Keywords: Cyclic microwave irradiation; Nanostructured AWO<sub>4</sub> (A = Ca, Sr); Spheres; Peaches with notches; Dumb-bells; Bundles

#### 1. Introduction

Metal tungstates are classified into two groups with different crystal structures; scheelites (CaWO<sub>4</sub>, SrWO<sub>4</sub>, BaWO<sub>4</sub> and PbWO<sub>4</sub>) and wolframites (MgWO<sub>4</sub>, ZnWO<sub>4</sub>, CdWO<sub>4</sub>, etc.) [1]. Among the crystals with scheelite structures, CaWO<sub>4</sub> and SrWO<sub>4</sub> have attracted particular interest in a variety of studies such as stimulated Raman scattering technique [2], electro-optical property [3] and microwave application [4]. They were prepared by chemical bath deposition [5], Czochralski technique [6], solvothermal-mediated microemulsion method [7], metathetic reaction [8] and the evaporation of a polymer based metal-complex precursor solution [9]. In this study, the influence of CTAB on the morphologies of AWO<sub>4</sub> (A = Ca, Sr) prepared by cyclic microwave irradiation was demonstrated. The reaction proceeded in an open system at atmospheric pressure without any further requirement of calcination. The

# 2. Experiment

Different moles (M) of CTAB and 3 mM Na<sub>2</sub>WO<sub>4</sub>·2H<sub>2</sub>O were separately dissolved in 10 ml water and mixed. Subsequently, a solution of 3 mM Ca(NO<sub>3</sub>)<sub>2</sub>·4H<sub>2</sub>O or Sr(NO<sub>3</sub>)<sub>2</sub> in 10 ml water was put in the mixture. The reactions cyclically proceeded using 300 W microwave for 10 min to produce AWO<sub>4</sub> (A = Ca, Sr). One cycle of the microwave irradiation consists of 10 s irradiation and 20 s interval. The products were washed with water and 95% ethanol, and dried at 70 °C for 12 h.

### 3. Results and discussion

XRD spectra of CaWO<sub>4</sub> and SrWO<sub>4</sub> prepared with different moles of CTAB are shown in Fig. 1. The spectra were compared with those of the JCPDS software (reference codes: 77-2234 and 85-0587) [10], and specified as AWO<sub>4</sub> (A = Ca, Sr). They have scheelite tetragonal structure and  $I4_1/a$  space-group symmetry

process is very simple, attractive and novel by focusing large amount of microwave irradiation into the solutions to produce pure products.

<sup>\*</sup> Corresponding author. Tel.: +66 89 7565189; fax: +66 53 892277. *E-mail addresses:* ttpthongtem@yahoo.com, ttpthongtem@hotmail.com (T. Thongtem).

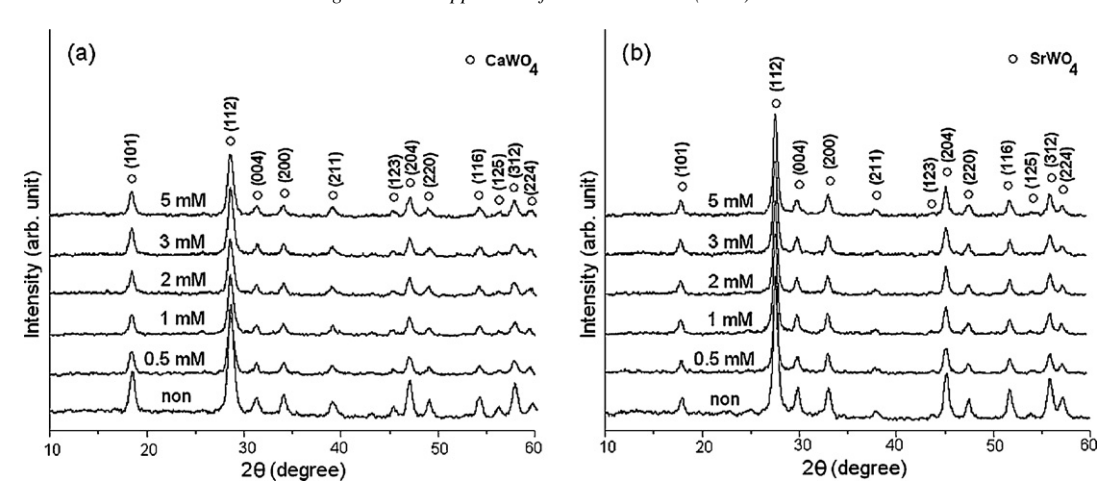


Fig. 1. XRD spectra of (a) CaWO<sub>4</sub> and (b) SrWO<sub>4</sub> prepared with different moles of CTAB.

[10]. Their strongest intensity peaks are at  $2\theta = 28.88^{\circ}$  and  $27.64^{\circ}$  for CaWO<sub>4</sub> and SrWO<sub>4</sub>, respectively, assigned to (1 1 2) plane. Calculated lattice parameters [11] for CaWO<sub>4</sub> ( $a = b = 0.5218 \pm 0.0013$  nm and  $c = 1.1316 \pm 0.0022$  nm) and SrWO<sub>4</sub> ( $a = b = 0.5417 \pm 0.0007$  nm and  $c = 1.1951 \pm 0.0000$  nm) are very close to those of the corresponding JCPDS software, and have the influence on their interplanar spaces. No other characteristic peaks of impurities were detected.

Vibrations of AWO<sub>4</sub> are classified into two types, the internal and external modes [6]. The first belongs to the vibration inside [WO<sub>4</sub>]<sup>2-</sup> molecular units of which the centers of mass are stationary. The second is called lattice phonon which corresponds to the motion of  $A^{2+}$  cations and the rigid molecular units. In free space,  $[WO_4]^{2-}$  tetrahedrons have  $T_d$  symmetry [6,12]. Their vibrations compose of four internal modes ( $\nu_1(A_1)$ ,  $\nu_2(E)$ ,  $\nu_3(F_2)$  and  $\nu_4(F_2)$ ), one free rotation mode ( $\nu_{\rm f.r.}(F_1)$ ), and one translation mode  $(F_2)$  [6]. In lattice space, the symmetry is reduced to  $S_4$ . All degenerative vibrations are split [6,12] due to the crystal field effect and Davydov splitting [6]. For tetragonal scheelite primitive cell (wavevector  $\mathbf{k} = \mathbf{0}$ ) [6,13], there are 26 different vibrations ( $\Gamma = 3A_g + 5A_u + 5B_g + 3B_u + 5E_g + 5E_u$ ) determined by group theory calculation [6,12]. Among them,  $3A_g$ ,  $5B_g$  and  $5E_g$  vibrations are Raman-active. Only  $4A_u$  and  $4E_u$ of the  $5A_u$  and  $5E_u$  vibrations are active in IR frequencies, and the others  $(1A_u \text{ and } 1E_u)$  are acoustic vibrations. The  $3B_u$  vibrations are silent modes [6,12].

For the present research, six different vibrations were detected on Raman spectra shown in Fig. 2a and b. Among them,  $\nu_1(A_g)$ ,  $\nu_3(B_g)$ ,  $\nu_3(E_g)$ ,  $\nu_4(B_g)$ ,  $\nu_2(A_g)$  and  $\nu_{f.r.}(A_g)$  are at 908, 835, 793, 399, 332 and 210 cm<sup>-1</sup> for CaWO<sub>4</sub>, and 917, 833, 795, 372, 336 and 192 cm<sup>-1</sup> for SrWO<sub>4</sub>, respectively. Each vibration mode is in accord with Raman vibrations analyzed by other researchers [12]. The spectra provide the evidence of scheelite structure for both products [12].

FTIR spectra shown in Fig. 2c and d were analyzed with a transmittance mode. For  $T_d$  symmetry,  $\nu_3(F_2)$  and  $\nu_4(F_2)$  are IR active and correspond to stretching and bending modes, respectively [14,15]. The spectra show a band of W–O stretching vibration in [WO<sub>4</sub>]<sup>2-</sup> tetrahedrons [3,14,15] at 793

and 807 cm $^{-1}$  for CaWO $_4$  and SrWO $_4$ , respectively. They are the internal modes specified as  $\nu_3(F_2)$  antisymmetric stretching vibrations [14,15]. Other weak W–O bending bands were detected at 438 and 410 cm $^{-1}$  for CaWO $_4$  and SrWO $_4$ , respectively. O–H stretching and bending vibrations of residual water in CaWO $_4$  were detected at 3435 and 1635 cm $^{-1}$ , and in SrWO $_4$  were at 3442 and 1637 cm $^{-1}$ , respectively.

Fig. 3 shows SEM images of CaWO<sub>4</sub> and SrWO<sub>4</sub> composing of microsized particles with different morphologies. For CaWO<sub>4</sub> in a CTAB-free solution, it composes of nano-scale particles clustering together in microspheres, shown in Fig. 3a. In the solution containing 0.5 mM CTAB, the spheres were cleft into two parts; peach-like particles with the notches, shown in Fig. 3b. Subsequently, the peach-like particles were transformed into dumb-bells (Fig. 3c) and bundles (Fig. 3d) in the solutions containing 2 and 5 mM CTAB, respectively. The CTAB (cationic surfactant) functioned as a template or shaped director. When Na<sub>2</sub>WO<sub>4</sub>·2H<sub>2</sub>O was mixed with CTAB, [WO<sub>4</sub>]<sup>2-</sup> and the cations formed complex molecules. Subsequently, Ca(NO<sub>3</sub>)<sub>2</sub>·4H<sub>2</sub>O was added in the mixture. The CTAB cations were replaced by Ca2+ ions to produce CaWO4 by a microwave irradiation. During the preparation, vibrating electric field of a microwave applied a force on electric charged particles. Vibrations of the reactants have the influence on the proceeded reaction effectively. Once the CaWO<sub>4</sub> nuclei (very fine particles) formed, their growth could relate to the interaction between oriented CTAB chains and the nuclei. A uniform and ordered long chain structured CTAB adsorbed on the nucleus surfaces which led to the nucleus growth along the longitudinal direction [16]. There was some growth in the normal direction as well, but its rate was the slowest. The influence of the shaped director was increased with the increase of the CTAB moles. The spherical particles in the CTAB-free solution were transformed step by step into bundles in the solution containing 5 mM CTAB. Some of the bundles were broken due to the microwave vibration frequency. For SrWO<sub>4</sub> in a CTAB-free solution, the products were the peach-like particles with the notches, as shown in Fig. 3e. When CTAB was added in the solution, the produced particles grew along the

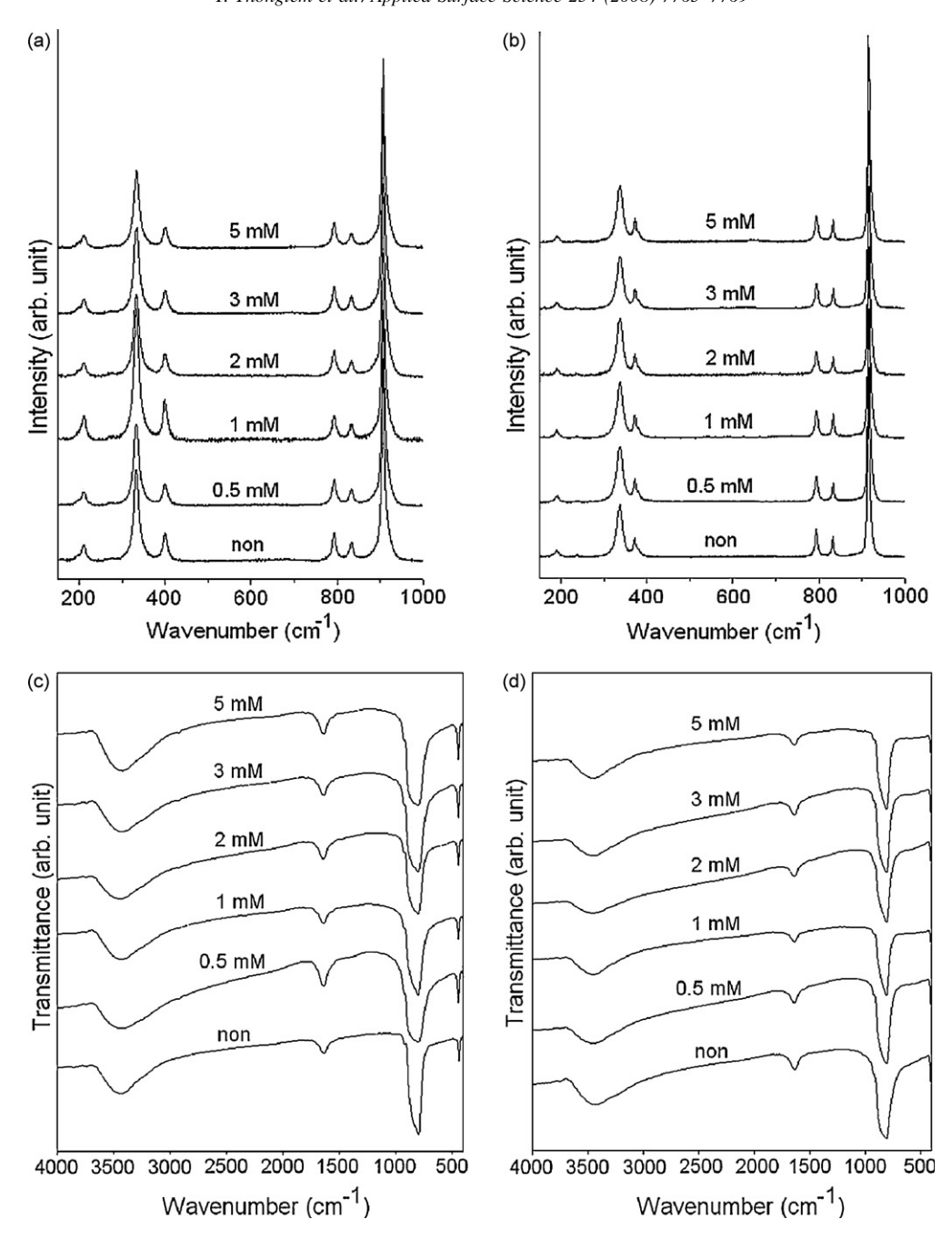


Fig. 2. Raman and FTIR spectra of (a, c) CaWO<sub>4</sub> and (b, d) SrWO<sub>4</sub> prepared with different moles of CTAB, respectively.

longitudinal direction. The products composed of a number of dumb-bells in the solutions containing 1 and 2 mM CTAB (Fig. 3f and g), and bundles in the 3 and 5 mM CTAB solutions (Fig. 3h and i). The cationic surfactant also had the same function as the above explanation.

The structures of the produced particles were also investigated with TEM and SAED. In Fig. 4, the TEM images show  $CaWO_4$  and  $SrWO_4$  the shape of dumb-bell prepared in the 3 and 1 mM CTAB solution (Fig. 4a and d), respectively. The interpretations of the SAED patterns at the markers in the corresponding TEM images are shown in Fig. 4b and e, respectively [11,17]. These patterns show that each of product

particles composes of single crystal. The calculated angles between any pair of the directions and the interplanar spaces determined from  $(h\,k\,l)$  are in accord with those of the diffraction patterns on their films. Calculated zone axes [11,17] are respectively in [0 4 1] and  $[\bar{4}\bar{3}\bar{2}]$  directions parallel or nearly parallel to the electron beams. The patterns for CaWO<sub>4</sub> and SrWO<sub>4</sub> were simulated [18] using the corresponding directions as zone axes and are shown in Fig. 4c and f, respectively. The patterns are symmetric and systematic, and are in good accord with those of the interpretations.

PL spectra with different excitation wavelengths of 280 nm for  $CaWO_4$  and 245 nm for  $SrWO_4$  are shown in Fig. 5. They

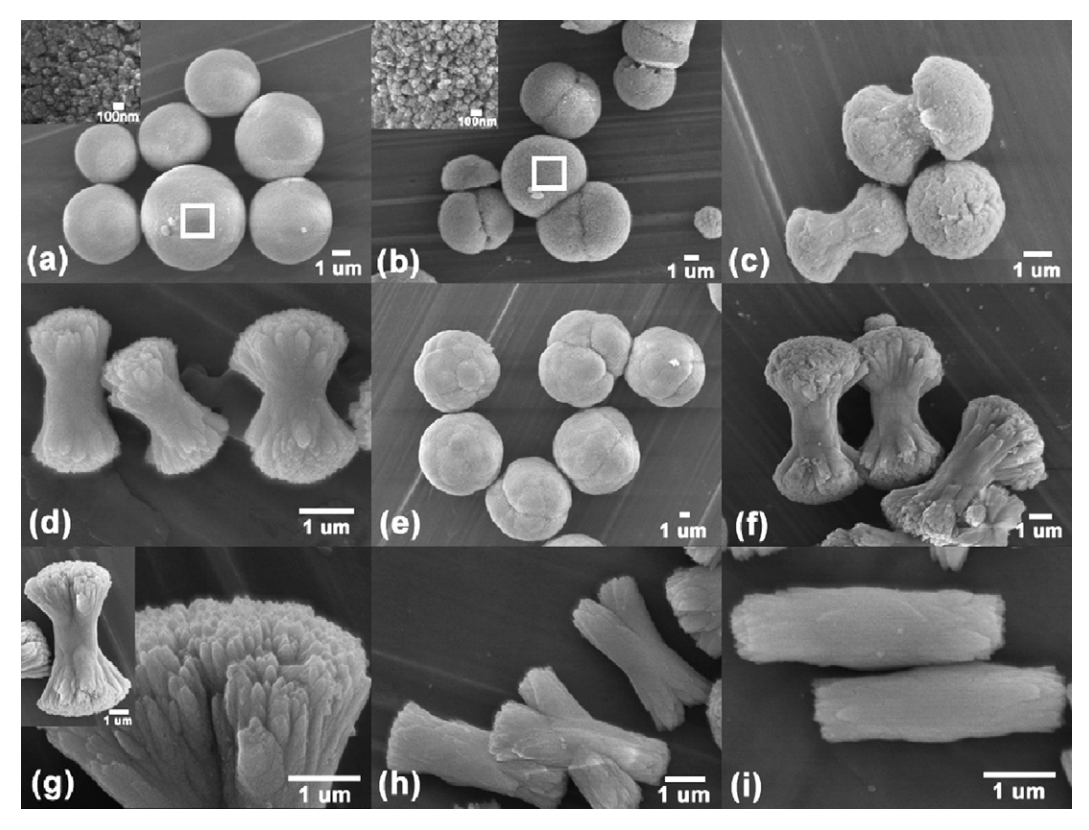


Fig. 3. SEM images of  $CaWO_4$  prepared in (a) the CTAB-free solution, and (b–d) the solutions of 0.5, 2 and 5 mM CTAB, and of  $SrWO_4$  prepared in (e) the CTAB-free solution, and (f–i) the solutions of 1, 2, 3 and 5 mM CTAB, respectively. The superimposed images at the upper lefts of the images (a) and (b) showed the closer view of the white rectangle areas of the corresponding images.

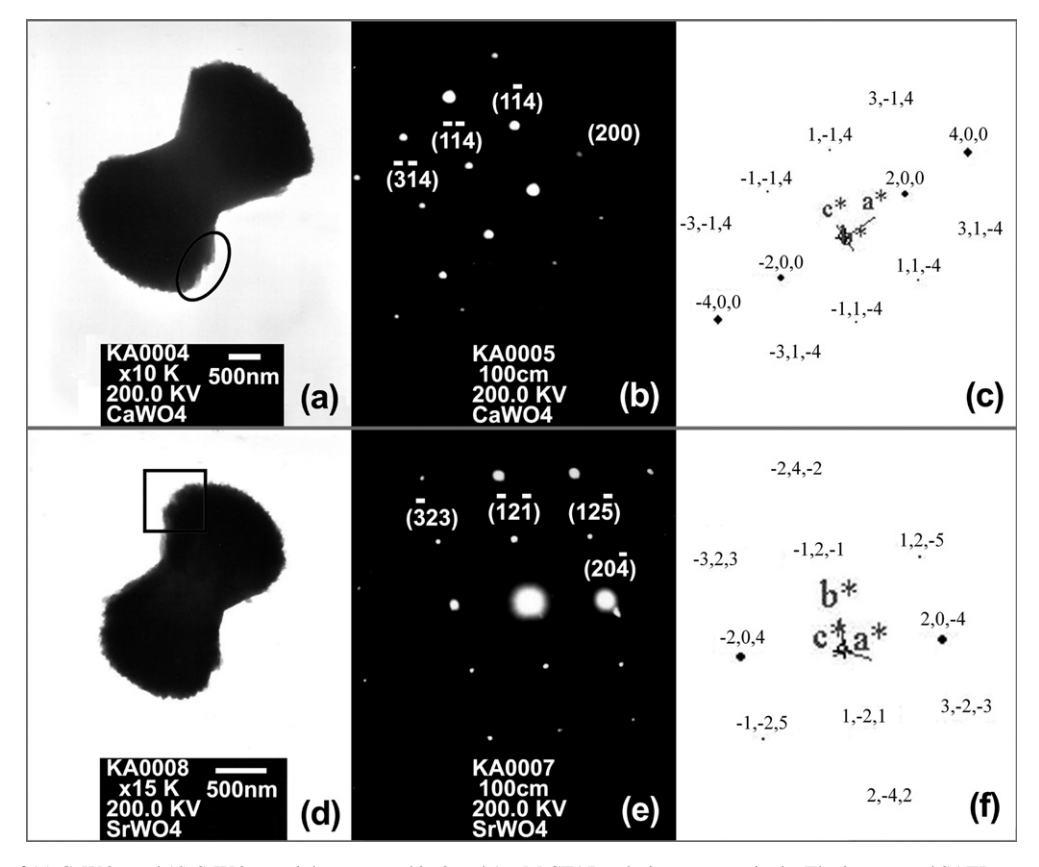


Fig. 4. TEM images of (a)  $CaWO_4$  and (d)  $SrWO_4$  particles prepared in 3 and 1 mM CTAB solutions, respectively. The interpreted SAED patterns were observed at the marked areas of ellipse (b) and square (e) in the TEM images. The schematic drawings of the corresponding SAED patterns are shown in (c) and (f).

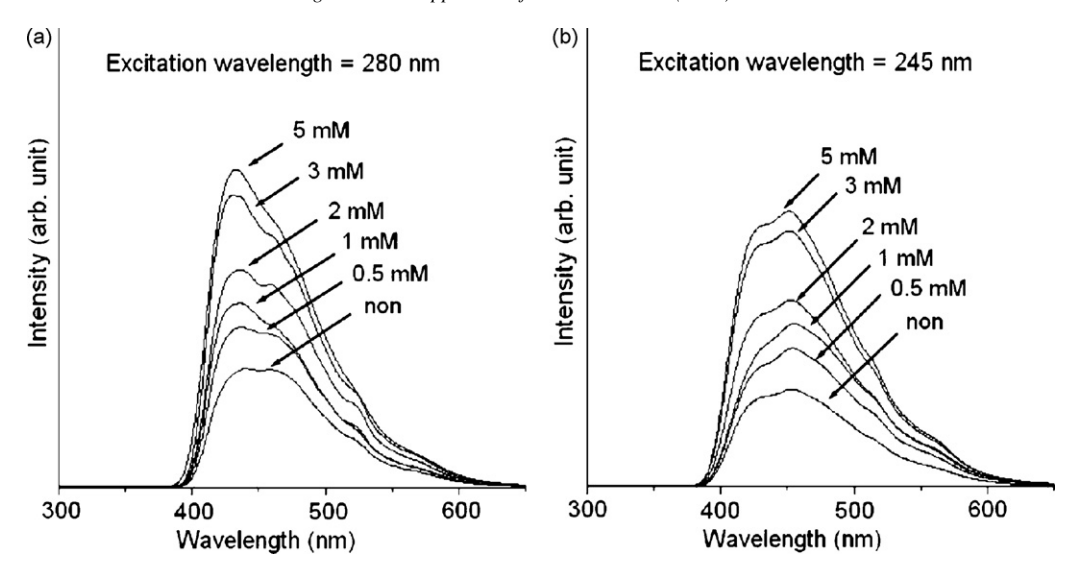


Fig. 5. PL spectra of (a) CaWO<sub>4</sub> and (b) SrWO<sub>4</sub> prepared with different moles of CTAB.

show the intrinsic peaks with their surrounding shoulders. The intrinsic peaks are considered to be from the  ${}^{1}T_{2} \rightarrow {}^{1}A_{1}$ transition of electrons within [WO<sub>4</sub>]<sup>2-</sup> anions [19–21], which can be treated as excitons [21]. The shoulders are from some defects and/or impurities, and interpreted as extrinsic transitions [21]. PL intensity is controlled by the number of charged transfers. For the present analysis, the emission peaks are in the spectral region at 428–434 nm for CaWO<sub>4</sub>, and 447–451 nm for SrWO<sub>4</sub>. For most PL studies, their blue emissions were at 440 nm for CaWO<sub>4</sub>, and 460 nm for SrWO<sub>4</sub> [5,22,23]. Comparing to the corresponding materials, the present emission peaks are blue-shift caused by the quantum-sized effect [24]. PL intensities are increased with the increase of the CTAB moles. They are the highest for the bundle-shaped CaWO<sub>4</sub> and SrWO<sub>4</sub> (5 mM CTAB solutions). Shape and size of the crystals can also play a role in their emission peaks.

#### 4. Conclusions

CaWO<sub>4</sub> and SrWO<sub>4</sub> were successfully synthesized with a cyclic microwave irradiation. The metal tungstates composed of nanosized particles in clusters with different shapes and sizes influenced by CTAB. They provided the evidence of scheelite structure with W–O stretching vibration in [WO<sub>4</sub>]<sup>2-</sup> tetrahedrons at 793 and 807 cm<sup>-1</sup> for CaWO<sub>4</sub> and SrWO<sub>4</sub>, respectively. The PL emission peaks are in the spectral region at 428–434 nm for CaWO<sub>4</sub>, and 447–451 nm for SrWO<sub>4</sub>.

# Acknowledgements

We are extremely grateful to the Thailand Research Fund, National Research Council of Thailand, and Institute for the Promotion of Teaching Science and Technology, Bangkok, Thailand, for funding the research.

- V.N. Kolobanov, I.A. Kamenskikh, V.V. Mikhailin, I.N. Shpinkov, D.A. Spassky, B.I. Zadneprovsky, L.I. Potkin, G. Zimmerer, Nuclear Instrum. Method Phys. Res. A 486 (2002) 496.
- [2] Z.C. Ling, H.R. Xia, D.G. Ran, F.Q. Liu, S.Q. Sun, J.D. Fan, H.J. Zhang, J.Y. Wang, L.L. Yu, Chem. Phys. Lett. 426 (2006) 85.
- [3] G. Zhang, R. Jia, Q. Wu, Mater. Sci. Eng. B 128 (2006) 254.
- [4] S.H. Yoon, D.W. Kim, S.Y. Cho, K.S. Hong, J. Eur. Ceram. Soc. 26 (2006) 2051
- [5] R. Zhai, H. Wang, H. Yan, M. Yoshimura, J. Cryst. Growth 289 (2006) 647.
- [6] T.T. Basiev, A.A. Sobol, Y.K. Voronko, P.G. Zverev, Opt. Mater. 15 (2000) 205
- [7] L. Sun, Q. Guo, X. Wu, S. Luo, W. Pan, K. Huang, J. Lu, L. Ren, M. Cao, C. Hu, J. Phys. Chem. C 111 (2007) 532.
- [8] V. Thangadurai, C. Knittlmayer, W. Weppner, Mater. Sci. Eng. B 106 (2004) 228.
- [9] A. Sen, P. Pramanik, J. Eur. Ceram. Soc. 21 (2001) 745.
- [10] Powder Diffract. File, JCPDS Internat. Centre Diffract. Data, PA 19073-3273, U.S.A., 2001.
- [11] T. Thongtem, A. Phuruangrat, S. Thongtem, Mater. Lett. 61 (2007) 3235.
- [12] S.P.S. Porto, J.F. Scott, Phys. Rev. 157 (1967) 716.
- [13] A. Golubović, R. Gajić, Z. Dohčević-Mitrović, S. Nikolić, J. Alloys Compd. 415 (2006) 16.
- [14] A.P. de Azevedo Marques, D.M.A. de Melo, C.A. Paskocimas, P.S. Pizani, M.R. Joya, E.R. Leite, E. Longo, J. Solid State Chem. 179 (2006) 671.
- [15] J.A. Gadsden, Infrar. Spectr. Miner. Related Inorg. Comp. Butterworths, 1975.
- [16] T. Saraidarov, R. Reisfeld, A. Sashchiuk, E. Lifshitz, Physica E 37 (2007) 173.
- [17] T. Thongtem, A. Phuruangrat, S. Thongtem, Mater. Lett. 62 (2008) 454.
- [18] C. Boudias, D. Monceau, CaRIne Crystallography 3.1, 17 rue du Moulin du Roy, F-60300 Senlis, France, 1989–1998.
- [19] Y. Zhang, N.A.W. Holzwarth, R.T. Williams, Phys. Rev. B 57 (1998) 12738.
- [20] M.J. Treadaway, R.C. Powell, J. Chem. Phys. 61 (1974) 4003.
- [21] V.B. Mikhailik, I.K. Bailiff, H. Kraus, P.A. Rodnyi, J. Ninkovic, Radiat. Measure. 38 (2004) 585.
- [22] Z. Lou, M. Cocivera, Mater. Res. Bull. 37 (2002) 1573.
- [23] W.S. Cho, M. Yashima, M. Kakihana, A. Kudo, T. Sakata, M. Yoshimura, Appl. Phys. Lett. 68 (1996) 137.
- [24] R. Jia, Q. Wu, G. Zhang, Y. Ding, J. Mater. Sci. 42 (2007) 4887.



Available online at www.sciencedirect.com





applied surface science

Applied Surface Science 254 (2008) 7581-7585

# Characterization of MeWO<sub>4</sub> (Me = Ba, Sr and Ca) nanocrystallines prepared by sonochemical method

Titipun Thongtem a,\*, Anukorn Phuruangrat b, Somchai Thongtem b

<sup>a</sup> Department of Chemistry, Faculty of Science, Chiang Mai University, Chiang Mai 50200, Thailand <sup>b</sup> Department of Physics, Faculty of Science, Chiang Mai University, Chiang Mai 50200, Thailand

Available online 2 February 2008

#### Abstract

Metal tungstates (MeWO<sub>4</sub>, Me = Ba, Sr and Ca) were successfully prepared using the corresponding Me(NO<sub>3</sub>)<sub>2</sub>·2H<sub>2</sub>O and Na<sub>2</sub>WO<sub>4</sub>·2H<sub>2</sub>O in ethylene glycol by the 5 h sonochemical process. The tungstate phases with scheelite structure were detected with X-ray diffraction (XRD) and selected area electron diffraction (SAED). Their calculated lattice parameters are in accord with those of the JCPDS cards. Transmission electron microscopy (TEM) revealed the presence of nanoparticles composing the products. Their average sizes are  $42.0 \pm 10.4$ ,  $18.5 \pm 5.1$  and  $13.1 \pm 3.3$  nm for Me = Ba, Sr and Ca, respectively. Interplanar spaces of the crystals were also characterized with high-resolution TEM (HRTEM). Their crystallographic planes are aligned in systematic array. Six different vibration wavenumbers were detected using Raman spectrometer and are specified as  $\nu_1(A_g)$ ,  $\nu_3(B_g)$ ,  $\nu_4(B_g)$ ,  $\nu_2(A_g)$  and free rotation. Fourier transform infrared (FTIR) spectra provided the evidence of scheelite structure with W–O anti-symmetric stretching vibration of  $[WO_4]^{2-}$  tetrahedrons at 786–883 cm<sup>-1</sup>. Photoluminescence emission of the products was detected over the range of 384–416 nm.

© 2008 Elsevier B.V. All rights reserved.

PACS: 81.16.Be

Keywords: Sonochemical method; BaWO<sub>4</sub>; SrWO<sub>4</sub>; CaWO<sub>4</sub>; Nanocrystallines

# 1. Introduction

Recently, the research on nanocrystallines has been increasingly progressive due to their novel properties. Among them, MeWO<sub>4</sub> (Me = Ba, Sr and Ca) with scheelite structure are such the materials [1,2]. There are W ions in tetrahedrons composing of O ions. Me ions are surrounded with eight O ions [3]. The properties of MeWO<sub>4</sub> nanocrystallines are influenced by the chemical composition, structure, phase and morphologies. The tungstates are very useful in a variety of applications, such as scintillators [2,3], stimulated Raman scattering [1], optoelectronic devices [4] and catalysts [5]. They were prepared by a variety of methods, such as a simple template-free precipitation technique [1], spray pyrolysis [2], microwave-assisted synthesis [5], chemical solution method [6], a

facile microemulsion-mediated hydrothermal process [7] and electrochemical method [8].

Currently, nano-structured materials have been found to exhibit anomalous properties which are totally different from their bulks [9]. The physical and chemical properties are influenced by the particle sizes, which were caused by quantum confinement effects [10]. For such the particles, percents of surface area per unit volume are very large. Their optical absorption wavelengths exhibited blue-shift comparing with the corresponding bulk materials [11]. Due to these favorable properties, the nanoparticles are being extensively studied for used in a variety of applications.

Sonochemical process has very attractive attention used for preparing materials. It can lead to more uniform distribution of nanoparticles, smaller sizes, slightly higher surface area and better thermal stability and phase purity than that achieved by the conventional method [12]. When ultrasonic radiation is supplied to chemical solutions, their molecules vibrate accordingly and heat develops. Vibration of molecules can solve the problems of concentration and temperature gradients.

<sup>\*</sup> Corresponding author. Tel.: +66 89 7565189; fax: +66 53 892 277. *E-mail addresses:* ttpthongtem@yahoo.com, ttpthongtem@hotmail.com (T. Thongtem).

The radiation has the influence on the reaction to proceed with efficiency and shorter time. Subsequently, pure products were produced.

Ethylene glycol (heat capacity at 25  $^{\circ}$ C = 150.4 J mol $^{-1}$  K $^{-1}$  [13]) is able to assist in forming the complex and stabilizing the nanoparticles. It promotes the particles to exist as non-cluster [14]. Temperature rising develops in ethylene glycol is two times slower than that in water (heat capacity at 25  $^{\circ}$ C = 75.4 J mol $^{-1}$  K $^{-1}$  [13]). Therefore, it is good choice for using ethylene glycol as the solvent for the synthesis of nanoparticles.

The purpose of the research is to prepare  $MeWO_4$  (Me = Ba, Sr and Ca) nanocrystallines with novel properties in ethylene glycol by the sonochemical method. The reaction proceeded in an open system at atmospheric pressure. No other additives were used. The process is very simple, attractive and novel for preparing pure products.

# 2. Experiment

Each of 5 mM Me(NO<sub>3</sub>)<sub>2</sub>·2H<sub>2</sub>O (Me = Ba, Sr and Ca) and Na<sub>2</sub>WO<sub>4</sub>·2H<sub>2</sub>O was dissolved in 30 ml ethylene glycol. The reactions proceeded for 5 h by the application of powerful ultrasonic radiation (35 kHz) on according to the following.

$$\begin{split} &\text{Me}(\text{NO}_3)_2 \cdot 2\text{H}_2\text{O} + \text{Na}_2\text{WO}_4 \cdot 2\text{H}_2\text{O} \underset{\text{sonochemical process}}{\overset{\text{ethylene glycol}}{\longrightarrow}} \text{MeWO}_4 \\ &+ 2\text{NaNO}_3 + 4\text{H}_2\text{O} \end{split}$$

The final products were washed with water and ethanol, dried at 70 °C for 12 h, and intensively characterized.

# 3. Results and discussion

Crystallographic planes on X-ray diffraction (XRD) spectra (Fig. 1) were indexed using Bragg's law for diffraction. The planes correspond to MeWO<sub>4</sub> (Me = Ba, Sr and Ca) (reference codes: 43–0646, 85–0587 and 41–1431) [15]. Their strongest intensity peaks diffracted from the same plane specified as (1 1 2). They have scheelite structure with tetragonal crystal system [1–3,6,16,17] and have I4<sub>1</sub>/a or C<sup>6</sup><sub>4h</sub> space-group symmetry [2,15,16]. Calculated lattice parameters [18] for BaWO<sub>4</sub> (a = b = 0.5618 nm, c = 1.2734 nm), SrWO<sub>4</sub> (a = b = 0.5415 nm, c = 1.1962 nm) and CaWO<sub>4</sub> (a = b = 0.5248 nm, c = 1.1394 nm) are very close to those of the corresponding JCPDS cards [15], and have the influence on the spaces between crystallographic planes. No other characteristic peaks of impurities were detected showing that the products are pure phase.

Raman vibrations of MeWO<sub>4</sub> are divided into two groups, the internal and external modes [19]. The internal mode is the W–O vibration within  $[WO_4]^{2-}$  tetrahedral units with immobile mass centers. The external one or lattice phonon corresponds to the vibration of  $Me^{2+}$  cations relative to the rigid tetrahedral units. In free space,  $[WO_4]^{2-}$  tetrahedrons have  $T_d$ -symmetry [17,19]. Their vibrations compose of four internal modes  $(\nu_1(A_1), \nu_2(E), \nu_3(F_2))$  and  $\nu_4(F_2)$ , one free rotation  $(\nu_{fr}(F_1))$  and one translation  $(F_2)$  [19]. In lattice space, they have

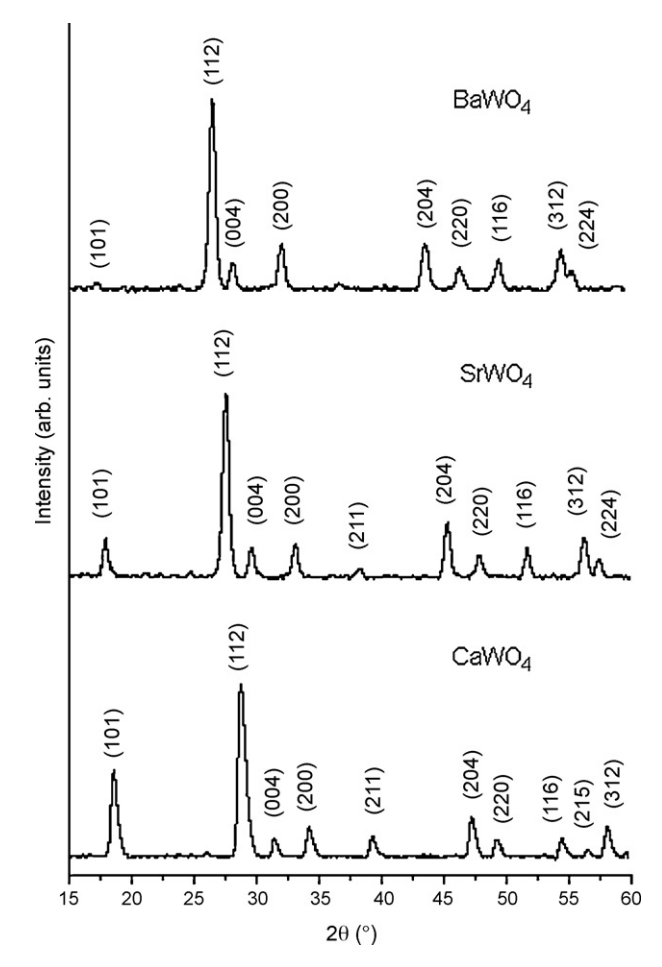


Fig. 1. XRD spectra of  $\rm BaWO_4, SrWO_4$  and  $\rm CaWO_4$  prepared by sonochemical method.

 $S_4$ -symmetry. All degenerative vibrations are split [17,19] due to the crystal field effect and Davydov splitting [19]. By using group-theory calculation, there are 26 different modes for tetragonal scheelite primitive cell (wavevector,  $\mathbf{k} = \mathbf{0}$ ), three for  $A_g$  and  $B_u$ , and five for  $A_u$ ,  $B_g$ ,  $E_g$  and  $E_u$  each [3,19]. All of  $A_g$ ,  $B_g$  and  $E_g$  modes are Raman-active. Only four of five  $A_u$  and  $E_u$  modes are active in IR range. Their remains are acoustic vibrations. Three vibrations of  $B_u$  are silent modes [3,19].

Six different modes ( $\nu_1(A_g)$ ,  $\nu_3(B_g)$ ,  $\nu_3(E_g)$ ,  $\nu_4(B_g)$ ,  $\nu_2(A_g)$ and free rotation) were detected on Raman spectra (Fig. 2a) at 921, 826, 791, 345, 332 and 191 cm<sup>-1</sup> for BaWO<sub>4</sub>, 922, 838, 799, 372, 337 and 190 cm $^{-1}$  for SrWO<sub>4</sub> and 913, 838, 798, 401, 337 and 211 cm<sup>-1</sup> for CaWO<sub>4</sub> respectively. Each of the modes is in accord with Raman vibrations analyzed by other researchers [17,19]. The spectra of the three products provide the evidence of scheelite structure [17,19]. Comparing to Ar laser ( $\lambda = 514.5$  nm), a great deal of energy was lost during the inelastic scattering process. In addition, Fourier transform infrared (FTIR) spectra (Fig. 2b) were analyzed using a transmittance mode. For T<sub>d</sub>-symmetry, vibration frequencies of  $[WO_4]^{2-}$  tetrahedrons are  $\nu_1(A_1)$ ,  $\nu_2(E)$ ,  $\nu_3(F_2)$  and  $\nu_4(F_2)$  [20]. In lattice space, their site symmetries become S<sub>4</sub>. The correlation of the two point groups  $(T_d \to S_4)$  is as follows:  $A_1 \rightarrow A, E \rightarrow A + B$  and  $F_2 \rightarrow B + E$ . Only bands corresponding to  $v_2$ ,  $v_3$  and  $v_4$  were detected [20]. Main transmittance

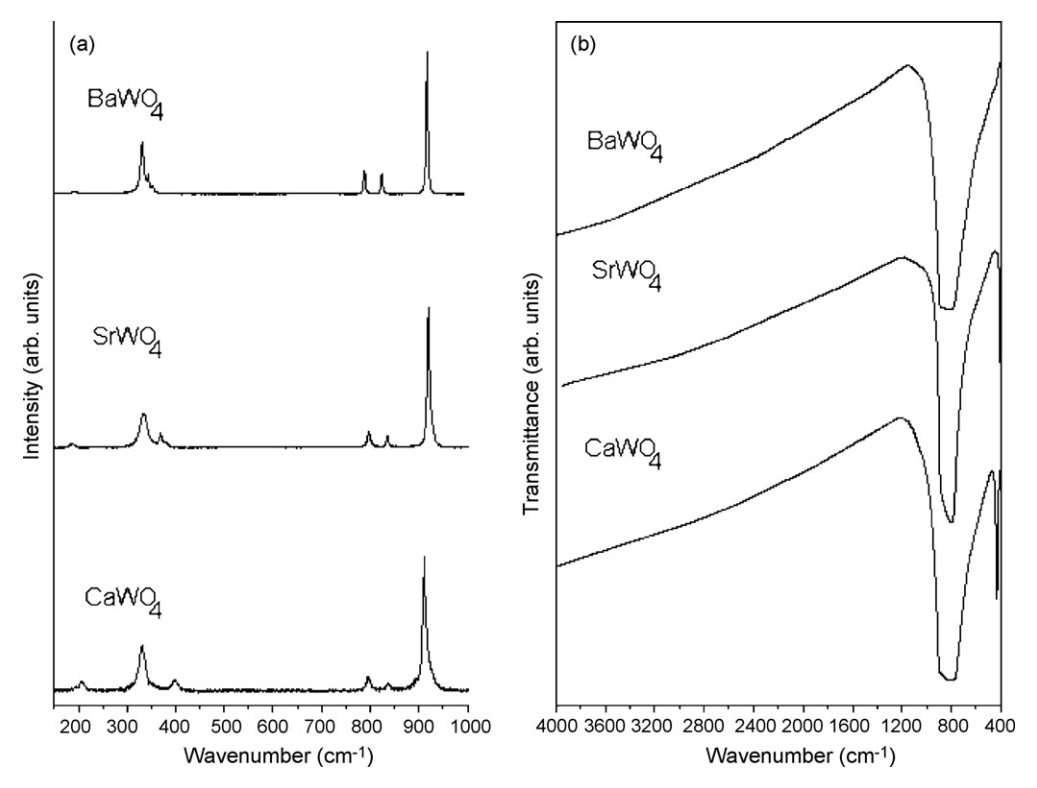


Fig. 2. (a) Raman and (b) FTIR spectra of BaWO<sub>4</sub>, SrWO<sub>4</sub> and CaWO<sub>4</sub> prepared by sonochemical method.

bands  $(\nu_3)$  specified as W–O anti-symmetric stretching vibration of  $[WO_4]^{2-}$  tetrahedrons in lattice space [21] were detected at 786–883 cm<sup>-1</sup>. Sometimes they split into two bands, sometimes they do not [20,22,23]. For present result, it appears as the strong broad band. The  $\nu_4$  splits into two bands at the wavenumbers of less than 400 cm<sup>-1</sup> [20]. Additional weak peak of W–O bending band was also detected at 447 cm<sup>-1</sup> for CaWO<sub>4</sub>. It was specified as  $\nu_2$  band [20,24]. The present analysis is in accord with other results [22,23].

For the resolution of 0.10 nm, transmission electron microscopy (TEM) images (Fig. 3) show that the three products compose of a number of dispersed nanosized particles with round shape. Among them, the sizes ranging from the biggest to the smallest are BaWO<sub>4</sub>, SrWO<sub>4</sub> and CaWO<sub>4</sub>, respectively. Selected area electron diffraction (SAED) patterns (Fig. 3) are diffuse showing that the products compose of nanosized particles. Each of them is polycrystal. They were also caused by a number of single crystals with different

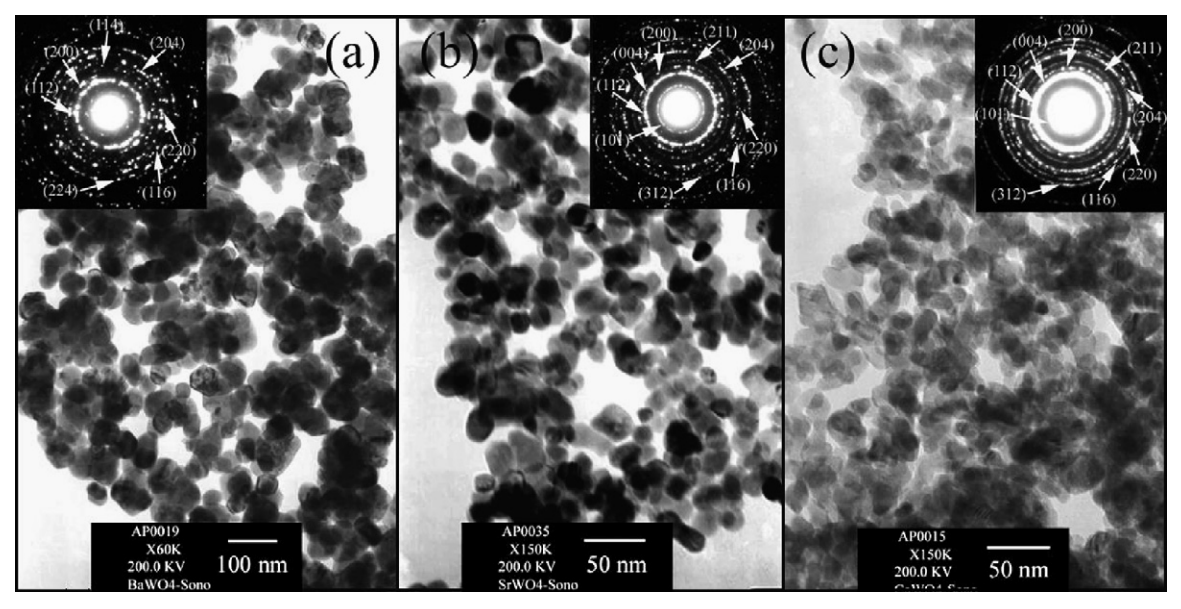


Fig. 3. TEM images and SAED patterns of (a) BaWO<sub>4</sub>, (b) SrWO<sub>4</sub> and (c) CaWO<sub>4</sub>.

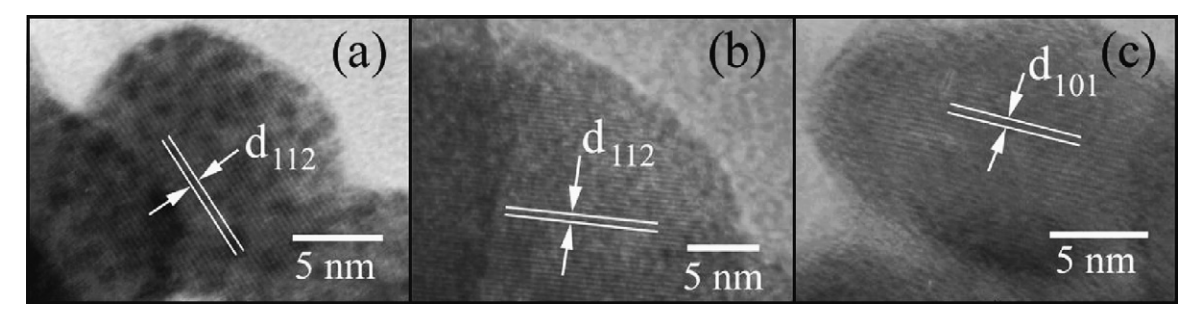


Fig. 4. HRTEM images of (a) BaWO<sub>4</sub>, (b) SrWO<sub>4</sub> and (c) CaWO<sub>4</sub>.

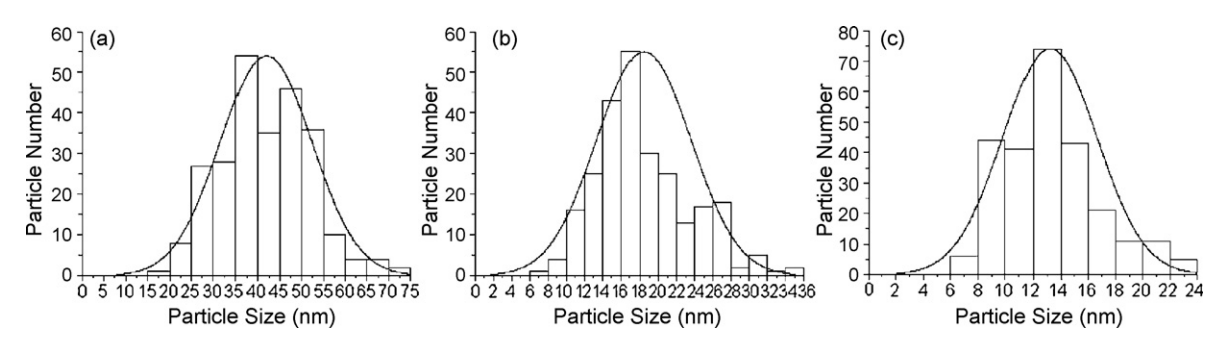


Fig. 5. Particle size distributions of (a) BaWO<sub>4</sub>, (b) SrWO<sub>4</sub> and (c) CaWO<sub>4</sub>.

orientations. The patterns appear as concentric rings, due to the diffraction of electrons through the nanosized particles. The rings were interpreted [25,26], and specified as (1 1 2), (2 0 0), (1 1 4), (2 0 4), (2 2 0), (1 1 6) and (2 2 4) planes for BaWO<sub>4</sub>,  $(1\ 0\ 1), (1\ 1\ 2), (0\ 0\ 4), (2\ 0\ 0), (2\ 1\ 1), (2\ 0\ 4), (2\ 2\ 0), (1\ 1\ 6)$ and (312) planes for SrWO<sub>4</sub> and (1 0 1), (1 1 2), (0 0 4), (2 0 0), (2 1 1), (2 0 4), (2 2 0), (1 1 6) and (3 1 2) planes for CaWO<sub>4</sub> [15]. The (1 1 2) plane has the strongest intensity composing the SAED patterns. Their strongest intensities are in accord with those of the corresponding XRD spectra. Lattice planes (Fig. 4) show that atoms are uniformly arranged in systematic array. The detected spaces correspond to (1 1 2), (1 1 2) and (1 0 1) planes for BaWO<sub>4</sub>, SrWO<sub>4</sub> and CaWO<sub>4</sub>, respectively. The particle sizes (Fig. 5) were determined [27]. The distributions are very close to the normal curves. They are in the ranges of 7.5-75, 1-35 and 2-24 nm with the average of  $42.0\pm10.4, 18.5\pm5.1$  and  $13.1\pm3.3$  nm for BaWO<sub>4</sub>, SrWO<sub>4</sub> and CaWO<sub>4</sub>, respectively. Their shapes and sizes have the influence on the photoluminescent (PL) properties as well.

The crystal-field splitting and hybridization of the molecular orbitals of  $[WO_4]^{2-}$  tetrahedrons [16] are shown in Fig. 6. The W 5d(t<sub>2</sub>) and W 5d(e) orbitals are hybridized with the O 2p( $\sigma$ ) and O 2p( $\pi$ ) ligand orbitals to form  $[WO_4]^{2-}$  tetrahedrons. The four ligand p( $\sigma$ ) orbitals are compatible with the tetrahedral representation for a<sub>1</sub> and t<sub>2</sub> symmetries and the eight ligand p( $\pi$ ) orbitals are for t<sub>1</sub>, t<sub>2</sub> and e symmetries. The top occupied state has t<sub>1</sub> symmetry formed from O 2p( $\pi$ ) states. The lowest unoccupied state has e symmetry formed from a combination of the W 5d(e) and O 2p( $\pi$ ) orbitals to give anti-bonding (\*). The hybridization between the W 5d and O 2p orbitals is specified as covalent bonding between the ions. For ground state system, all one-electron states below band gap are filled to give a many-electron  $^1A_1$  state. At the lowest excited state, there are one hole

in  $t_1$  (primarily O  $2p(\pi)$ ) state and one electron in e (primarily W 5d) state which give rise to many-electron  ${}^1T_1$ ,  ${}^3T_1$ ,  ${}^1T_2$  and  ${}^3T_2$  states. Among them, only  ${}^1T_2 \to {}^1A_1$  transition is electric dipole allow [16,28].

By respective using of 344, 270 and 214 nm exciting wavelengths for BaWO<sub>4</sub>, SrWO<sub>4</sub> and CaWO<sub>4</sub>, photoluminescent spectra (Fig. 7) have the narrow central peaks with their surrounding shoulders. The central (intrinsic) peaks are considered to be from the  ${}^{1}T_{2} \rightarrow {}^{1}A_{1}$  transition of electrons within [WO<sub>4</sub>]<sup>2-</sup> anions [16,28,29]. The transition can be treated as an exciton [29]. The shoulders are from some defects and impurities, and are specified as extrinsic transition [29]. PL intensity is controlled by the number of charged transfers. For the present analysis, the emission peaks are in the spectral region at 384–416 nm. The results are in the same range as

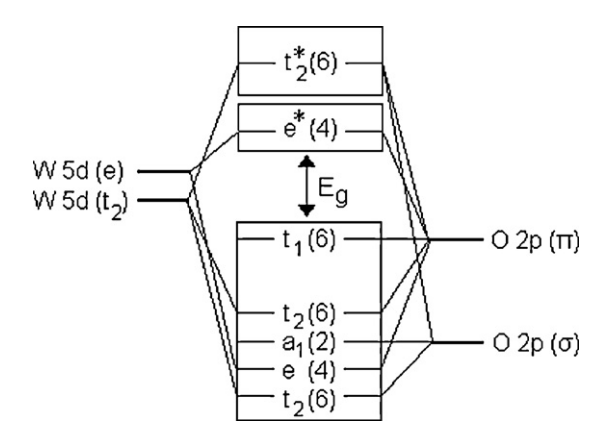


Fig. 6. Diagram of the crystal-field splitting and hybridization of the molecular orbitals of  $[WO_4]^{2-}$  tetrahedrons.  $[E_g:$  Energy band gap; (\*): Anti-bonding (Unoccupied) states; Degeneracy of each cluster state is specified in parentheses.]

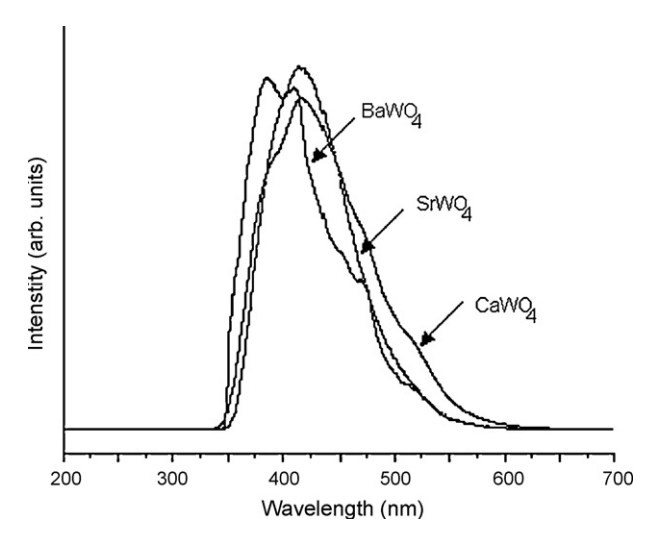


Fig. 7. PL spectra of BaWO<sub>4</sub>, SrWO<sub>4</sub> and CaWO<sub>4</sub>.

others [22,29,30]. Comparing to the corresponding bulks, their emission peaks are blue-shift [22] caused by the quantum-sized effect [10].

#### 4. Conclusions

BaWO<sub>4</sub>, SrWO<sub>4</sub> and CaWO<sub>4</sub> were successfully prepared by sonochemical method. Each of them is pure phase, and composes of dispersed nanocrystallines. They are in the ranges of 7.5–75, 1–35 and 2–24 nm for BaWO<sub>4</sub>, SrWO<sub>4</sub> and CaWO<sub>4</sub>, respectively. Their atoms are uniformly arranged in lattice array. The evidence of scheelite structured products was provided. Main transmittance bands specified as W–O antisymmetric stretching vibration were detected at 786–883 cm<sup>-1</sup>. Their emission peaks are due to the  $^1T_2 \rightarrow ^1A_1$  electronic transition of  $[WO_4]^{2-}$  tetrahedrons in the spectral region at 384–416 nm. They are blue-shift relative to the corresponding bulks.

# Acknowledgement

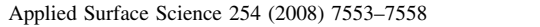
We are grateful to the Thailand Research Fund for supporting the research.

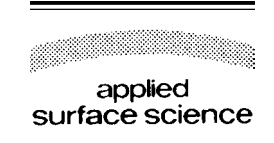
- [1] X. Wang, H. Xu, H. Wang, H. Yan, J. Cryst. Growth 284 (2005) 254.
- [2] Z. Lou, M. Cocivera, Mater. Res. Bull. 37 (2002) 1573.
- [3] A. Golubović, R. Gajić, Z. Dohčević-Mitrović, S. Nikolić, J. Alloys Compd. 415 (2006) 16.
- [4] C. Zhang, E. Shen, E. Wang, Z. Kang, L. Gao, C. Hu, L. Xu, Mater. Chem. Phys. 96 (2006) 240.
- [5] J.H. Ryu, J.W. Yoon, C.S. Lim, W.C. Oh, K.B. Shim, Ceram. Int. 31 (2005) 883.
- [6] M.A.M.A. Maurera, A.G. Souza, L.E.B. Soledade, F.M. Pontes, E. Longo, E.R. Leite, J.A. Varela, Mater. Lett. 58 (2004) 727.
- [7] L. Sun, M. Cao, Y. Wang, G. Sun, C. Hu, J. Cryst. Growth 289 (2006) 231.
- [8] W.S. Cho, M. Yashima, M. Kakihana, A. Kudo, T. Sakata, M. Yoshimura, Appl. Phys. Lett. 68 (1996) 137.
- [9] A. Datta, A. Saha, A.K. Sinha, S.N. Bhattacharyya, S. Chatterjee, J. Photochem. Photobiol. B 78 (2005) 69.
- [10] N.M. Huang, C.S. Kan, P.S. Khiew, S. Radiman, J. Mater. Sci. 39 (2004) 2411.
- [11] J.R. Lakowicz, I. Gryczynski, Z. Gryczynski, C.J. Murphy, J. Phys. Chem. B 103 (1999) 7613.
- [12] A. Gedanken, Ultrason. Sonochem. 11 (2004) 47.
- [13] J.Y. Huot, E. Battistel, R. Lumry, G. Villeneuve, J.F. Lavallee, A. Anusiem, C. Jolicoeur, J. Solution Chem. 17 (1988) 601.
- [14] D. Chen, G. Shen, K. Tang, H. Zheng, Y. Qian, Mater. Res. Bull. 38 (2003) 1783.
- [15] Powder Diffract. File, JCPDS Internat. Centre Diffract. Data, PA 19073– 3273, U.S.A., 2001.
- [16] Y. Zhang, N.A.W. Holzwarth, R.T. Williams, Phys. Rev. B 57 (12) (1998) 738
- [17] S.P.S. Porto, J.F. Scott, Phys. Rev. 157 (1967) 716.
- [18] T. Thongtem, A. Phuruangrat, S. Thongtem, Mater. Lett. 61 (2007) 3235.
- [19] T.T. Basiev, A.A. Sobol, Y.K. Voronko, P.G. Zverev, Opt. Mater. 15 (2000) 205.
- [20] G.M. Clark, W.P. Doyle, Spectrochim. Acta 22 (1966) 1441.
- [21] Z.C. Ling, H.R. Xia, D.G. Ran, F.Q. Liu, S.Q. Sun, J.D. Fan, H.J. Zhang, J.Y. Wang, L.L. Yu, Chem. Phys. Lett. 426 (2006) 85.
- [22] G. Zhang, R. Jia, Q. Wu, Mater. Sci. Eng. B 128 (2006) 254.
- [23] F.A. Miller, C.H. Wilkins, Anal. Chem. 24 (1952) 1253.
- [24] R.L. Frost, L. Duong, M. Weier, Spectrochim Acta A 60 (2004) 1853.
- [25] T. Thongtem, S. Kaowphong, S. Thongtem, J. Mater. Sci. 42 (2007) 3923.
- $[26]\ A.\ Phuruangrat,\ T.\ Thongtem,\ S.\ Thongtem,\ Mater.\ Lett.\ 61\ (2007)\ 3805.$
- [27] Scion Image, Scion Corp., 82 Worman's Mill Ct., Suite H, Frederick, MD 21701, 1997–2005.
- [28] M.J. Treadaway, R.C. Powell, J. Chem. Phys. 61 (1974) 4003.
- [29] V.B. Mikhailik, I.K. Bailiff, H. Kraus, P.A. Rodnyi, J. Ninkovic, Radiat. Meas. 38 (2004) 585.
- [30] G. Zhou, M. Lü, Z. Xiu, S. Wang, H. Zhang, W. Zou, J. Cryst. Growth 276 (2005) 116.



Available online at www.sciencedirect.com







www.elsevier.com/locate/apsusc

# Characterization of PbS with different morphologies produced using a cyclic microwave radiation

Anukorn Phuruangrat<sup>a</sup>, Titipun Thongtem<sup>b,\*</sup>, Somchai Thongtem<sup>a</sup>

<sup>a</sup> Department of Physics, Faculty of Science, Chiang Mai University, Chiang Mai 50200, Thailand
 <sup>b</sup> Department of Chemistry, Faculty of Science, Chiang Mai University, 239 Hauy Kaew Road,
 Suthep District Amphur Maung, Chiang Mai 50200, Thailand

Available online 18 January 2008

#### Abstract

PbS was produced from different lead (Pb(CH<sub>3</sub>COO)<sub>2</sub>·H<sub>2</sub>O, PbCl<sub>2</sub>·2.5H<sub>2</sub>O, Pb(NO<sub>3</sub>)<sub>2</sub>) and sulfur (CH<sub>3</sub>CSNH<sub>2</sub>, CH<sub>5</sub>N<sub>3</sub>S, NH<sub>2</sub>CSNH<sub>2</sub>) sources in propylene glycol using a cyclic microwave radiation at different powers and prolonged times. PbS (cubic) was detected using X-ray diffraction (XRD) and selected area electron diffraction (SAED) techniques. The interpreted and simulated patterns are in good accord. Raman spectrometer revealed the presence of vibrations at 138, 273 and 439 cm<sup>-1</sup>. Different morphologies (nano-sized particles, hexapods, cubes, ferns and magic squares) were characterized using a scanning electron microscope (SEM) and a transmission electron microscope (TEM). The product morphologies were influenced by the starting agents, microwave powers and prolonged times.

© 2008 Elsevier B.V. All rights reserved.

PACS: 81.07.Bc

Keywords: Cyclic microwave radiation; PbS; Nano-sized particles; Hexapods; Cubes; Ferns; Magic squares

# 1. Introduction

At present, luminescent materials with different morphologies have become increasingly important. One of them is PbS, which has a small band gap (0.41 eV) and a large exciton Bohr radius (18 nm) [1,2]. The sulfide with nanoparticles possesses the third-order nonlinear optical property, which has the potential for being used in optical devices [3]. PbS nanocrystals (irregular nanoparticles, star-shaped dendrites, truncated nanocubes and nanocubes) showed an emission spectrum at the same wavelength of 632 nm although their morphologies are different. Nanocubes with the best crystals contain very low defect concentration. The intensity is highest, compared with other nanocrystals. But for irregular nanoparticles, the intensity is the lowest. The emission properties are influenced by several parameters, such as shapes, sizes, size distributions and defects [4]. In addition, absorption UV spectra of PbS nanocrystals

having the shapes of nanorods, nanobelts, nanodendrites and nanovelvet-flowers were very large blue-shift relative to its bulk due to the quantum size effect [3]. The product with different morphologies was produced using a variety of methods such as dendritic PbS nanostructures by ultrasonic method [5], hollow nanospheres by sonochemical method [6], nanoparticles by a simple polyol route [7], cross-shaped PbS nanostructures by a surfactant-assisted reflux process [8] and nanocrystals in ethanol by a microwave heating synthesis [9]. Microwave radiation is very attractive and used for preparing materials. It can rapidly lead to very high temperatures which have an influence on the reaction rates. When microwave is supplied to solutions, one or more of the components is capable of coupling with the radiation. Vibrating electric field applied a force on charged particles which vibrated accordingly. It can lead to higher heating rate than that achieved by conventional method, and can solve the problems of temperature and concentration gradients. Subsequently, pure products were produced [10]. The present research is to investigate the role of lead and sulfur sources on the morphologies of PbS produced in propylene glycol using a cyclic microwave radiation without any further calcination.

<sup>\*</sup> Corresponding author. Tel.: +66 53 943341; fax: +66 53 892 277. *E-mail addresses:* ttpthongtem@yahoo.com, ttpthongtem@hotmail.com (T. Thongtem).

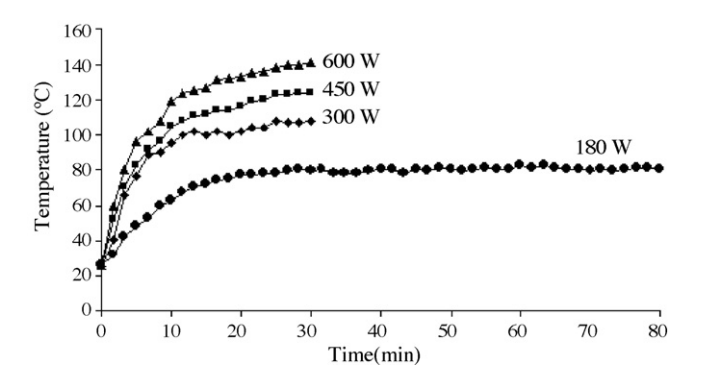


Fig. 1. Test temperatures at different microwave powers and prolonged times.

Table 1 Lead and sulfur sources, product codes and the products morphologies

Lead sources	Sulfur sources	Product codes	Product morphologies
Pb(CH <sub>3</sub> COO) <sub>2</sub> ·H <sub>2</sub> O	CH <sub>3</sub> CSNH <sub>2</sub>	AA	Nano-sized particles
	$CH_5N_3S$	AC	Hexapods
	$NH_2CSNH_2$	AT	Hexapods
PbCl <sub>2</sub> ·2.5H <sub>2</sub> O	CH <sub>3</sub> CSNH <sub>2</sub>	CA	Cubes
	CH <sub>5</sub> N <sub>3</sub> S	CC	Nano-sized particles
	$NH_2CSNH_2$	CT	Nano-sized particles
Pb(NO <sub>3</sub> ) <sub>2</sub>	CH <sub>3</sub> CSNH <sub>2</sub>	NA	Cubes
	CH <sub>5</sub> N <sub>3</sub> S	NC	Ferns
	NH <sub>2</sub> CSNH <sub>2</sub>	NT	Magic squares

# 2. Experiment

PbS with different morphologies was produced from 0.005 mol each of lead and sulfur sources (Table 1) in 30 ml propylene glycol using a cyclic microwave radiation at different powers and prolonged times. One cycle of 100 s prolonged time composed of 30 s radiation and 70 s non-radiation. Test temperatures for the present research are shown in Fig. 1. They were increased with the increase in the microwave powers and

prolonged times. The temperatures rapidly increased during the first 15 min. Their rates decreased afterwards. For 180 W, the temperature tended to be constant at 80 °C after 20-min test. At the conclusion of the test, the final products were washed with water and ethanol, and dried at 80 °C for 12 h. Then, they were characterized using an X-ray diffractometer (XRD) operated at 20 kV, 15 mA and using Cu K $\alpha$  radiation in the 2 $\theta$  angular range of 15–60°, a transmission electron microscope (TEM) as well as the use of the selected area electron diffraction (SAED) technique operated at 200 kV, a scanning electron microscope (SEM) operated at 15 kV and a Raman spectrometer using 50 mW Ar Laser with  $\lambda$  = 514.5 nm at room temperature.

#### 3. Results and discussion

Crystallographic planes of XRD spectra (Figs. 2 and 3) were indexed using Bragg's law for X-ray diffraction and compared with those of the JCPDS software (reference code: 05-0592) [11]. At 180 W for 30 min, the product is so less that it is not able to collect from the filter paper. For longer times (Fig. 2a), higher powers (Fig. 2b), and different lead and sulfur sources at 600 W for 15 min (Fig. 3a-c), the products were specified as cubic PbS with Fm-3m space group. Their intensities increased with the increase in the prolonged times and microwave powers. These reflect the degree or extent of the crystals. For present analysis, well-crystallized PbS was successfully synthesized [12]. The products composed of a number of atoms aligning in a periodic lattice. The strongest intensity is at  $2\theta = 30.08^{\circ}$  and diffracted from (2 0 0) plane of the crystalline products. No other impurities were detected although the products were produced using different conditions. XRD spectra were characterized over the  $2\theta$  angular ranges of 15– 60°, which cover the main peaks with high intensities. The peaks with  $2\theta > 60^{\circ}$ , such as (4 0 0) and (3 3 1), were off-scale and were not detected.

SEM and TEM images (Figs. 4 and 5) show that the products were successfully produced in a variety of shapes and sizes

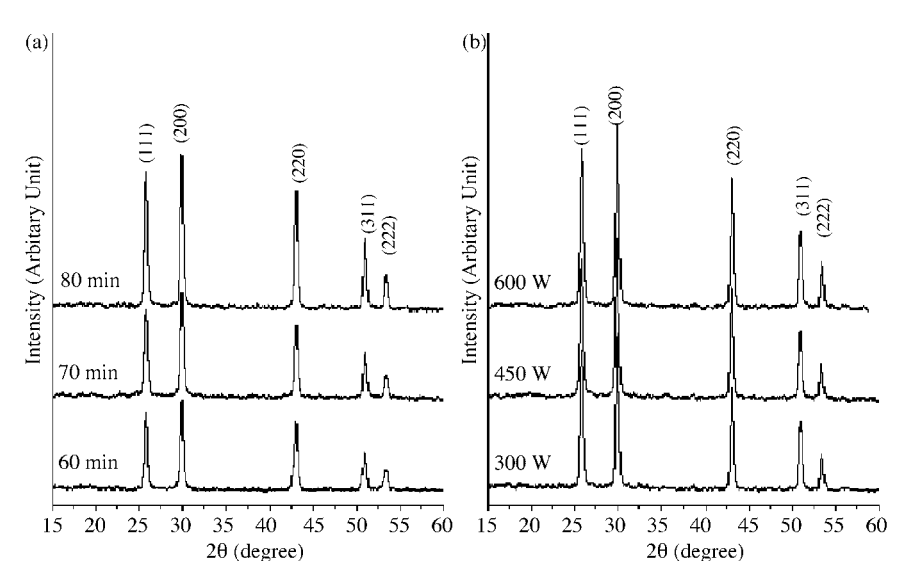


Fig. 2. XRD spectra of CA product produced using PbCl<sub>2</sub>·2.5H<sub>2</sub>O and CH<sub>3</sub>CSNH<sub>2</sub> at (a) 180 W microwave power for different prolonged times, and (b) different microwave powers for 15 min.

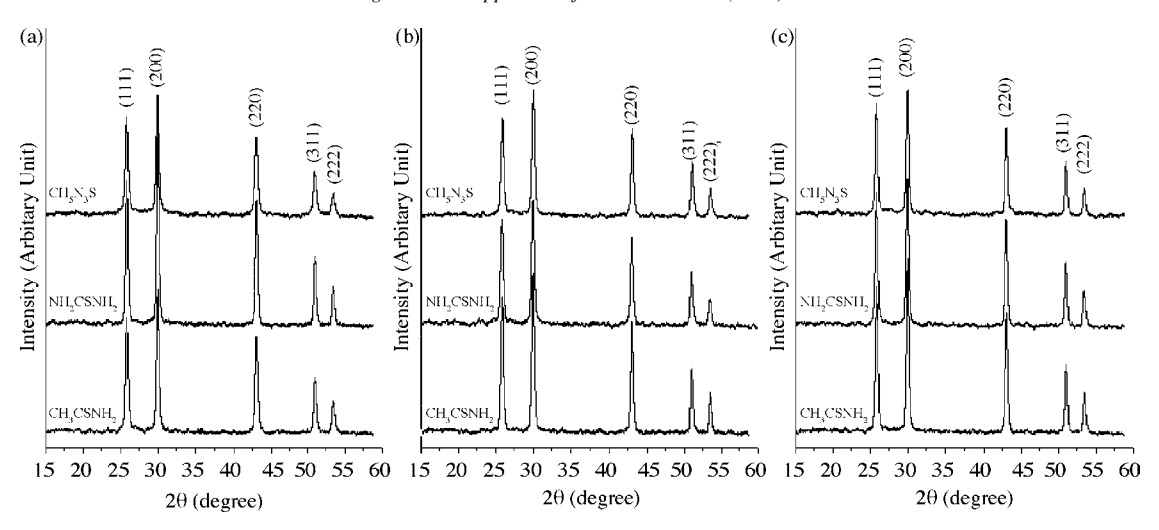


Fig. 3. XRD spectra of PbS produced using (a)  $Pb(CH_3COO)_2 \cdot H_2O$ , (b)  $PbCl_2 \cdot 2.5H_2O$  and (c)  $Pb(NO_3)_2$  with different sulfur sources at 600 W microwave power for 15 min.

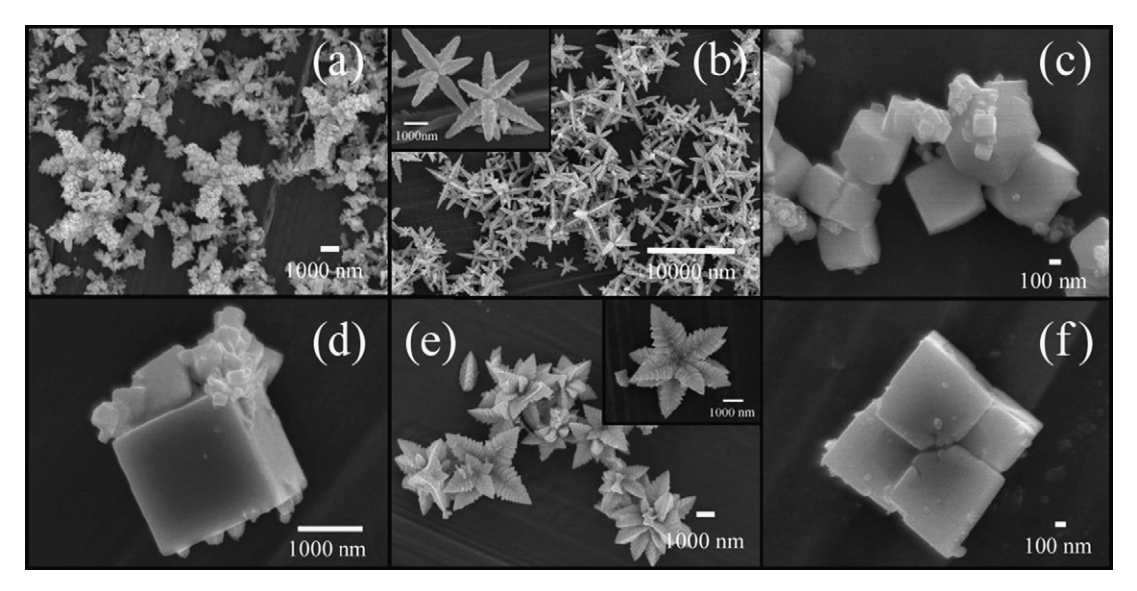


Fig. 4. Surface morphologies of PbS produced using 600 W microwave power for 15 min. (a-f) are AC, AT, CA, NA, NC and NT, respectively.

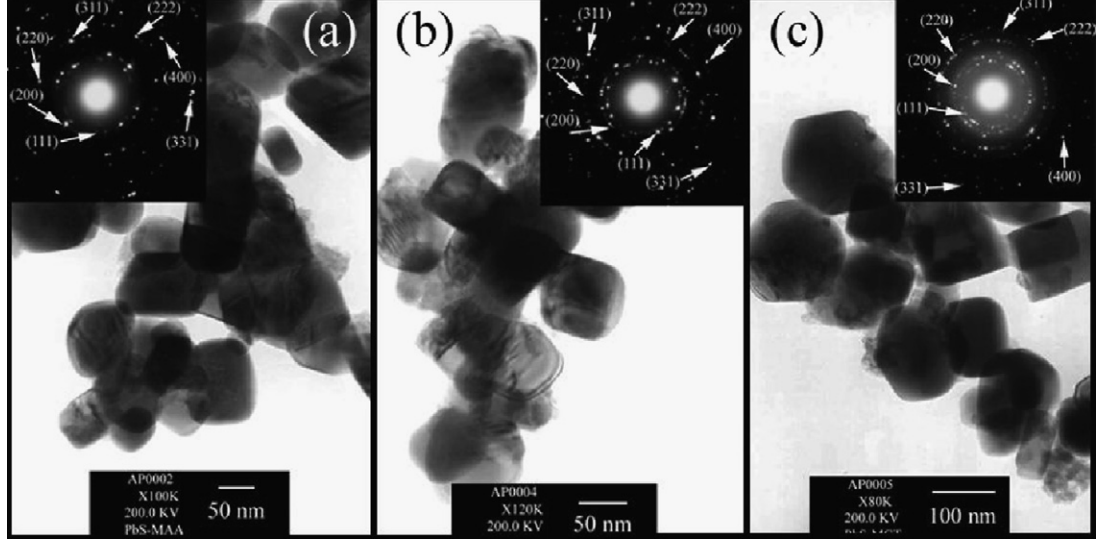


Fig. 5. TEM images and SAED patterns of PbS produced using 600 W microwave power for 15 min. (a-c) are AA, CC and CT, respectively.

which are summarized in Table 1. The AC and AT products (Fig. 4a and b) composed of hexapods at right angle. Four pods are in the same plane. The other two pods are at right angle to the four-pod structure. One pod is on the top, and the other is at the bottom. The CA and NA products (Fig. 4c and d) composed of a number of cubes with different sizes. Their facets are very smooth like a mirror. The NC product (Fig. 4e) shaped like fern. Each of its leaves slopes up to a point, and has two halves with the same size and shape. The NT (Fig. 4f) is similar to a magic square. It composed of four cubes in cubic cluster. The number of cubes present along any row, column or diagonal has the same sum. Those for AA, CC and CT (Fig. 5a–c), they are rather round particles with nanometer in size. The crystalline degree can play the role in the morphologies as well.

Different product morphologies were influenced by lead and sulfur sources which have different structural formulas. Nucleation and growth of the particles can play roles in the morphology. The crystal growth of some preferred structures or planes relates to the surface energy of the planes in the specified condition. It is described as the shape selective surface absorption process [13]. The amount of starting agents in the solution also has the influence on different orientation of the particles which reflects the nucleation and the growth of the crystals. The particle orientations were increased with the increase in the amount of starting agents [14]. Phase with the lowest free energy is thermodynamically stable, and has more chance to exist in the process [15]. This reflects the product morphologies. Apart from the above, crystal growth is influenced by the solubility of the precursors in the particular solvent and synthesized temperature which reflects the morphologies [13]. Microwave powers and irradiation times also have the influence on the product shape, size and crystallinity.

Their SAED patterns (Fig. 5) composed of a number of bright spots arranging into concentric rings. They show the character of crystalline products. Electron beam diffracts from

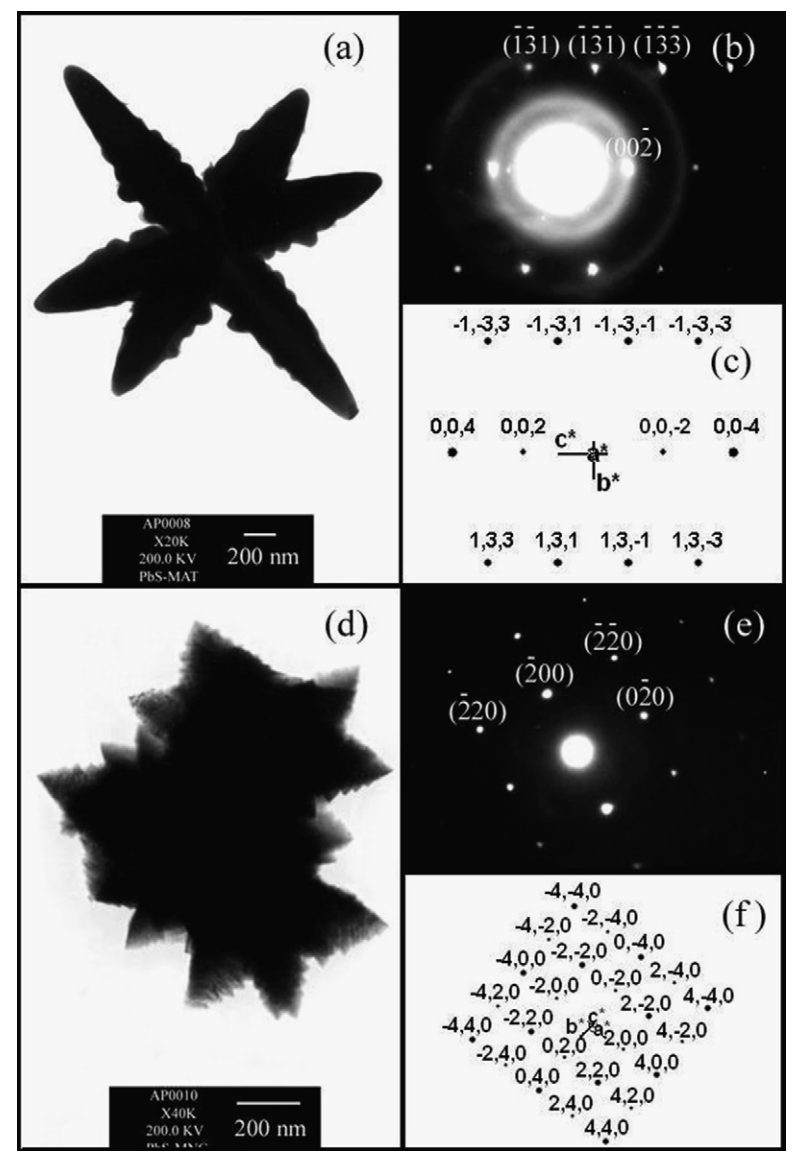


Fig. 6. TEM images, and SAED and simulated patterns of PbS produced using 600 W microwave power for 15 min. (a-c) and (d-f) are for AT and NC, respectively.

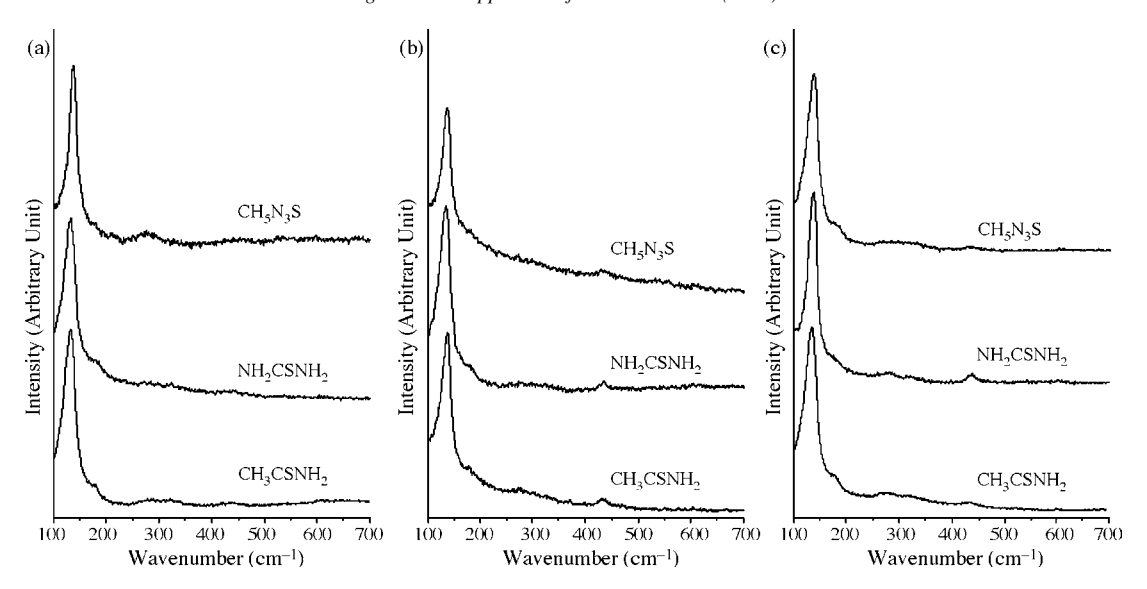


Fig. 7. Raman spectra of PbS produced from (a-c) Pb(CH<sub>3</sub>COO)<sub>2</sub>·H<sub>2</sub>O, PbCl<sub>2</sub>·2.5H<sub>2</sub>O and Pb(NO<sub>3</sub>)<sub>2</sub> and different sulfur sources, using 600 W microwave power for 15 min, respectively.

the crystallographic planes of the unit cells composing the products. The interpreted patterns [16,17] correspond to  $(1\ 1\ 1)$ ,  $(2\ 0\ 0)$ ,  $(2\ 2\ 0)$ ,  $(3\ 1\ 1)$ ,  $(2\ 2\ 2)$ ,  $(4\ 0\ 0)$  and  $(3\ 3\ 1)$ . Comparing the diffraction planes to those of the JCPDS software [11], they were specified as cubic PbS.

The AT and NC products were also analyzed using TEM. Their morphologies (Fig. 6a and d) are in accord with those of the SEM images (Fig. 4b and e). SAED patterns (Fig. 6b and e) appear as symmetric and systematic array of bright spots showing that a number of atoms are arranged in their crystal lattices. The patterns were interpreted [18], and specified as cubic PbS crystal [11]. Calculated electron beams [18] are in the  $\begin{bmatrix} 3 \ \overline{1} \ 0 \end{bmatrix}$  and  $\begin{bmatrix} 0 \ 0 \ 1 \end{bmatrix}$  directions for AT and NC products, respectively. They are the directions that electron beams were sent to the crystal facets. Diffraction patterns for AT and NC with  $\begin{bmatrix} 3 \ \overline{1} \ 0 \end{bmatrix}$  and  $\begin{bmatrix} 0 \ 0 \ 1 \end{bmatrix}$  zone axes were simulated (Fig. 6c and f), respectively [19]. The simulated spots with the specified crystallographic planes are in systematic and symmetric arrays. Comparing the interpreted and simulated patterns, they are in good accord. The a\*, b\* and c\* lattice vectors for both patterns are in the [1 0 0], [0 1 0] and [0 0 1] directions, respectively. For one crystal structure, the corresponding lattice vectors are the same although their zone axes are different. Additional concentric rings were also detected for the AT product (Fig. 6b). They were caused by the C grid.

A definite existence of the products was analyzed using a Raman spectrometer. Test specimens are non-destructive and are able to re-use for other purposes. Generally, Raman shifts correspond to the longitudinal optical (LO) mode in crystalline semiconductors. Transverse optical (TO) and surface phonon (SP) modes are not detectable due to symmetry restrictions and low intensities, respectively [20]. The detection of SP mode is possible in the nanostructured materials of which the surface to volume ratio is large. This shows that surface roughness and crystallite size can play the role in the Raman spectra [20]. For the present research, the spectra (Fig. 7) contain prominent bands at the same wavenumbers although the products have different

morphologies (synthesized using different lead and sulfur sources). They imply that the vibrations are independent of the morphologies. The frequencies are influenced by some parameters, such as the atomic masses of Pb and S, and vibration constant of bonding between Pb and S atoms arranged in the lattice. Among the different spectra, their peaks are at 138, 273 and 439 cm<sup>-1</sup>. The peak below 150 cm<sup>-1</sup> is tentatively attributable to the so-called plasma line of the excitation laser [21,22]. The 273  $\mathrm{cm}^{-1}$  peak corresponds to two-phonon process [21]. The peak at 439 cm<sup>-1</sup> is allowed in the rock-salt structure [23]. It was specified as the first overtone mode [22], which involves two phonons with equal but opposite k [23]. The fundamental LO of the rock-salt structure at approximately 219.5 cm<sup>-1</sup> was unable to detect due to the rising in intensity of baseline (disorder in PbS lattice) at low wavenumbers. Baseline intensity covered the fundamental LO mode, which was forbidden [22,23].

# 4. Conclusions

Different shapes and sizes of PbS crystals were successfully produced from different lead and sulfur sources in propylene glycol using the cyclic microwave radiation at different powers and prolonged times. XRD, SAED and Raman analyses revealed the presence of PbS phase with the first overtone mode at 439 cm<sup>-1</sup>. The crystalline degree was increased with the increase in the microwave powers and prolonged times. The nano-sized particles, hexapods, cubes, ferns and magic squares were characterized using SEM and TEM. They were influenced by the microwave powers, prolonged times and starting agents.

# Acknowledgements

We are grateful to the Thailand Research Fund for supporting the research, and the Graduate School of Chiang Mai University for general funding.

- [1] S. Wang, A. Pan, H. Yin, Y. He, Y. Lei, Z. Xu, B. Zou, Mater. Lett. 60 (2006) 1242.
- [2] L. Xu, W. Zhang, Y. Ding, W. Yu, J. Xing, F. Li, Y. Qian, J. Cryst. Growth 273 (2004) 213.
- [3] L. Dong, Y. Chu, Y. Liu, M. Li, F. Yang, L. Li, J. Colloid Interface Sci. 301 (2006) 503.
- [4] G. Zhou, M. Lü, Z. Xiu, S. Wang, H. Zhang, Y. Zhou, S. Wang, J. Phys. Chem. B 110 (2006) 6543.
- [5] P. Zhao, G. Chen, Y. Hu, X. He, K. Wu, Y. Cheng, K. Huang, J. Cryst. Growth 303 (2007) 632.
- [6] S.F. Wang, F. Gu, M.K. Lü, Langmuir 22 (2006) 398.
- [7] Y.J. Yang, Colloid Surf. A 276 (2006) 192.
- [8] S.F. Wang, F. Gu, M.K. Lü, D.Z. Wang, Z.S. Yang, H.P. Zhang, Y.Y. Zhou, A.Y. Zhang, Mater. Lett. 60 (2006) 2759.
- [9] T. Ding, J.J. Zhu, Mater. Sci. Eng. B 100 (2003) 307.
- [10] C. Gabriel, S. Gabriel, E.H. Grant, B.S.J. Halstead, D.M.P. Mingos, Chem. Soc. Rev. 27 (1998) 213.

- [11] Powder Diffract. File, JCPDS Internat. Centre Diffract. Data, PA 19073-3273, U.S.A. (2001).
- [12] T. Thongtem, S. Thongtem, Ceram. Int. 31 (2005) 241.
- [13] S. Biswas, S. Kar, S. Chaudhuri, J. Cryst. Growth 299 (2007) 94.
- [14] Y.C. Zhang, X.Y. Hu, T. Qiao, Solid State Commun. 132 (2004) 779.
- [15] K. Sopunna, T. Thongtem, M. McNallan, S. Thongtem, Surf. Sci. 566–568 (2004) 810.
- [16] T. Thongtem, S. Kaowphong, S. Thongtem, J. Mater. Sci. 42 (2007) 3923.
- [17] A. Phuruangrat, T. Thongtem, S. Thongtem, Mater. Lett. 61 (2007) 3805.
- [18] T. Thongtem, A. Phuruangrat, S. Thongtem, Mater. Lett. 61 (2007) 3235.
- [19] C. Boudias, D. Monceau, CaRIne Crystallography 3.1, 17 rue du Moulin du Roy, F-60300 Senlis, France (1989–1998).
- [20] K.K. Nanda, S.N. Sahu, Phys. Rev. B 58 (1998) 15 405.
- [21] A.M. Qin, Y.P. Fang, W.X. Zhao, H.Q. Liu, C.Y. Su, J. Cryst. Growth 283 (2005) 230.
- [22] G.D. Smith, S. Firth, R.J.H. Clark, M. Cardona, J. Appl. Phys. 92 (2002) 4375
- [23] R. Sherwin, R.J.H. Clark, R. Lauck, M. Cardona, Solid State Commun. 134 (2005) 565.



Contents lists available at ScienceDirect

# Materials Letters

journal homepage: www.elsevier.com/locate/matlet



# Preparation of ear-like, hexapod and dendritic PbS using cyclic microwave-assisted synthesis

Anukorn Phuruangrat <sup>a,\*</sup>, Titipun Thongtem <sup>b,\*</sup>, Somchai Thongtem <sup>a</sup>

- <sup>a</sup> Department of Physics, Faculty of Science, Chiang Mai University, Chiang Mai 50200, Thailand
- <sup>b</sup> Department of Chemistry, Faculty of Science, Chiang Mai University, Chiang Mai 50200, Thailand

#### ARTICLE INFO

Article history: Received 24 November 2008 Accepted 18 December 2008 Available online 25 December 2008

Reywords:
Cyclic microwave-assisted synthesis
PbS
Ear-like structure
Hexapod
Dendrite

#### ABSTRACT

Different morphologies of PbS were prepared using microwave-assisted synthesis of 1:4, 1:1 and 4:1 molar ratios of Pb(CH<sub>3</sub>COO)<sub>2</sub> to NH<sub>2</sub>CSNH<sub>2</sub> in propylene glycol. Cubic PbS was detected using X-ray diffraction (XRD) and selected area electron diffraction (SAED). Raman spectrometry revealed the presence of vibrations at 134, 274 and 430 cm<sup>-1</sup>. The product morphologies for different molar ratios of Pb(CH<sub>3</sub>COO)<sub>2</sub> to NH<sub>2</sub>CSNH<sub>2</sub> were also characterized using a scanning electron microscope (SEM) and a transmission electron microscope (TEM). The obtained morphologies changed with molar ratios used for the starting agents. The simulated diffraction pattern was also in accordance with the interpretation of the experimental results.

© 2008 Elsevier B.V. All rights reserved.

#### 1. Introduction

PbS is one of luminescent materials which have novel semiconducting and optical properties [1]. It has a small band gap of 0.41 eV (for bulk at room temperature), large excitonic Bohr radius of 18 nm [2–4], and is very sensitive to the quantum-size effect [2,3]. Different morphologies can play the roles in the properties. They are nanocrystals [5], nanorods [6,7], nanotubes [6], nanocubes [8], starshapes [9], dendrites [8,10] and flower-like crystals [11], which can be prepared by different methods, such as hydrothermal and solvothermal routes [4,8], electroless chemical deposition [12], microwave-assisted synthesis [11] and sonochemistry method [6].

Microwave-assisted synthesis [13] is a very attractive process for producing a variety of materials. When microwave radiation is applied to chemicals, at least one of the components is capable of coupling with the radiation. It is able to promote the reaction rates, and consumes shorter reaction time, comparing to a conventional method. Temperature and concentration gradients are able to be solved by the vibration of microwave radiation. Due to a large amount of microwave energy focused onto solutions, the vibrating electric field applies a force on the charged particles to vibrate accordingly. The radiation can play the role in promoting the reaction kinetics with high efficiency.

To the best of our knowledge, there are not many reports on the preparation of ear-like, hexapod and dendritic PbS, and using only

hydrothermal process [14,15]. In the present research, these PbS nanostructures were prepared from different molar ratios of Pb and S sources, using cyclic microwave-assisted synthesis. The final products were intensively analyzed for further discussion.

# 2. Experiment

Difference PbS morphologies were prepared from 1:4, 1:1 and 4:1 molar ratios of  $Pb(CH_3COO)_2$  to  $NH_2CSNH_2$  in propylene glycol, using 600 W cyclic microwave radiation for 9 cycles. A cyclic duration of 100 s, the radiation was on for 30 s every 70 s interval. At the conclusion of the process, the system naturally cooled down to room temperature. The products were washed with water and ethanol, and dried at 80 °C for 12 h. Then they were characterized by using X-ray diffraction (XRD), Raman spectrometry, scanning electron microscopy (SEM), transmission electron microscopy (TEM) as well as selected area electron diffraction (SAED) techniques. The electron diffraction patterns were simulated by CaRIne Crystallography 3.1 program [16] and compared with those of the experimental results.

#### 3. Results and discussion

XRD patterns (Fig. 1a) were indexed by using ICDD-JCPDS database (card no. 05-0592) [17]. The examined products were cubic PbS, with the Fm-3 m space group. No characteristic peaks of impurities were detected showing that each of the products is a pure phase. Their lattice parameters were calculated from the equation of plane spacing for cubic crystal system and Bragg's law for diffraction [18]. The averages and standard deviations are 5.9494±0.0105, 5.9482±0.0095 and 5.9516±0.0121 Å for the products prepared using 1:4,1:1 and 4:1 molar ratios of Pb(CH<sub>3</sub>COO)<sub>2</sub> to NH<sub>2</sub>CSNH<sub>2</sub>, respectively. They are very close to those of the ICDD-JCPDS reference data [17].

<sup>\*</sup> Corresponding authors.

E-mail addresses: phuruangrat@hotmail.com (A. Phuruangrat),
ttpthongtem@yahoo.com (T. Thongtem).

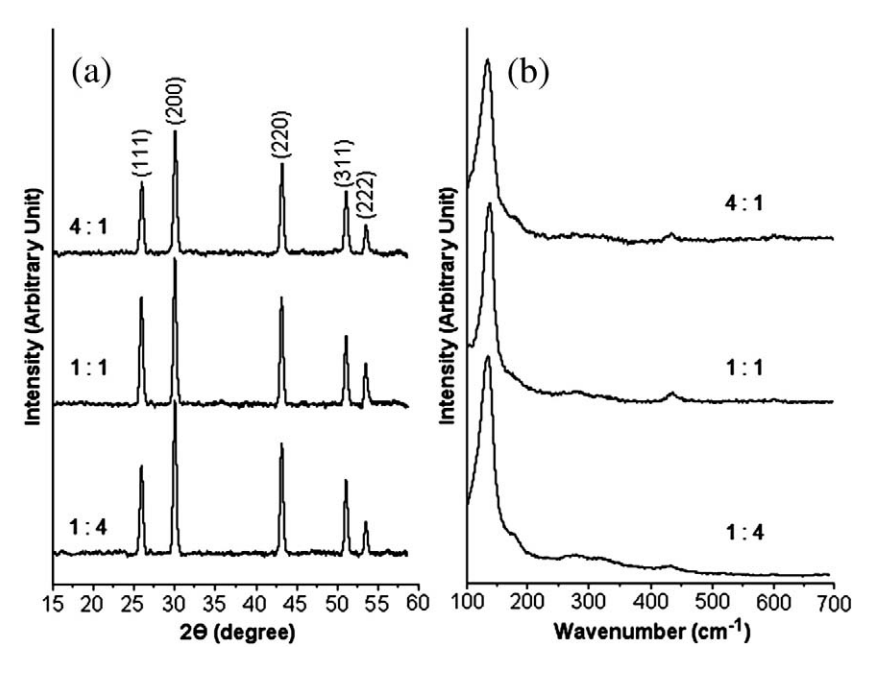


Fig. 1. (a) XRD patterns and (b) Raman spectra of the products prepared using different molar ratios of Pb(CH<sub>3</sub>COO)<sub>2</sub> to NH<sub>2</sub>CSNH<sub>2</sub>.

The chemical process leading to PbS formation is considered to proceed according to the following.

$$Pb(CH3COO)2 \rightarrow Pb2+ + 2(CH3COO)-$$
(1)

$$NH_2CSNH_2 + H_2O \rightarrow NH_2CONH_2 + H_2S$$
 (2)

$$Pb^{2+} + S^{2-} \rightarrow PbS \tag{3}$$

Theoretically, 1 mol  $Pb(CH_3COO)_2$  and 1 mol  $NH_2CSNH_2$  were used to produce 1 mol PbS. The products were able to be produced even when either of the reactants was excessive.

A definite existence of PbS was analyzed using Raman spectrometry. The Raman spectra (Fig. 1b) contain prominent bands at the same wavenumbers. They are influenced by some parameters, such as atomic masses of Pb and S, and vibration constant of bonding between Pb and S atoms residing in the lattice. Among the different spectra, their peaks are at 134, 274 and 430 cm $^{-1}$ . The peak below 150 cm $^{-1}$  is tentatively attributable to the so-called plasma line of the excitation laser [1,19]. The 274 cm $^{-1}$  peak corresponds to two-phonon process [1]. The peak at 430 cm $^{-1}$  is allowed in the rock-salt structure [20]. It is specified as the first overtone of the longitudinal optical (2LO) mode at the center ( $\Gamma$ ) of Brillouin zone [19], which involves two phonons with equal but opposite wave vectors (k) [20]. The fundamental longitudinal optical (1LO) mode of the rock-salt structure at approximately 215.5 cm $^{-1}$  was unable to be detected due to the rising in intensity of baseline, caused by disordering in PbS lattice, at low wavenumbers. The baseline intensity covered the 1LO mode, which was forbidden [19,20].

The SEM images from Fig. 2 show that the products are ear-like structure, hexapod and dendrite for 1:4, 1:1 and 4:1 molar ratios of Pb(CH $_3$ COO) $_2$  to NH $_2$ CSNH $_2$ . The hexapods composed four coplanar pods, with the other two pods at right angle with

respect to the four-pod structure. One pod is on the top, and the other is at the bottom. The length of the trunk and the diameter of the branches of PbS dendrites are about 5–8  $\mu m$  and 700–800 nm, respectively. The product morphologies were controlled by the different growth direction and rate [14,15]. Each arm of hexapod PbS is along the [100] direction. When NH2CSNH2 is added excess, the independent arm of hexapod is broken from core to form a crystal dendrite. When Pb(CH3COO)2 is in excess, it seems to favor the faster growth in [011] relative to [100] directions. The result is the formation of the ear-like structure [14].

TEM images (Fig. 3) were used to specify the product morphologies. The results obtained using TEM are in accordance with those provided by SEM. For the present research, TEM images are 2D. But for SEM images, they are 3D. The SAED patterns from Fig. 4a and b, for the products prepared using 4:1 and 1:4 molar ratios of Pb(CH<sub>3</sub>COO)<sub>2</sub> to NH<sub>2</sub>CSNH<sub>2</sub> appear as a symmetric and systematic array of bright spots showing that a number of atoms are arranged in respective crystalline structures. The patterns were interpreted [21], and specified as cubic PbS [17]. The electron beam used for the analysis was in the [001] direction. The electron diffraction simulated pattern (Fig. 4c) is composed of systematic and symmetric array of bright spots as well. It is in good accordance with those obtained from the experiment.

# 4. Conclusions

Ear-like, hexapod and dendritic PbS nano-structures were successfully prepared from 1:4, 1:1 and 4:1 molar ratios of Pb(CH<sub>3</sub>COO)<sub>2</sub> to NH<sub>2</sub>CSNH<sub>2</sub> in propylene glycol, using cyclic microwave-assisted synthesis. XRD and SAED analyses revealed the presence of PbS with a cubic structure. The experimental and simulated patterns are in good accordance. Both SEM and TEM analyses revealed the presence of earlike, hexapod and dendritic PbS which were prepared using different

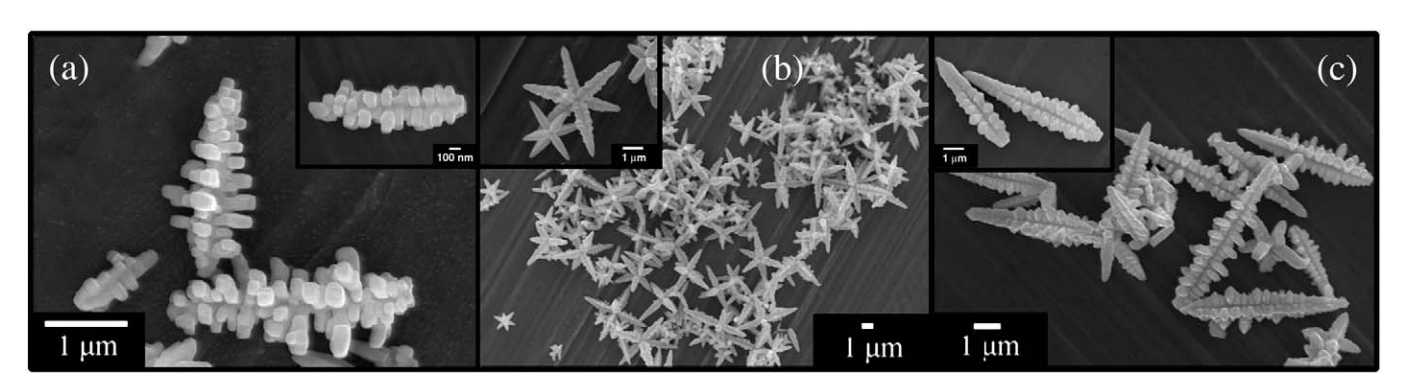


Fig. 2. SEM images of the products prepared using (a-c) 1:4, 1:1, and 4:1 molar ratios of Pb(CH<sub>3</sub>COO)<sub>2</sub> to NH<sub>2</sub>CSNH<sub>2</sub>, respectively.

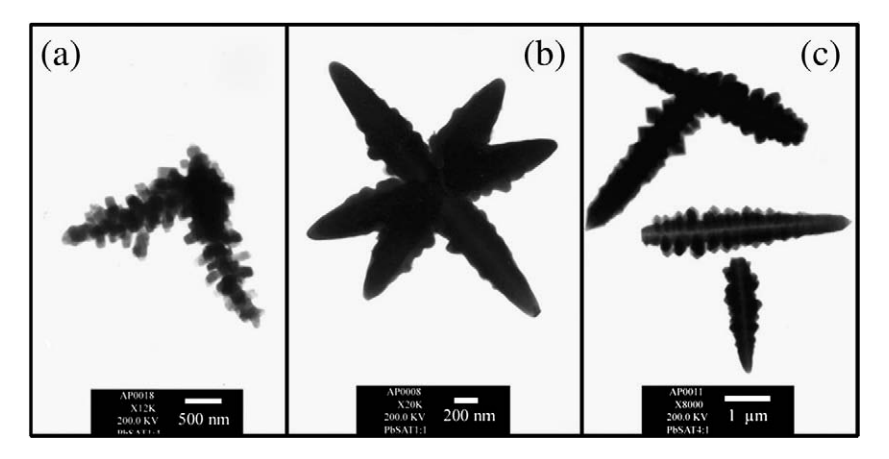


Fig. 3. TEM images of the products prepared using (a-c) 1:4, 1:1, and 4:1 molar ratios of Pb(CH<sub>3</sub>COO)<sub>2</sub> to NH<sub>2</sub>CSNH<sub>2</sub>, respectively.

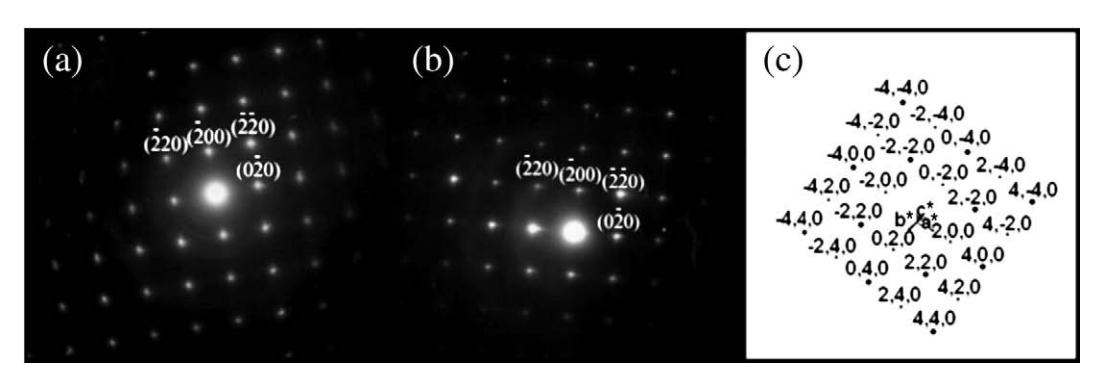


Fig. 4. SAED patterns of the products prepared using (a) 4:1 and (b) 1:4 molar ratios of Pb(CH<sub>3</sub>COO)<sub>2</sub> to NH<sub>2</sub>CSNH<sub>2</sub>, and (c) simulated electron diffraction pattern.

molar ratios of Pb and S sources. The 430 cm<sup>-1</sup> first overtone mode was detected using Raman spectrometry, but the fundamental one was forbidden.

#### Acknowledgements

We are extremely grateful to the Thailand Research Fund (TRF), Commission on Higher Education (CHE), and National Research Council of Thailand (NRCT) for financial support, and Graduate School of Chiang Mai University for general funding.

- [1] Qin AM, Fang YP, Zhao WX, Liu HQ, Su CY. J Cryst Growth 2005;283:230-41.
- Xu L, Zhang W, Ding Y, Yu W, Xing J, Li F, et al. J Cryst Growth 2004;273:213–9. Zhang YC, Qiao T, Hu XY, Wang GY, Wu X. J Cryst Growth 2005;277:518–23.
- [4] Wang S, Pan A, Yin H, He Y, Lei Y, Xu Z, et al. Mater Lett 2006;60:1242-6.
- [5] Gautam UK, Seshadri R. Mater Res Bull 2004;39:669-76.
- [6] Wang SF, Gu F, Lü MK, Zhou GJ, Zhang AY. J Cryst Growth 2006;289:621–5.

- [7] Saraidarov T. Reisfeld R. Sashchiuk A. Lifshitz E. Physica E 2007:37:173-7.
- Zhang W, Yang Q, Xu L, Yu W, Qian Y. Mater Lett 2005;59:3383-8.
- Zhou G, Lü M, Xiu Z, Wang S, Zhang H, Zhou Y, et al. J Phys Chem B 2006;110:6543-8. [10] Zhang Z, Lee SH, Vittal JJ, Chin WS. J Phys Chem B 2006;110:6649-54.
- [11] Ni Y, Wang F, Liu H, Yin G, Hong J, Ma X, et al. J Cryst Growth 2004;262:399–402.
- [12] Minceva-Sukarova B, Najdoski M, Grozdanov I, Chunnilall CJ. J Mol Struct
- 1997;410–411:267–70. [13] Gabriel C, Gabriel S, Grant EH, Halstead BSJ, Mingos DMP. Chem Soc Rev 1998;27:213–23.
- [14] Shao S, Zhang G, Zhou H, Sun P, Yuan Z, Li B, et al. Solid State Sci 2007;9:725-31.
- [15] Ji Y, Ma X, Zhang H, Xu J, Yang D. J Phys Condens Matter 2003;15:7611-5.
- [16] Boudias C, Monceau D. CaRlne Crystallography 3.1, 17 rue du Moulin du Roy, F-60300 Senlis, France; 1989-1998.
- [17] Powder Diffract. File, JCPDS Internat. Centre Diffract. Data, PA 19073-3273, U.S.A. 2001.
- [18] Suryanarayana C, Norton MG. X-ray Diffract, A Practical Approach. New York: Plenum Press; 1998.
- [19] Smith GD, Firth S, Clark RJH, Cardona M. J Appl Phys 2002;92:4375-80.
- [20] Sherwin R, Clark RJH, Lauck R, Cardona M. Solid State Commun 2005;134:565-70.
- [21] Thongtem T, Phuruangrat A, Thongtem S. Mater Lett 2007;61:3235–8.



# Carboxymethyl Cellulose-Assisted Hydrothermal Synthesis of PbS with Nano- and Micro-Crystals

Titipun Thongtem<sup>1</sup>\*, Sulawan Kaowphong<sup>2</sup>, and Somchai Thongtem<sup>2</sup>

<sup>1</sup>Department of Chemistry, Faculty of Science, Chiang Mai University, Chiang Mai 50200, Thailand <sup>2</sup>Department of Physics, Faculty of Science, Chiang Mai University, Chiang Mai 50200, Thailand

PbS with nano- and micro-crystals was hydrothermally synthesized from Pb(NO<sub>3</sub>)<sub>2</sub> and thiosemicar-bazide using carboxymethyl cellulose (CMC) as a template at 140, 180 and 200 °C for 12 h. CMC, NaOH and hydrothermal temperatures have the influence on the product morphologies characterized using a scanning electron microscope (SEM) and a transmission electron microscope (TEM). PbS (cubic) composing of Pb and S was detected using an X-ray diffractometer (XRD), a selected area electron diffraction (SAED) technique and an energy dispersive X-ray (EDX) analyzer. The interpreted patterns are in accordance with those of the simulations. Raman spectrometer revealed the presence of the vibration modes at 136, 278, 432, 602 and 967 cm<sup>-1</sup>. Emission spectra of the products were detected at 384-388 nm using a photoluminescence (PL) spectrometer.

**Keywords:** Hydrothermal Synthesis, Carboxymethyl Cellulose (CMC), PbS with Nano- and Micro-Crystals.

#### 1. INTRODUCTION

At present, nano- and micro-crystalline luminescent materials have become increasingly important. One of them is PbS which has a small band gap (0.41 eV) and a large exciton Bohr radius (18 nm).1-3 It has novel semiconducting and optical properties influenced by different shapes and sizes.4 It was synthesized using different methods, such as nanocubic and dendritic crystals by a complex solvothermal synthetic route,5 star-shaped dendrites, multipods, truncated nanocubes and nanocubes by a simple solution route,6 nanorods, nanobelts, nanovelvet-flowers and dendritic nanostructures using aqueous solution at low temperature assisted by CTAB,7 nanoclusters using a powder method on ionomers,8 thin solid films by electroless chemical deposition,9 magic-square structure by hydrothermal preparation,10 and nanobelts by sonochemical synthesis.11 The purpose of the research is to study the influence of carboxymethyl cellulose (CMC) and NaOH on PbS with nano- and micro-crystals synthesized using the home-made stainless steel autoclaves. Carboxymethyl cellulose, a non-toxic and inexpensive biomolecule, was used for shaping the product morphologies. It is a capping agent in the solutions as well. 12 The final products were then analyzed for further discussion.

# 2. EXPERIMENTAL DETAILS

For the present research, 0.003 mol Pb(NO<sub>3</sub>)<sub>2</sub> in 15 ml water, and 0.05 g carboxymethyl cellulose (CMC) in 10 ml water were thoroughly mixed to form the CMC/Pb2+ solution.<sup>12</sup> Subsequently, 0.003 mol thiosemicarbazide (NH2CSNHNH2) in 15 ml water and different molarities of 10 ml NaOH were put in the CMC/Pb2+ solution.To produce PbS with different morphologies, the reaction proceeded in the home-made stainless steel autoclaves at 140, 180 and 200 °C for 12 h.The precipitates were washed with water and 95% ethanol, and dried at 80 °C for 24 h. The final products were analyzed using an X-ray diffractometer (XRD) operated at 20 kV, 15 mA and using Cu K radiation in the 2 angular range of 15-60 deg, a transmission electron microscope (TEM) as well as the use of the selected area electron diffraction (SAED) technique operated at 200 kV, a scanning electron microscope (SEM) and an energy dispersive X-ray (EDX) analyzer operated at 15 kV, a Raman spectrometer using 50 mW Ar laser with 514.5 nm wavelength, and a luminescence spectrometer using the 250 nm exciting wavelength.

# 3. RESULTS AND DISCUSSION

XRD spectra (Fig.1) were indexed using Bragg's law for diffraction and compared to that of the JCPDS software with reference code no.05-0592. <sup>13</sup> They were specified as

<sup>\*</sup> Author to whom correspondence should be addressed.

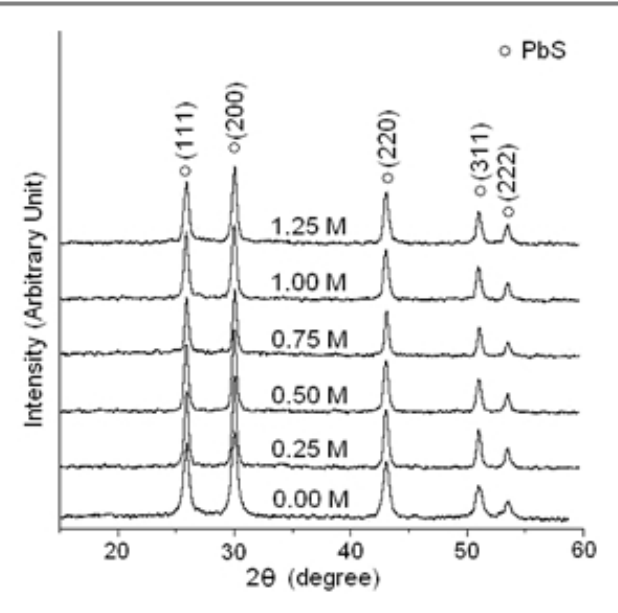


Fig. 1. XRD spectra of the products synthesized in the solutions containing 0.05 g CMC and different molarities of NaOH by the 140  $^{\circ}\text{C}$  hydrothermal reaction for 12 h.

cubic PbS with Fm-3m space group. The spectra are very sharp showing that well-crystallized PbS was successfully synthesized. The products were composed of a number of atoms aligning in a periodic lattice. The strongest intensity is at 2  $\theta$  = 30.08 deg and diffracts from (200) plane of the crystalline products. No other characteristic peaks of impurities such as different oxide-sulfates were detected showing that the products are pure phase. The results are in accordance with that detected by other researchers.

A definite existence of the products was analyzed using a Raman spectrometer. The spectra (Fig.2) contain prominent bands at the same wavenumbers although the products were synthesized using different conditions. Among the different spectra, their peaks are at 136, 278, 432, 602 and 967 cm<sup>-1</sup>. The peak below 150 cm<sup>-1</sup> is tentatively attributable to the so-called plasma line of the excitation laser.<sup>4,15</sup> The 278 cm<sup>-1</sup> peak was caused by the two-phonon process.4 Those at 432 and 602 cm<sup>-1</sup> are specified as the first and second overtone modes, respectively.15 The peak above 960 cm<sup>-1</sup> is attributable to oxide-sulfates.4 15 During Raman analysis, PbS could possibly be oxidized by air, and the undesired phases were produced on the product surface.<sup>16</sup> The constituents of the products were also characterized using EDX.The spectra (Fig.3) reveal the presence of Pb and S.

TEM images and SAED patterns (Fig.4) are used to specify the morphologies and phases of the products. In NaOH-free solution containing 0.05 g CMC (pH = 47), the product is flower-like at 140 °C hydrothermal reaction (Fig.4(a)). At 180 and 200 °C (Figs.4(b) and (c)), the flower becomes larger and more complete. During processing, PbS nuclei were produced. They grew into different morphologies controlled by growth rates of their crystallographic planes. Ratios (R) of growth rates along

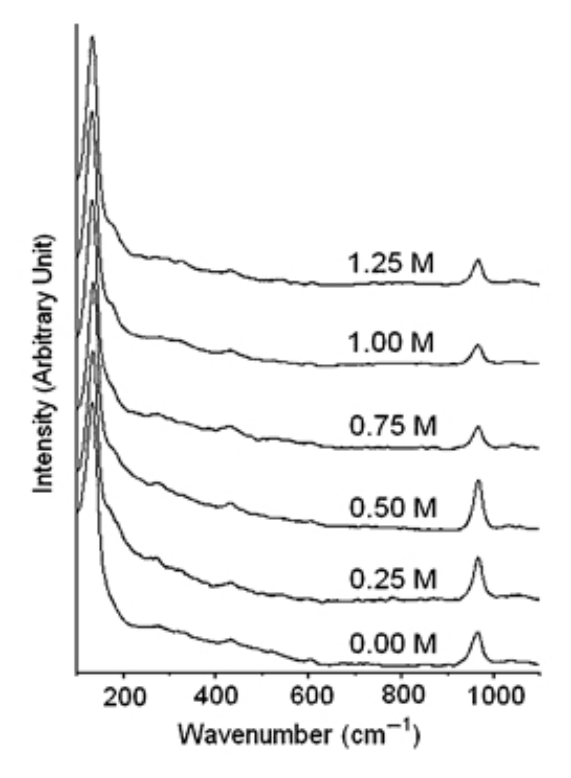


Fig. 2. Raman spectra of the products synthesized in the solutions containing 0.05 g CMC and different molarities of NaOH by the 140  $^{\circ}\text{C}$  hydrothermal reaction for 12 h.

[100] to [111] directions are used to determine shapes of the crystalline products.<sup>6,17,18</sup> Among them, nanocubes bounded by (100) planes were produced for *R* approaching or less than 0.58, spherical nanocrystals for *R* approaching 0.87, and one dimension rod-based single- and multi-pod

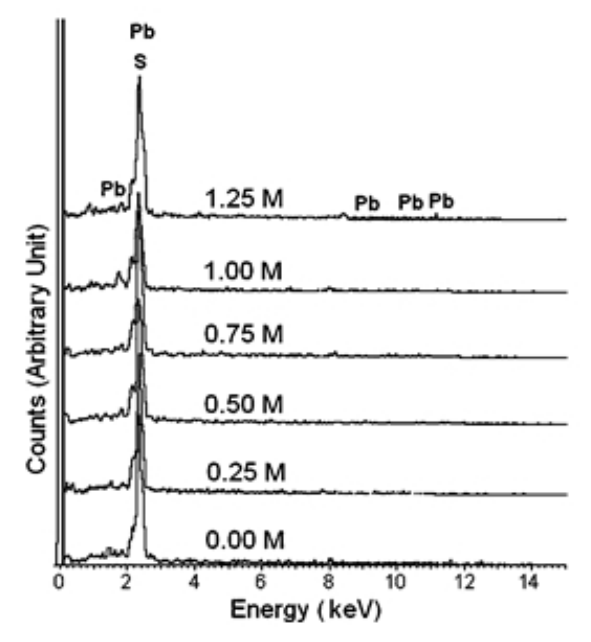


Fig. 3. EDX spectra of the products synthesized in the solutions containing 0.05 g CMC and different molarities of NaOH by the 140  $^{\circ}\text{C}$  hydrothermal reaction for 12 h.

J. Nanosci. Nanotechnol. 10, 2853-2857, 2010

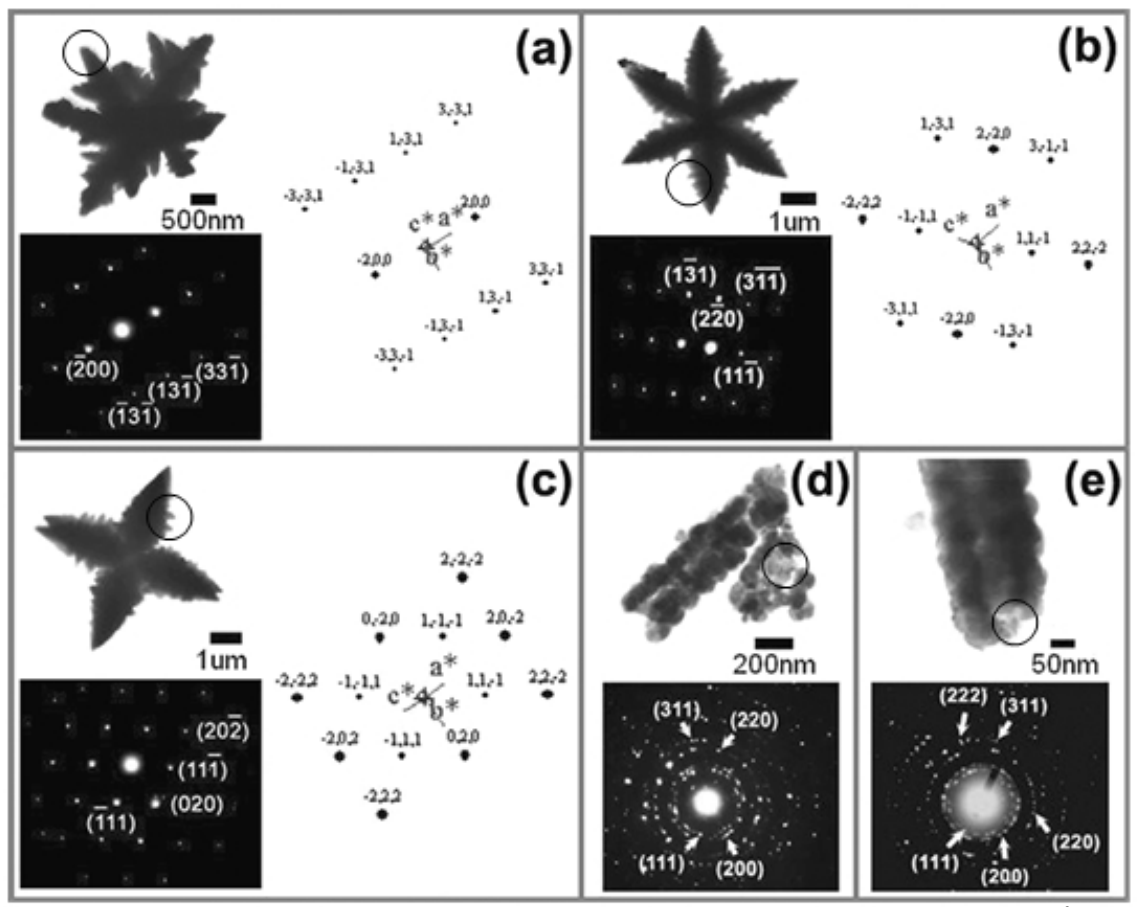


Fig. 4. TEM images and SAED patterns of PbS synthesized in (a-c) NaOH-free solution containing 0.05 g CMC at 140, 180 and 200 °C, and (d, e) 1.00 M and 1.25 M NaOH solutions containing 0.05 g CMC at 140 °C, respectively. The corresponding simulated patterns are also shown in (a-c). The products marked with the circles on the corresponding images were used for SAED analysis.

structured nanocrystals as well as flower-like crystals and star-shaped dendrites for R closing to or even above 1.73.6, 19 Growth rates of different crystallographic planes dominate by their corresponding surface energies.6 For cubic PbS crystal, surface energies ( $\gamma$ ) of different planes are different, and are in a sequence as  $\gamma$  (111) <  $\gamma$  (100) < γ (110).6,17 Thus CMC preferentially adsorbed on (111) plane. 17 18 Growth of PbS crystals along [111] direction was inhibited, and the process is in favor of growth along [100] direction.18 These have the influence on the growth rate ratio (R) to become higher. It is reasonable to assume R to be above 1.73, which led to the production of flower-like nanocrystals in the process.<sup>19</sup> Their SAED patterns (Figs.4(a-c)) appear as systematic array of bright spots showing that a number of atoms are aligned in their normal lattice. The patterns were interpreted, 20 and specified as cubic PbS crystal.13 Calculated electron beams or zone axes<sup>20</sup> are in the [013], [112] and [101] directions for the products produced at 140, 180 and 200 °C hydrothermal reactions, respectively. They are the directions that electron beams were sent to the corresponding crystalline facets. For the present research, simulated patterns (Figs.4(a-c)) were created 21 using the corresponding zone

axes. They are systematic and symmetric, and are in good accordance with the corresponding interpreted patterns. For the simulated patterns,  $a^{*}$ ,  $b^{*}$  and  $c^{*}$  lattice vectors are in the [100], [010] and [001] directions, respectively. The corresponding lattice vectors are the same although their zone axes are different. In the solution containing 0.05 g CMC and 1.00 M NaOH, a tubular cluster of nanoparticles at 140 °C hydrothermal reaction (Fig.4(d)) was produced. SAED pattern is composed of several concentric rings characterized as polycrystals. Interplanar spaces were calculated<sup>22, 23</sup> using their diffraction ring diameters, and compared with those of the JCPDS software. 13 They correspond to (111), (200), (220) and (311) crystallographic planes of the products and were specified as PbS.<sup>13</sup> When NaOH concentration was increased to 1.25 M, a tubular cluster of nano-particles (Fig.4(e)) became more complete. The shape of a tube was clearer. It has the dark and light contrast bands with 220 nm outside diameter. External surface of the tube is highly irregular, caused by an arrangement of nano-particles in sequence along its axial length. The SAED pattern composes of (111), (200), (220), (311) and (222) planes and were specified as PbS as well.

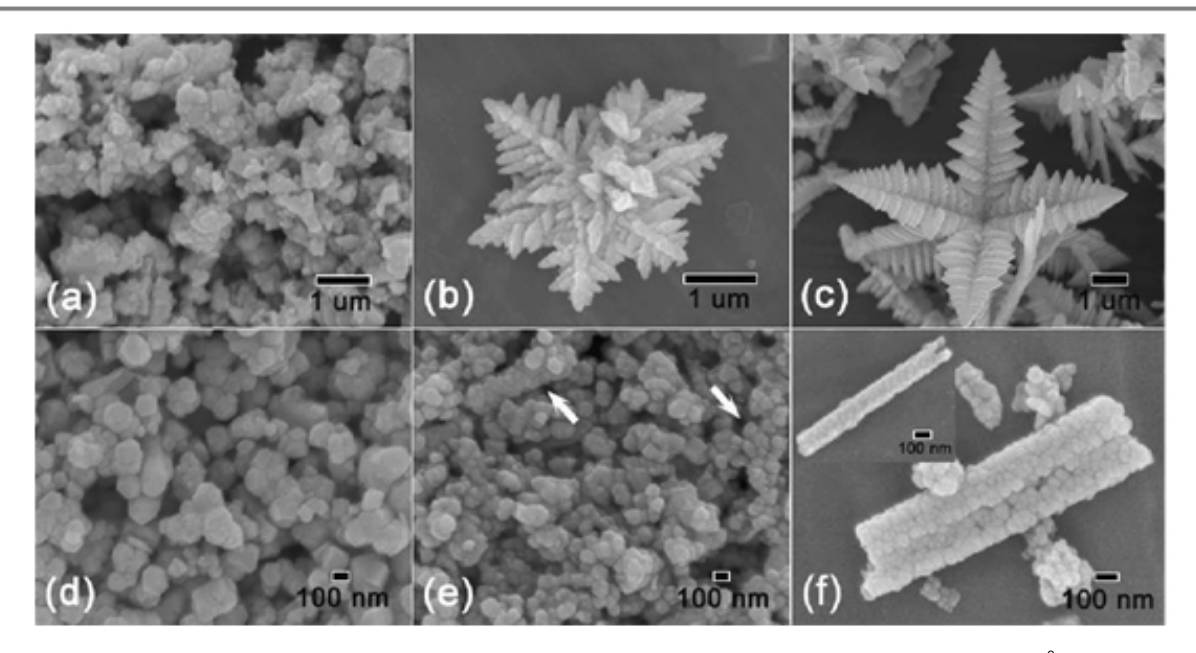


Fig. 5. Surface morphologies of PbS synthesized using different conditions (0 or 0.05 g CMC/0-1.25 M NaOH/140 or 200  $^{\circ}$ C).(a) (0/0/140), (b) (0.05/0/140), (c) (0.05/0/200), (d) (0.05/0.5/140), (e) (0.05/1.00/140) and (f) (0.05/1.25/140).

SEM images or surface morphologies (Fig.5) show that the products were successfully synthesized in a variety of shapes and sizes which were influenced by CMC, NaOH and hydrothermal temperatures. At 140 °C, and in CMC and NaOH-free solution (Fig.5(a)), Pb(NO<sub>3</sub>)<sub>2</sub> with thiosemicarbazide (NH2CSNHNH2) to produce PbS with submicro-sized particles in irregular clusters. When 0.05 g CMC was used in the process (NaOH-free solutions), Pb(NO<sub>3</sub>)<sub>2</sub> reacted with CMC to form CMC/Pb<sup>2+</sup> solution.12 Following the addition of thiosemicarbazide in the CMC/Pb2+ solution, H2S gradually evolved and further combined with lead ions to produce PbS.12 CMC is rich in carboxylate groups which can play a key role in the formation of nanostructured flowers by coordinating with Pb2+. The process determined the nucleation sites and growth of the products,12 composing of nanostructured flower (Fig.5(b)).It is more complete and becomes larger at 200 °C hydrothermal reaction (Fig.5(c)). The flower is made up of several petals.A distance between two apices of the two petals across the center of the flower is approximately 8,400 nm long. Each of the petals is composed of a number of small plates arranged in systematic order. For 0.05 g CMC, 0.5 M NaOH and 140 °C (Fig.5(d)), the product was composed of nano-sized particles in clusters. When 1.00 M NaOH was used (Fig. 5(e)), some clusters (marked with arrows) are similar to the tubes. The added NaOH coordinated with carboxylate groups which resulted to the decrease in the efficiency of CMC/Pb2+ coordination. Nucleation and growth processes were changed. OH- ions seemed to limit the growth of particles in all directions. The nano-particles were assembled in the perfectly tubular structure in 0.05 g CMC and 1.25 M

NaOH solution (Fig.5(f)). The diameters of the tubes are 162-387 nm.

Photoluminescence (PL) property of the products (Fig.6) was characterized using a 250 nm exciting wavelength. The maximum intensities were detected over the range 384-388 nm although their intensities are different. Their PL emission is in accordance with other result.<sup>24</sup> Morphologies have the influence on the intensities, which were increased with the decrease in the NaOH molarities (acidity increase).At a constant hydrothermal temperature and time, and different NaOH molarities, PL intensity of nanostructured flower (NaOH-free solution) is at the highest.The intensities are also very sensitive to the number of electronic transfers and defects in the products.<sup>25</sup>

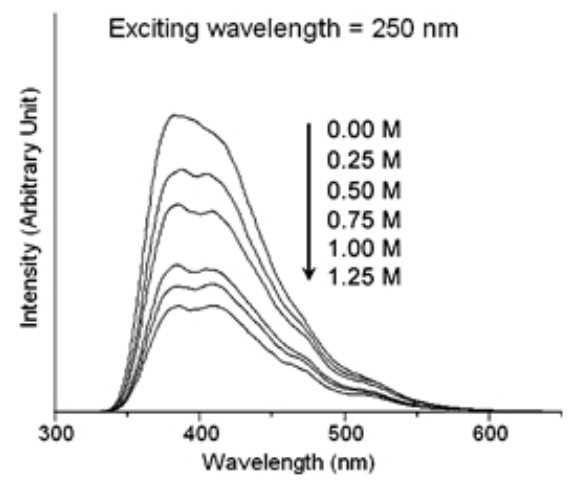


Fig. 6. PL spectra of the products synthesized in the solutions containing 0.05 g CMC and different molarities of NaOH by the 140  $^{\circ}\text{C}$  hydrothermal reaction for 12 h.

J. Nanosci. Nanotechnol. 10, 2853-2857, 2010

## 4. CONCLUSIONS

PbS with nano- and micro-crystals was successfully synthesized using hydrothermal reaction at different temperatures.Both CMC and NaOH can play the role in the reaction by producing a variety of product morphologies.XRD, SEM, EDX, TEM, SAED and Raman analyses revealed the presence of nano- and micro-crystalline PbS (cubic) composing of Pb and S with the first and second overtone modes at 432 and 602 cm<sup>- 1</sup>, respectively. The interpreted and simulated patterns are in good accordance.PL emission spectra of the products were detected at 384-388 nm, and PL intensity of the nanostructured flowers is at the highest.

Acknowledgments: We are extremely grateful to the Thailand Research Fund (TRF), National Research Council of Thailand (NRCT), and Institute for the Promotion of Teaching Science and Technology, for supporting the research.

### References and Notes

- L. Xu, W. Zhang, Y. Ding, W. Yu, J. Xing, F. Li, and Y. Qian, J. Cryst. Growth 273, 213 (2004).
- Y. C. Zhang, T. Qiao, X. Y. Hu, G. Y. Wang, and X. Wu, J. Cryst. Growth 277, 518 (2005).
- S. Wang, A. Pan, H. Yin, Y. He, Y. Lei, Z. Xu, and B. Zou, Mater. Lett. 60, 1242 (2006).
- A. M. Qin, Y. P. Fang, W. X. Zhao, H. Q. Liu, and C. Y. Su, J. Cryst. Growth 283, 230 (2005).
- W. Zhang, Q. Yang, L. Xu, W. Yu, and Y. Qian, Mater. Lett. 59, 3383 (2005).

- G. Zhou, M. Lu, Z. Xiu, S. Wang, H. Zhang, Y. Zhou, and S. Wang, J. Phys. Chem. B 110. 6543 (2006).
- 7. L. Dong, Y. Chu, Y. Liu, M. Li, F. Yang, and L. Li, *J. Coll. Interf.* Sci. 301, 503 (2006).
- 8. G. R. Deen and M. Hara, Polymer 46, 10883 (2005).
- 9. B. Minceva-Sukarova, M. Najdoski, I. Grozdanov, and C.J. Chunnilall, J. Molec. Struct. 410-411, 267 (1997).
- Y. Ni, X. Wei, J. Hong, and X. Ma, Mater. Res. Bull. 42, 17 (2007).
- S. M. Zhou, X. H. Zhang, X. M. Meng, X. Fan, S. T. Lee, and S. K. Wu, J. Solid State Chem. 178, 399 (2005).
- M. Wu, X. Pan, X. Qian, J. Yin, and Z. Zhu, *Inorg.* Chem. Comm. 7,359 (2004).
- 13. Powder Diffract. File, JCPDS-ICDD , 12 Campus Boulevard, Newtown Square PA 19073-3273, U.S.A. (2001).
- 14. T. Thongtem and S. Thongtem, Ceram. Internat. 30, 1463 (2004).
- G. D. Smith, S. Firth, R. J. H. Clark, and M. Cardona, J. Appl. Phys. 92,4375 (2002).
- J. G. Shapter, M. H. Brooker, and W. M. Skinner, Internat. J. Miner. Process. 60, 199 (2000).
- P. Zhao, G. Chen, Y. Hu, X. L. He, K. Wu, Y. Cheng, and K. Huang, J. Cryst. Growth 303, 632 (2007).
- 18. X. Zhao, J. Yu, and B. Cheng, *Mater*. Chem. Phys. 101,379 (2007).
- B. Haobo, H. Wei, and G. Mingyuan, Chin. Sci. Bull. 51, 2576 (2006).
- 20. T. Thongtem, A. Phuruangrat, and S. Thongtem, *Mater. Lett.* 61, 3235 (2007).
- C. Boudias, D. Monceau, CaRIne Crystallography 3.1, DIVERGENT S. A., Centre de Transfert, 60200 Compiegne, France (1989-1998).
- 22. A. Phuruangrat, T. Thongtem and S. Thongtem, *Mater. Lett.* 61, 3805 (2007).
- T. Thongtem, S. Kaowphong and S. Thongtem, J. Mater. Sci. 42,3923 (2007).
- 24. S. Ye, Y. Ye, Y. Ni, and Z. Wu, J. Cryst. Growth 284, 172 (2005).
- T. Thongtem, A. Phuruangrat, and S. Thongtem, Appl. Surf. Sci. 254, 7581 (2008).

Received: 3 December 2008. Accepted: 20 January 2009.